UNIVERSITA' VITA-SALUTE SAN RAFFAELE

CORSO DI DOTTORATO DI RICERCA INTERNAZIONALE IN MEDICINA MOLECOLARE

Curriculum in Neuroscienze e Neurologia Sperimentale

A chemical screening approach targeting new autophagy modulators against ischemic brain damage

DoS: Dr. Luca Muzio

Second Supervisor: Prof.ssa Michela Matteoli

Tesi di DOTTORATO di RICERCA di Alice Viotti

Matricola 013851

Ciclo di dottorato XXXIV

SSD BIO/13

Anno Accademico 2020/2021

CONSULTAZIONE TESI DI DOTTORATO DI RICERCA

La sottoscritta / *I*	Alice Viotti
Matricola / *registration number*	013851
Nata a / *born at*	Alessandria
Il / *on*	03/08/1993

Autrice della tesi di Dottorato di ricerca dal titolo / *author of the PhD Thesis titled* ***A chemical screening approach targeting new autophagy modulators against ischemic brain damage***

X AUTORIZZA la Consultazione della tesi / AUTHORIZES *the public release of the thesis*

□ NON AUTORIZZA la Consultazione della tesi per …… mesi / DOES NOT AUTHORIZE *the public release of the thesis for …… months*

a partire dalla data di conseguimento del titolo e precisamente */ from the PhD thesis date, specifically*

Dal / *from* ……/……/…… Al / *to* ……/……/……

Poiché / *because*:

□ l'intera ricerca o parti di essa sono potenzialmente soggette a brevettabilità / *The whole project or part of it might be subject to patentability;*

□ ci sono parti di tesi che sono già state sottoposte a un editore o sono in attesa di pubblicazione / *Parts of the thesis have been or are being submitted to a publisher or are in press;*

□ la tesi è finanziata da enti esterni che vantano dei diritti su di esse e sulla loro pubblicazione / *the thesis project is financed by external bodies that have rights over it and on its publication.*

Data / Date 31/01/2022 Firma / Signature

DECLARATION

This thesis has been composed by myself and has not been used in any previous application for a degree. Throughout the text I use both 'I' and 'We' interchangeably.

All the results presented here were obtained by myself, except for:

1) *In silico* compounds prioritization was performed in collaboration with Dr. Chiara Parravicini and Prof. Ivano Eberini, Department of Pharmacological and Biomolecular Sciences, University of Milan, Milan, Italy;
2) Transmission Electron Microscopy samples were processed, and images were acquired by Dr. Alessia Loffreda and Dr. Andrea Raimondi, Experimental Imaging Center, IRCCS San Raffaele Scientific Institute, Milan, Italy;
3) Middle Cerebral Artery Occlusion surgeries were performed by Dr. Andrea Bergamaschi under the supervision of Dr. Marco Bacigaluppi, Neuroimmunology Unit, IRCCS San Raffaele Scientific Institute, Milan, Italy.

All sources of information are acknowledged by means of reference.

ACKNOWLEDGEMENTS

I thank Professor Gianvito Martino for allowing me to initiate my Ph.D. in his laboratory, and for always providing constructive feedback.

A special thank goes to Dr. Luca Muzio for his constant supervision and scientific support.

I also thank Professor Michela Matteoli for supervising my research work and for her precious suggestions.

I thank Dr. Ivano Eberini and Dr. Chiara Parravicini for their collaboration and for helping me with the *in silico* analysis and data management.

I also acknowledge the technical contribution of Dr. Alessia Loffreda and Dr. Andrea Raimondi to the Electron Microscopy experiment.

I thank Dr. Marco Bacigaluppi and Professor Paola Panina for their important advice.

I also thank Dr. Marco Piccoli and Professor Luigi Anastasia for allowing me to perform the chemical screening in their laboratory and share instrumentation.

I finally acknowledge the valuable contribution of *each* member of the Neuroimmunology and Clinical Neuroimmunology Units.

ABSTRACT

Introduction - Autophagy is a self-eating process involved in the maintenance of cell homeostasis, that dominates physiological and pathological conditions. Many studies show that brain ischemia activates the autophagic flux in neurons. However, the role of such activation is far to be completely understood. The identification of selective autophagy modulators will foster the discovery of novel neuroprotective strategies, as well as gain insight into the functional outcomes of this biological process.

Methods - In this study, I developed a sensitive and robust assay to explore novel autophagy modulators in brain ischemia. Using a cell clone constitutively expressing Microtubule-Associated Protein 1A/1B-Light Chain 3 (LC3) coupled with the Green Fluorescent Protein (GFP) variant pHluorin, I monitored the autophagic flux in murine neuronal cells (Neuro-2a). I performed a fluorescence-based Low Throughput Screening by semi-automated flow cytometry. I introduced in the experimental setting Oxygen-Glucose Deprivation to stress cells, mimicking the toxic environment that features the ischemic brain. Following the primary screening assay, selected molecules were further evaluated by western blot analysis on Neuro-2a and *ad hoc* stressed primary cortical neurons. I finally employed Middle Cerebral Artery Occlusion (MCAO), an experimental animal model of brain ischemia, to validate best hits.

Results - We prioritized a library of 6839 bioactive compounds through an *in silico* screening based on physically significant descriptors and pharmaceutically relevant properties. I screened 898 compounds using the established *in vitro* model. The primary screening revealed 27 putative autophagy modulators. Nineteen selected compounds underwent three different validation rounds, involving an immortalized cell line and primary neuronal cultures. Eight of the nineteen molecules passed the first validation step and were further tested for their dose-response efficacy properties. Four molecules were tested on nutrient-deprived mouse cortical neurons, and three of them efficiently modulated autophagy in this model.

Conclusions - I set up a platform to screen small molecules potentially modulating the autophagic process. With this screening strategy, I applied stringent-threshold *in vitro* tests on different cell types. Best hits are currently under *in vivo* evaluation using the MCAO mouse model to finalize the pre-clinical study. This study will shed light on the complexity of the autophagy flux in ischemic stroke and its neuroprotective clinical potential.

TABLE OF CONTENTS

ACRONYMS AND ABBREVIATIONS

3-MA	3-Methyladenine
ADME	Absorption, Distribution, Metabolism, and Excretion
Akt	Ak strain transforming protein
AMBRA1	Activating Molecule in Beclin1-Regulated Autophagy protein 1
AMP	Adenosine Monophosphate
AMPA	Amino-3-hydroxy-5 methyl-4-isoazole Propionic Acid
AMPK	AMP-activated Protein Kinase
ANOVA	Analysis of Variance
AP-1	Activating Protein-1
ATG	AuTophaGy-related
ATP	Adenosine Triphosphate
AVs	Autophagic Vacuoles
Baf	Bafilomycin A1
BCA	Bicinchronic Acid
Bcl-2	B-cell lymphoma 2
Bif-1	Bax-interacting factor 1
BNIP3	Bcl2 and adenovirus E1B 19-kDa-Interacting Protein 3
BNIP3L	BNIP3-like
BSA	Bovine Serum Albumin
CAMKKβ	Calcium/calmodulin-dependent protein Kinase Kinase beta
CBF	Cerebral Blood Flow
CES	Cardioembolic Stroke
ClpP	Caseinolytic protease P
CMA	Chaperon-Mediated Autophagy
CNS	Central Nervous System
CT	Computed Tomography
DALY	Disability-Adjusted Life-Years
DIV	Days *In Vitro*
DMEM	Dulbecco's Modified Eagle Medium
DMPK	Drug Metabolism and Pharmacokinetics
DMSO	Dimethyl Sulfoxide
DNA-PK	DNA-dependent Protein Kinase
ECL	Enhanced Chemiluminescence
EDTA	Ethylenediamine Tetra acetic Acid

EGFR	Epidermal Growth factor Receptor
EPO	Erythropoietin
ER	Endoplasmic Reticulum
ERGIC	ER-Golgi Intermediate Compartment
ETC	Electron Transport Chain
FACS	Fluorescence-Activated Cell Sorter
FAD	Flavin Adenine Dinucleotide
FBS	Fetal Bovine Serum
FDA	Food and Drug Administration
FIP200	Focal adhesion kinase family Interacting Protein of 200 kDa
GABARAP	Gamma-Aminobutyric Acid Receptor-Associated Protein
GBD	Global Burden of Disease
GEF	Guanine nucleotide Exchange Factor
GFAP	Glial Fibrillary Acidic Protein
GFP	Green Fluorescent Protein
GPR132	G Protein-Coupled Receptor 132
Gαq	Gq alpha subunit
HER1	Human Epidermal growth factor Receptor 1
HER2	Human Epidermal growth factor Receptor 2
HIF	Hypoxia Inducible Factor
HMGCR	3-Hydroxy-3-Methylglutaryl Co-enzyme A Reductase
HOPS	Homotypic vacuole fusion and Protein Sorting
I/R	Ischemia-Reperfusion
IM	Isolation Membrane
IV	Intravenous
KAT2B	Lysine Acetyltransferase 2B
LAMP2A	Lysosome-Associated Membrane Protein type 2A
LAS	Large-artery Atherosclerotic Stroke
LC3	Microtubule-Associated Protein 1A/1B-Light Chain 3
LDF	Laser Doppler Flowmeter
LIR	LC3 Interaction Region
LTS	Low-Throughput Screening
LVO	Large Vessel Occlusions
MAD	Median Absolute Deviation
MAP2	Microtubule-Associated Protein 2
MAPK	Mitogen-Activated Protein Kinase
MAPK14	Mitogen-Activated Protein Kinase 14

MCA	Middle Cerebral Artery
MCAO	Middle Cerebral Artery Occlusion
miRNA	MicroRNA
MMP	Matrix Metalloproteinase
MOA	Mechanism Of Action
MRI	Magnetic Resonance Imaging
mTORC1	Mechanistic Target Of Rapamycin Complex 1
NA-1	Nerinetide
NAD^+	Nicotinamide Adenine Dinucleotide
NADPH	Nicotinamide Adenine Dinucleotide Phosphate
ND	Nutrient Deprivation
NF-κB	Nuclear Factor kappa B
NINDS	National Institute of Neurological Disorders and Stroke
NMDA	N-Methyl-D-Aspartate
NRBF2	Nuclear Receptor Binding Factor 2
OGD	Oxygen-Glucose Deprivation
OMM	Outer Mitochondrial Membrane
OPTN	Optineurin
p70S6K	p70 Ribosomal Protein S6 Kinase
PAS	Phagophore Assembly Site
PB1	Phox and Bem1p
PIK3C3	Phosphatidylinositol 3-Kinase Catalytic subunit type 3
PIK3C3-C1	PIK3C3 complex 1
PIK3C3-C2	PIK3C3 complex 2
PIK3R4	Phosphoinositide 3-Kinase Regulatory subunit 4
PINK1	PTEN-Induced Kinase 1
PK-hLC3	pHluorin-mKate2-human LC3
PKA	Protein Kinase A
PLA2	Phospholipase A2
PLC	Phospholipase C
pMCAL	permanent Middle Cerebral Artery Ligation
pMCAO	permanent Middle Cerebral Artery Occlusion
PRKN	Parkin
PSD-95	Post-Synaptic Density protein 95
PtdIns3K	Phosphatidylinositol 3-kinase
PTEN	Phosphatase and Tensin homolog
RAG	RAS-related small GTPase

Rb1	RB Transcriptional Corepressor 1
RIC	Remote Ischemic Conditioning
RNS	Reactive Nitrogen Species
ROS	Reactive Oxygen Species
RRAGD	Ras-related GTP-binding protein D
rt-PA	recombinant tissue Plasminogen Activator
S/N	Signal-to-Noise ratio
SAR	Selective Autophagy Receptor
SD	Standard Deviation
SNARE	SNAP Receptor
SPAN	Stroke Preclinical Assessment Network
SSMD	Strictly Standardized Mean Difference
STAIR	Stroke Therapy Academy Industry Roundtable
SVS	Small-Vessel Stroke
TEM	Transmission Electron Microscopy
TFEB	Transcription Factor EB
TIA	Transient Ischemic Attack
tMCAO	transient Middle Cerebral Artery Occlusion
TRPM2	Transient Receptor Potential Melastatin 2
TSC1	Tuberous Sclerosis 1
TSC2	Tuberous Sclerosis 2
TUJ1	Neuron-specific class III beta-tubulin
Ub	Ubiquitin
UBA	Ubiquitin-Binding domain
UBL	Ubiquitin-Like
ULK1	Unc-51-Like Kinase 1
ULK2	Unc-51-Like Kinase 2
UPR	Unfolded Protein Response
UVRAG	Ultraviolet irradiation Resistant-Associated Gene
V-ATPase	Vacuolar H^+-ATPase
VAM7	Vacuolar Morphogenesis protein 7
VAM9	Vacuolar Morphogenesis protein 9
VEFG	Vascular Endothelial Growth Factor
WIPI	WD-repeat protein Interacting with Phosphoinositides

LIST OF FIGURES AND TABLES

1. INTRODUCTION

1.1 Ischemic Stroke

1.1.1 Definition and epidemiology

Stroke is a neurological disease affecting the neurovascular system. It can be generally classified into *ischemic* and *hemorrhagic* stroke, with the ischemic stroke constituting the largest proportion of all new strokes annually (over 60%) (Shakir, 2018; Roth *et al*, 2018).

Ischemic stroke is described as an episode of neurological dysfunction caused by focal cerebral, spinal, or retinal infarction attributable to ischemia. Subtypes of ischemic stroke comprise Large-artery Atherosclerotic Stroke (LAS), Small-Vessel Stroke (SVS), and Cardioembolic Stroke (CES). Different classification systems are available and provide a precise etiological classification of each subtype: the TOAST classification (based on the Trial of ORG 10172 in Acute Stroke Treatment) (Adams *et al*, 1993), the ASCOD phenotyping system (A: atherosclerosis: S: small-vessel disease; C: cardiac pathology; O: other causes; D: dissection) (Amarenco *et al*, 2009), and the web-based Causative Classification System (Ay *et al*, 2007).

Hemorrhagic strokes are caused by leaky blood vessels causing intracerebral bleeding and are subdivided into intracerebral hemorrhage and subarachnoid hemorrhage. In this case, the classification relies on the specific anatomical site or presumed etiology. In 2019, intracerebral and subarachnoid hemorrhages constituted about 30% and 10% of all strokes, respectively (GBD 2019 Stroke Collaborators, 2021).

The global stroke epidemiology is rapidly changing. According to a report from the Global Burden of Disease (GBD) 2019 (GBD 2019 Stroke Collaborators, 2021), the annual number of deaths caused by stroke increased from 1990 to 2019, particularly in lower-income and middle-income countries. Globally in 2019, stroke was the second-leading cause of death and the third-leading cause of death and disability combined. Specifically, there were 6.55 million deaths from stroke and 143 million Disability-Adjusted Life-Years (DALYs – the sum of life-years lost due to premature death and the years of productive life lost due to disability) due to stroke. Over the study period, the age-standardized rates of stroke incidence decreased by 17%. However, age-specific incidence rates increased by 15% among those younger than 70 years. In addition, at the global level, age-standardized death and DALY rates

were higher in males than in females, although there were no significant sex differences in incidence rates.

The large increase in the global burden of stroke is due to population growth, aging, and the increase in exposure to several risk factors. Leading risk factors are high systolic blood pressure, high body-mass index, high fasting plasma glucose, pollution, and smoking (GBD 2019 Stroke Collaborators, 2021). There is also evidence that stroke can be genetically driven. A large multi-ethnic genome-wide association meta-analysis conducted in 2018 reported 32 genetic loci, including 22 not previously identified, associated with stroke risk. Some of the loci showed association specific to major etiological stroke subtypes. Approximately half of the identified loci correlate with multiple related vascular traits. Moreover, risk loci associated with stroke were enriched in drug targets for thrombolytic treatment (Malik *et al*, 2018).

1.1.2 Pathophysiology

Ischemic stroke is generally caused by arterial occlusion. This results in the abrupt Cerebral Blood Flow (CBF) decrease, hypoxia, and initiation of a series of molecular events that trigger tissue damage with consequent neuronal, glial, and endothelial cells death. From the morphological point of view, after an ischemic insult, it is possible to discriminate between two regions: the **core** and the ischemic **penumbra**. The ischemic core is the region more severely affected by ischemia, where the CBF is almost completely abolished. It is characterized by irreversibly damaged neurons that typically die from necrosis. On the other hand, the penumbra is defined as the perinecrotic region. It is functionally silent but metabolically active due to the presence of residual blood flow provided by collaterals. The ischemic penumbra is characterized by a slower cell death that typically occurs from apoptosis (Heiss, 2011). If a timely, efficient restoration of CBF does not occur, the infarction matures and spreads from the core to the surrounding hypoperfused regions. The propagation of the irreversible tissue damage is a dynamic process involving both space and time. Ischemic lesion maturation can either lead to delayed cell death or to recovery. This maturation process can last hours or days, depending on the insult intensity and other systemic or local factors (Berardelli & Cruccu, 2015; Mergenthaler *et al*, 2016) (**Figure 1**).

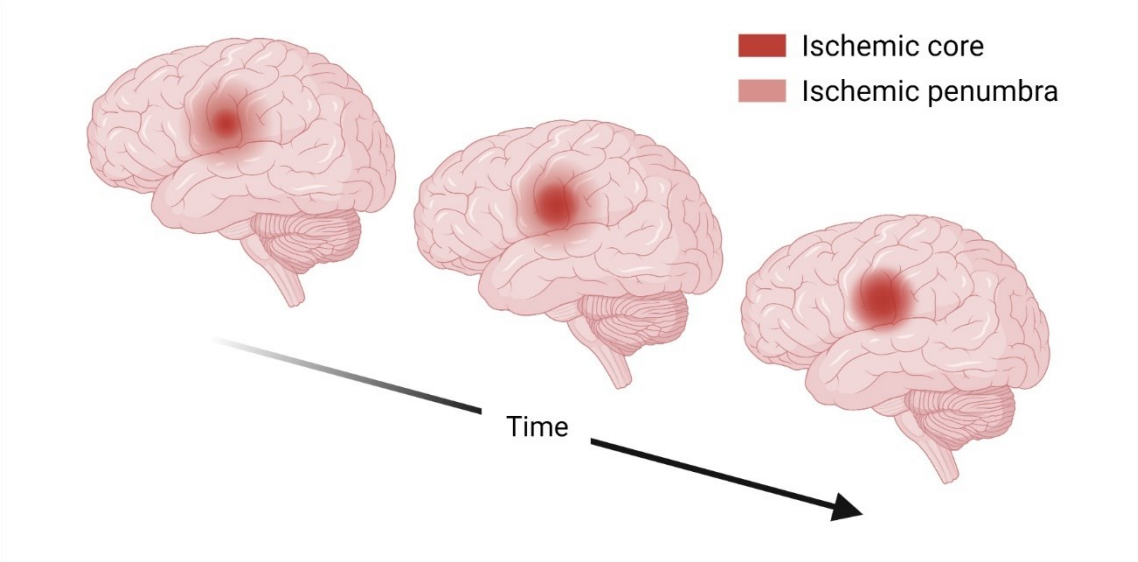

Figure 1 – Necrotic lesion maturation. *Following an ischemic event, it is possible to discriminate between irreversibly damaged tissue (ischemic core) and a surrounding hypoperfused region (ischemic penumbra). If prompt recanalization does not occur, the lesion can dynamically spread, leading to permanent tissue damage. Created with BioRender.com.*

Right after the ischemic insult, the brain can sustain cerebral oxygen metabolism through local compensatory mechanisms that involve vasodilation and augmented oxygen transfer from blood to the infarcted tissue. However, if the CBF is not restored, a metabolic crisis can occur (Powers *et al*, 1984). Diminished cerebral perfusion and oxygenation in the penumbra initiate a series of molecular events, termed *ischemic cascade*, leading to delayed neuronal cell death (**Figure 2**). The major consequence of CBF decrease is the inability of neurons to pursue aerobic respiration. This leads to anaerobic metabolism and excessive lactic acid production, with consequent tissue acidification (Kelmanson *et al*, 2021). The net result of this detrimental cascade is a strong impairment of the efficiency of the Electron Transport Chain (ETC), leading to the reduction of Adenosine Triphosphate (ATP) production and the failure of Na^+/K^+ ATPase. Membrane ion gradients quickly dissipate, facilitating selective and unselective ion channels opening. Membrane depolarization finally leads to neuronal swelling and cytotoxic edema, both caused by altered osmotic gradients. Moreover, impairment of the ionic gradient also increases Ca^{2+} influx and glutamate release in neurons. Glutamate-mediated activation of low and high-affinity kainate, N-methyl-D-aspartate (NMDA), and amino-3-hydroxy-5 methyl-4-isoazole propionic acid (AMPA) receptors further depolarizes the membrane causing large Ca^{2+} influx in neuronal cells (Choi & Rothman, 1990; Macdonald & Stoodley, 1998; Peng *et al*, 2006). Ca^{2+}-dependent events include proteases and lipid

peroxidases activation (Siesjö & Bengtsson, 1989). Among the enzymes that are aberrantly activated, phospholipase A2 (PLA_2) and C (PLC) are involved in membrane degradation. This process leads to the release of arachidonic acid, whose metabolism causes lipid peroxidation, and Reactive Oxygen Species (ROS) and prostaglandin production. As a result, cellular components are further damaged, linking the ischemic cascade to apoptosis and inflammation (Bach, 2017).

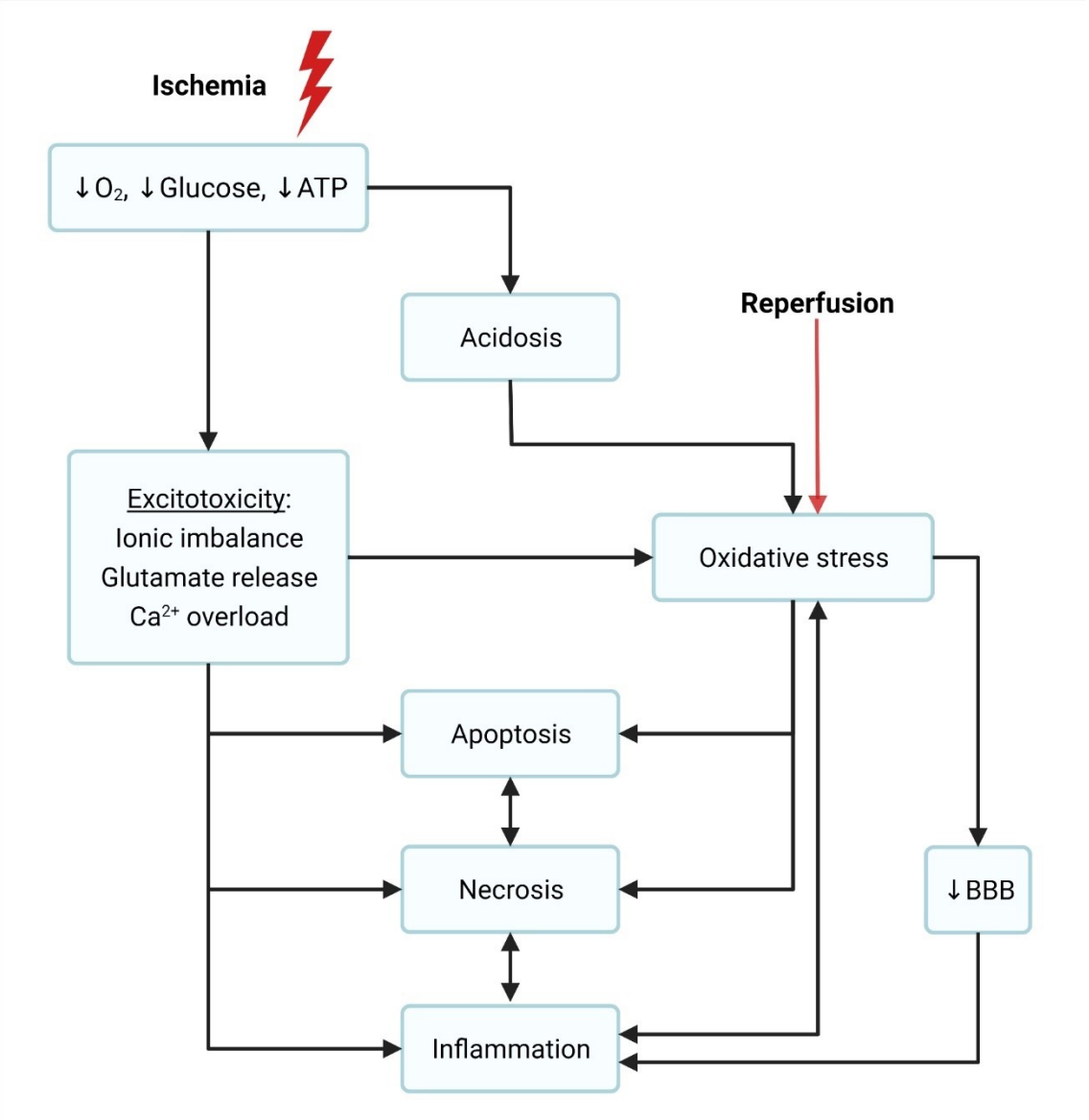

Figure 2 – Ischemic cascade. *Schematic diagram highlighting the major molecular events that follow ischemic stroke, finally leading to cellular death. Created with BioRender.com.*

Together with ROS, majorly produced by mitochondria, NADPH oxidases, and flavoproteins, also Reactive Nitrogen Species (RNS) concur to ischemic damage exacerbation. Indeed, ROS and RNS can harm cells in different ways, targeting lipids, DNA, and proteins (Girouard *et al*, 2009; Förstermann, 2010).

Along with metabolic reactions, ischemic stroke also triggers the expression of a wide range of genes. Activated genes mainly include those belonging to the inflammatory pathway, such as cytokines, chemokines, and factors promoting cell infiltration (Paoni *et al*, 2002). Oxidative stress and excitotoxicity can activate microglia, leading to the release of inflammatory mediators in the extracellular space. This also results in matrix metalloproteinases (MMPs) activation, which in turn tackle the brain barrier system (Yang & Rosenberg, 2011). BBB disruption is a reversible event, but it can persist for 72 hours after the initial ischemic insult, causing potentially negative implications in stoke management (Candelario-Jalil *et al*, 2007).

Hypoxic stress is also a direct cause of multiple transcription factors activation, including Activating Protein-1 (AP-1), Hypoxia-Inducible Factor-1 (HIF-1), and Nuclear Factor kappa B (NF-κB). Downstream activated genes comprise factors that significantly contribute to the adaptive response to oxygen deprivation (Safronova & Morita, 2010).

Given the complex mechanisms triggered by an ischemic insult, an effective stroke treatment should consider a synergistic and combined approach. Due to its residual viability, the penumbra region is the major target for all the therapeutic strategies adopted so far.

1.1.3 Diagnosis, management, and therapy

The diagnosis of symptomatic cerebral ischemic events is primarily clinic and further supported by modern imaging procedures, such as Computed Tomography (CT) and Magnetic Resonance Imaging (MRI), that help clinicians to provide evidence of infarction. Based on the duration of the symptoms, stroke can be distinguished from a Transient Ischemic Attack (TIA). Symptoms of a stroke last longer than 24 hours and can lead to an earlier death. TIA has a lower duration and, typically, no infarction evidence is detectable by imaging techniques (Sacco *et al*, 2013).

Among the available stroke treatments, there are pharmacological approaches that are strongly influenced by other factors, including hemodynamic management, monitoring of the ischemic edema, and adequate management of systemic complications that follow the primary ischemic event. Of note, an important role is played by what happens in intensive care or stroke unit soon after hospitalization. As

a principle, there are three main points to consider for appropriate management of ischemic stroke: (1) timely recanalization achievement, (2) collateral flow optimization, and (3) secondary brain injury avoidance (Rabinstein, 2017).

To date, the first primary therapeutic options for ischemic stroke mainly rely on prompt recanalization and reperfusion strategies, aiming to reduce infarct size and preserve neurological functions. The benefit of the therapy is time-dependent; thus, it is crucial to determine or estimate the time of stroke symptoms onset and follow updated clinical recommendations (Powers *et al*, 2019). The use of intravenous (IV) chemical thrombolytics for stroke treatment began more than 25 years ago and has been followed by endovascular procedures as an alternative or an adjunct to improve patients' outcomes. Specifically, recombinant tissue plasminogen activator (rt-PA), or other proteins displaying a similar activity, and mechanical thrombectomy with retrievable stents are the two evidence-based strategies to open the occluded vessel. Approved in 1996 by the Food and Drug Administration (FDA), rt-PA (Alteplase™) has been proven to be effective up to 4.5 hours after the onset of the ischemic symptoms (Lapchak & Boitano, 2017). Nevertheless, it must be considered that only a small percentage of stroke patients are eligible for rt-PA therapy. Indeed, although the improved clinical outcome in 50% of treated patients, rt-PA treatment is associated with an increased incidence of hemorrhagic complications (National Institute of Neurological Disorders and Stroke rt-PA Stroke Study Group, 1995). As regards endovascular technology, the first FDA approval came in 2004. Stent retrievers are particularly effective against Large Vessel Occlusions (LVO) and include self-expanding and aspirating devices (Gogela *et al*, 2017). According to updated guidelines, patients can be selected for mechanical thrombectomy between 6 and 24 hours from stroke symptoms onset (Powers *et al*, 2019).

Along with stroke therapy, the role of primary prevention should not be underestimated. This is more important considering that 77% of strokes are first events (Virani *et al*, 2021). Modifiable and behavioral factors, including hyperglycemia, renal dysfunction, smoking, unhealthy diet, and low physical activity, strongly concur to the development of an ischemic stroke (Vos *et al*, 2020). For every risk factor, guidelines exist to implement primary prevention and select the best therapeutic intervention for each individual patient (Goldstein *et al*, 2006).

1.1.4 Ischemia-reperfusion injury

Further considerations are needed about reperfusion. Although its undoubted necessary role in the therapeutic context, reperfusion causes additional damage that

is of great impact on patients' outcomes. Ischemia-Reperfusion (I/R) injury is defined as a multifactorial process that follows CBF restoration, leading to the paradoxical worsening of tissue dysfunction (Fitridge & Thompson, 2011). A major role in this sense is played by mitochondria, as the brain almost exclusively relies on oxidative phosphorylation for energy production. As ischemia occurs, electrons' transport through the ETC slows down, leading to electron stalling, ATP degradation, and proton gradient dissipation. This results in the alteration of mitochondrial membrane potential ($\Delta\Psi_m$), further promoted by the increased [Ca^{2+}] (Puka-Sundvall *et al*, 2000; Liu & Murphy, 2009). Upon reperfusion, the compromised ETC is not able to properly respond to the sudden oxygen influx mainly because of the unavailability of autoxidizable electron carriers (NAD^+ and FAD). The net result of this condition is a secondary burst of ROS/RNS production that further supports cellular decline.

1.1.5 Neuroprotection

Given the limits of current therapeutic options, successful treatments for stroke are strongly needed. Adjuvant approaches have been considered to protect brain cells from I/R injury, as well as to extend the narrow therapeutic window for recanalization strategies.

The term *neuroprotection* has been in use for about 60 years and can be considered a second therapeutic strategy for ischemic stroke treatment. It differs from the vascular approach based on early reperfusion as it is a cell-based strategy. The concept of neuroprotection aims to preserve brain tissue until CBF is restored, either by interfering with specific targets of the harmful ischemic cascade or by enhancing protective mechanisms. However, although several preclinical evidence demonstrated that neuroprotection is achievable, translation from animal models to patients encountered a high failure rate (Sacchetti, 2008; Braeuninger & Kleinschnitz, 2009). In 2006, an evaluation revealed that more than 1000 drugs and non-pharmacological strategies had been tested for neuroprotection in animal models. Among them, at least 114 candidates targeting the ischemic cascade, including NMDA and AMPA antagonists, and radical scavengers, have been administered to patients. Most of the tested drugs did not result in an amelioration of the clinical outcome (O'Collins *et al*, 2006). Major contributors to the high failure rate of proposed drugs are sub-optimal experimental design, poor consideration of age-related comorbidities, and limited read-outs while assessing stroke outcomes. As a result, the Stroke Therapy Academy Industry Roundtable (STAIR) updated its recommendations, highlighting the importance of focusing on agents with multiple

mechanisms of action, assessing long-term recovery using non-invasive MRI and complex motor and cognitive tests, as well as including aged animal models of stroke with comorbidities in both sexes.

Of note, to promote the effective translation of neuroprotectants into future pivotal clinical trials, the National Institute of Neurological Disorders and Stroke (NINDS) in the USA announced support for the Stroke Preclinical Assessment Network (SPAN). This approach is intended to screen and select therapeutic candidates in combination with thrombectomy, thrombolysis, or both. Selected candidates include Fingolimod, Fasudil, Remote Ischemic Conditioning (RIC), Tocilizumab, Uric acid, and Veliparib (Paul & Candelario-Jalil, 2021).

In the last decade, only a few candidates were evaluated in clinical trials. Among those candidates that completed phase III/IV clinical trials (**Table 1**), one has available results (ClinicalTrials.gov, NCT02930018). The efficacy and safety profile of Nerinetide (NA-1), an eicosapeptide interfering with Post-Synaptic Density protein 95 (PSD-95), were evaluated in a multicenter, double-blind, randomized placebo-controlled trial. PSD-95 potential in the neuroprotective context has already been extensively described (Haugaard-Kedström *et al*, 2017). The trial enrolled 1105 stroke patients with LVO within a 12-hour therapeutic window. Results showed that treatment with a single dose of NA-1 along with endovascular thrombectomy was not effective in reducing disability from stroke due to LVO at 90 days when compared with placebo. However, improved outcomes were observed in a subpopulation of patients receiving the NA-1 treatment alone (Hill *et al*, 2020). Authors hypothesized a drug-drug interaction between NA-1 and Alteplase, which could lead to plasmin-dependent NA-1 cleavage. Therefore, further confirmatory studies are needed to extensively explore NA-1 neuroprotective effects in patients.

In addition, four drugs are currently undergoing phase III/IV clinical trials (**Table 2**). Two of them aim to evaluate Cerebrolysin®'s efficacy. Cerebrolysin® is a multi-target neuropeptide preparation that displayed neurotrophic and neuroprotective effects. It is currently recommended in various clinical practice guidelines for both acute stroke and post-stroke rehabilitation phases (Beghi *et al*, 2021). A recent comprehensive meta-analysis highlight a very good safety profile of Cerebrolysin®, although there was a tendency for serious adverse events when used at high dosage (Strilciuc *et al*, 2021). Thus, further evaluations are needed to complete the safety and efficacy test of this molecule.

Table 1 – Completed phase III/IV clinical trials for ischemic stroke. *Data source: ClinicalTrials.gov. Research updated to January 2022; focus on "stroke" AND "neuroprotection", over the 2012-2022 period.*

ID	*Phase*	*Title*	*Interventions*	*Target*
NCT02930018	III	Safety and Efficacy of Nerinetide (NA-1) in Subjects Undergoing Endovascular Thrombectomy for Stroke (ESCAPE-NA1)	Nerinetide (NA.1), 2.6 mg/kg	PSD-95 inhibition
NCT03686163	IV	Effects of Intranasal Nerve Growth Factor for Acute Ischemic Stroke	Nerve Growth Factors	N/A

Table 2 – Ongoing phase III/IV clinical trials for ischemic stroke. *Data source: ClinicalTrials.gov. Research updated to January 2022; focus on "stroke" AND "neuroprotection", over the 2012-2022 period.*

ID	*Phase*	*Title*	*Interventions*	*Target*
NCT04904341	III	Efficacy of Cerebrolysin Treatment as an add-on Therapy to Mechanical Thrombectomy in Acute Ischemic Stroke.	Cerebrolysin	Other
NCT05041010	III	Rescues On Reperfusion Damage In Cerebral Infarction by Nelonemdaz	Neu2000KWL	NMDA inhibition; ROS scavenging
NCT05124353	II/III	Early Administration of Cerebrolysin on the Outcome of Patients With Acute Stroke Undergoing EVT	Cerebrolysin	Other
NCT04657133	III	Remote Ischemic Conditioning for the Treatment of Intracerebral Hemorrhage (RICH-2)	Remote ischemic conditioning	Other

There are other ongoing trials aim to evaluate the clinical safety of remote ischemic conditioning and Neu2000KWL. Neu2000KWL is a sulfasalazine derivative, described as a multi-target neuroprotectant that affects NMDA-receptors and acts as a free radical scavenger (Hong *et al*, 2018).

In conclusion, while deepening the safety profile of the described drugs, these works also suggest that, unlike previous unsuccessful attempts to achieve neuroprotection, novel candidates should probably not be specific but should target the ischemic cascade at different levels.

1.2 Autophagy

1.2.1 Overview

The term *autophagy*, denoting a self-eating process, was coined by Christian de Duve (Nobel Prize in Physiology or Medicine in 1974) in 1963 during a talk on the discovery of lysosomes. Since the concept of autophagy emerged, research studies remained largely observational until the early 1990s, when Yoshinori Ohsumi used baker's yeast to dissect the process, identifying 15 genes involved in autophagy regulation (Takeshige *et al*, 1992; Tsukada & Ohsumi, 1993). For his discoveries on autophagy mechanisms, Ohsumi was awarded the Nobel Prize in Physiology or Medicine in 2016, and from his findings the field largely increased in knowledge. To date, more than 40 yeast AuTophaGy-related (ATG) genes have been described and many of them have orthologues in humans. Indeed, autophagy is a highly conserved cellular degradation and recycling process. The major roles of autophagy are the maintenance of cellular homeostasis and providing nutrients to sustain cellular metabolism during different forms of stress.

In contrast to the ubiquitin-proteasome system, which mainly degrades short-living proteins, the autophagic pathway is involved in the bulk degradation of long-lived cytosolic components, including proteins and entire organelles (Yorimitsu & Klionsky, 2005). Moreover, in contrast to endocytic processes, which originate at the plasma membrane, all the autophagic substrates are freely accessible to the cytosolic components of the autophagic machinery.

Mammalian cells display three different types of autophagy: Chaperon-Mediated Autophagy (CMA), microautophagy, and macroautophagy. Although at the morphological level each type is unique, all three culminate with cargo delivery to the lysosome, with its subsequent degradation and recycling (Cuervo, 2004) (**Figure 3**). However, despite the marked morphological differences, there might be a strong

interplay between the diverse autophagic machinery, as they share common protein complexes and regulatory mechanisms (Wu *et al*, 2015; Mejlvang *et al*, 2018; Schuck, 2020).

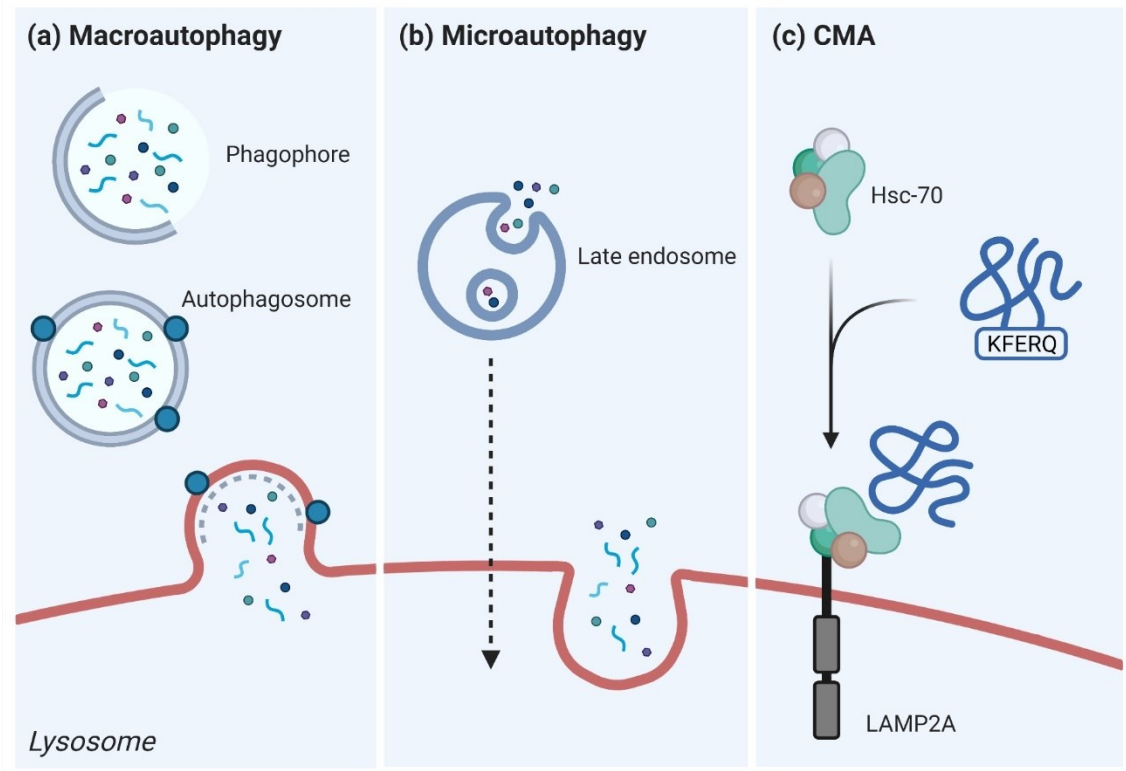

Figure 3 – Autophagy in mammalian cells. *Graphical representation of the three major autophagic pathways described in mammals: (a) macroautophagy, (b) microautophagy, and Chaperon-Mediated Autophagy (CMA). Created with BioRender.com.*

CMA is a selective degradative pathway for KFERQ-like motif-bearing proteins. The pentapeptide is recognized by the cytosolic chaperone Heat-Shock Cognate 71 kDa (Hsc70), which drives lysosomal translocation. Once at the lysosome, the substrate/chaperone complex triggers the multimerization of the Lysosome-Associated Membrane Protein type 2A (LAMP2A), which forms a translocation complex (Cuervo & Dice, 1996). Altered CMA has been proven to contribute to functional alterations, proteotoxicity, and a general loss of proteostasis in neurons (Kaushik & Cuervo, 2018; Bourdenx *et al*, 2021).

Microautophagy occurs when cargoes are directly sequestered by the lysosome through invaginations or protrusions of the lysosomal membrane. Although in the past two decades studies carried out in yeast revealed much information regarding the mechanisms of lysosomal membrane invagination and the major proteins

involved in this process (Krick *et al*, 2008; Morshed *et al*, 2020), little is still known about microautophagy in mammalian cells. In 2011, Sahu *et al*. described a microautophagy-like process in which cytosolic proteins were delivered to late endosomes in a Hsc70-dependent, but LAMP2A-independent manner (Sahu *et al*, 2011).

Macroautophagy is the most studied and well-characterized autophagic pathway. Generally, it occurs at a low level constitutively and can be enhanced by different stresses, such as nutrient deprivation or energy starvation. In contrast to microautophagy and CMA, during macroautophagy, the initial sequestration step involves the formation of cytosolic double-membrane vesicles that transport cargoes to the lysosome. In yeast, autophagic membranes generate *de novo* at a single perivacuolar site named Phagophore Assembly Site (PAS) (Suzuki *et al*, 2001). On the contrary, in mammalian systems, the initiation step occurs at multiple sites (Mizushima *et al*, 2011; Dikic & Elazar, 2018).

Following autophagy initiation, the membrane starts to expand, forming a cup-shaped structure named the **phagophore**. As expansion proceeds, the membrane elongates and curves around cytosolic cargoes. Once the elongation step is completed, the two ends of the phagophore seal into a double-membrane structure termed the **autophagosome**. Autophagosomes vary in size, depending on the organism and the specific cargo type. Mammalian autophagosomes' diameter ranges from 0.5 to 1.5 μm. In mammals, the autophagosome is destined to deliver the autophagic cargos to the lysosomal compartment, fusing with the lysosomal membrane to form the **autolysosome**. The movement of autophagic cargos to the lysosomal endpoint is commonly referred to as **autophagic flux**.

Macroautophagy can converge with endocytosis. For this reason, as an intermediate step, autophagosomes may also fuse with early- or late-endosomes to form the **amphisomes**, before fusing with lysosomes. Within the autolysosome, the acidic pH and the presence of lysosomal hydrolases determine the degradation of the autophagosome inner membrane and autophagic cargoes. Degradation products are then recycled back to the cytoplasm to serve for energy generation or cellular biosynthetic pathways (Mizushima & Komatsu, 2011; Parzych & Klionsky, 2014; Dikic & Elazar, 2018).

Each of the above-mentioned steps is finely regulated and promoted by dedicated protein complexes. Major players involved in the mammalian macroautophagic process are hereafter described and summarized in **Figure 4**.

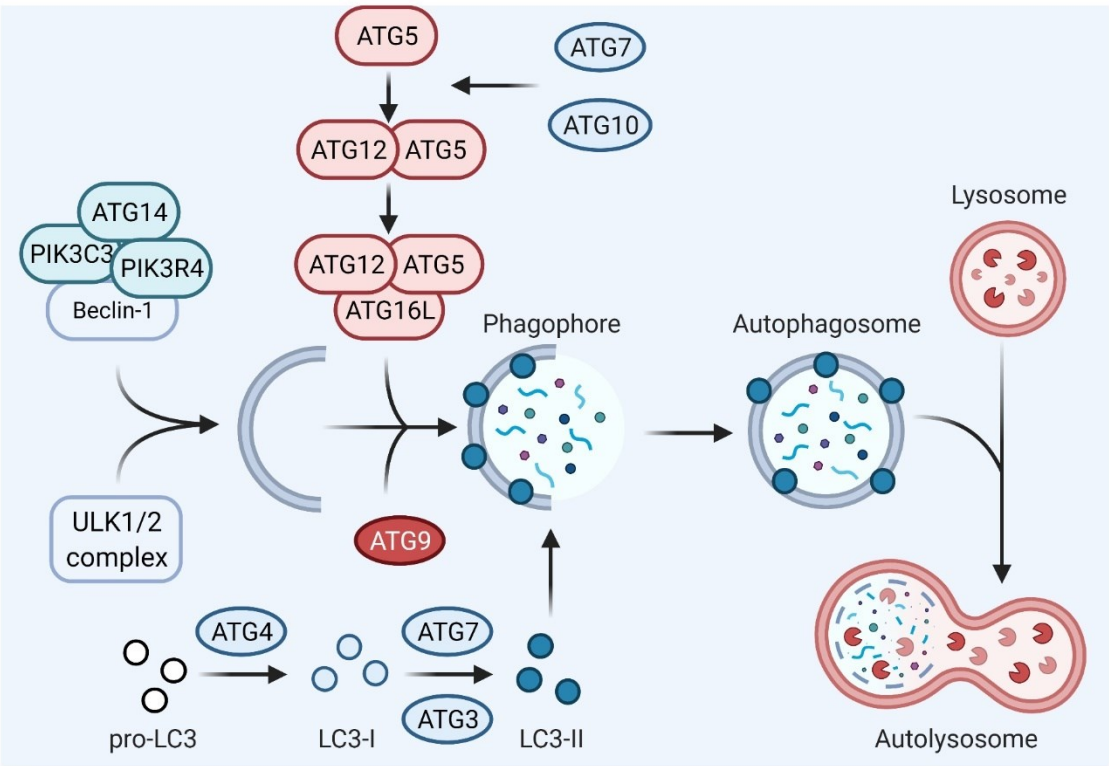

Figure 4 – Macroautophagy in mammalian cells. *Graphical representation of the major proteins and complexes involved in macroautophagic machinery regulation. Created with BioRender.com.*

Induction – Autophagy initiation requires a protein complex consisting of one protein belonging to the Unc-51-like kinase family (either ULK1 or ULK2), the mammalian homolog of Atg13 (ATG13), and the Focal adhesion kinase family Interacting Protein of 200 kDa (FIP200; also known as RB1CC1) (Hara *et al*, 2008). The ULK1/2-ATG13-FIP200 complex is not regulated by the nutrient status of the cell, and it is stably assembled. Another protein, ATG101 (also known as C12orf44), associates with the complex and is essential for autophagy initiation. A key regulator of the initiation step is the mechanistic Target Of Rapamycin Complex 1 (mTORC1). Its activity is dependent on the nutrient status of the cell (Bar-Peled & Sabatini, 2014; González & Hall, 2017; Saxton & Sabatini, 2017). Specifically, under nutrient-rich conditions, mTORC1 associates with the ULK1/2-ATG13-FIP200 complex. Upon association, it directly phosphorylates ULK1/2 and ATG13 for inactivation. Conversely, upon starvation or rapamycin treatment, mTORC1 dissociates from the complex, leading to ULK1 autophosphorylation. In turn, ULK1 phosphorylates both ATG13 and FIP200, leading to macroautophagy induction (Jung *et al*, 2009).

Phagophore nucleation – The next step relies on the recruitment of the ATG14-containing class III phosphatidylinositol 3-kinase (PtdIns3K) complex (Itakura & Mizushima, 2010). This complex is necessary for the phagophore's nucleation and is composed of Phosphatidylinositol 3-Kinase Catalytic subunit type 3 (PIK3C3; also known as VPS34), Phosphoinositide 3-Kinase Regulatory subunit 4 (PIK3R4; also known as p150), and Beclin-1. This complex participates both in macroautophagy, by associating with ATG14 to form the PIK3C3 complex 1 (PIK3C3-C1), or in the endocytic pathway, interacting with Ultraviolet Irradiation Resistant-Associated Gene (UVRAG) to form the PIK3C3 complex 2 (PIK3C3-C2) (Liang *et al*, 2006). Regulation of the elongation process occurs by protein interaction with Beclin-1. Nuclear Receptor Binding Factor 2 (NRBF2) is a component of the PIK3C3-C1, identified as a key regulatory subunit of the complex (Ohashi *et al*, 2016). NRBF2 interaction with the PIK3C3-C1 and, in particular, with Beclin-1 is strongly dependent on ATG14 (Lu *et al*, 2014). Negative regulators of the PtdIns3K complex include the antiapoptotic protein B-cell lymphoma 2 (Bcl-2), which binds Beclin-1 preventing its interaction with PIK3C3, and Rubicon, which interacts with the UVRAG-associated PtdIns3K complex. Conversely, the Activating Molecule in Beclin-1-Regulated Autophagy protein 1 (AMBRA1) and Bax-interacting factor 1 (Bif-1) act as positive regulators, which interact with Beclin-1 directly and indirectly, respectively (Takahashi *et al*, 2007).

The phagophore generation and elongation typically occur within Ω-shaped ER subdomains, termed **omegasomes**, which are enriched in the lipid molecule PtdIns-3-phosphate (PI3P) (Axe *et al*, 2008). PI3P recruits the WD-repeat protein Interacting with Phosphoinositides (WIPI) protein family and the WIPI-binding proteins ATG2A/B (Velikkakath *et al*, 2012; Proikas-Cezanne *et al*, 2015), providing a scaffold to recruit the autophagic machinery for phagophore assembly and maturation (Ren *et al*, 2020).

Critical membrane sources for autophagosome formation include the Golgi apparatus, endosomes, mitochondria, and the plasma membrane (Ravikumar *et al*, 2010; Longatti *et al*, 2012; Hamasaki *et al*, 2013). In addition, studies in mammalian cells pointed out the ER-Golgi Intermediate Compartment (ERGIC; a network of vesicular and tubular membrane structures devoted to the two-way trafficking between the two compartments) as a phospholipids source for autophagosomes biogenesis and maturation (Ge *et al*, 2013).

Elongation – For phagophore elongation, there are two conjugation systems involving ubiquitin-like (UBL) proteins (Weidberg *et al*, 2011). ATG7 serves as an E1

activating enzyme, while ATG3 and ATG10 are two E2 conjugating enzymes. The first system relies on the ATG12—ATG5-ATG16L1 complex, with ATG12 and ATG5 covalently conjugated in an ATG7/ATG10-dependent manner. The ATG12—ATG5-ATG16L1 complex associates with the phagophore until the autophagosome is completed (Ichimura *et al*, 2000). Regulation systems involve the Golgi protein RAB33A, which can inhibit ATG16L1, and the Lysine Acetyltransferase 2B (KAT2B), which can independently target ATG5, ATG7, and ATG12. The other UBL system is the Microtubule-Associated Protein 1A/1B-Light Chain 3 (LC3, homolog of the yeast Atg8) system. It requires the LC3 processing by the cysteine protease ATG4 to form LC3-I, exposing an LC3's glycine residue at the C-terminus. ATG7 activates LC3-I and transfers it to the E2-like enzyme ATG3, where it is covalently conjugated to the lipid phosphatidylethanolamine (PE) to form LC3-II (Geng & Klionsky, 2008). The ATG12—ATG5-ATG16L1 complex is reported to facilitate the latter step, acting as an E3 ligase. LC3-II is the membrane-associated LC3 form and can localize to the phagophore membrane. A second ATG4 cleavage step is possible, leading to LC3 deconjugation and release from the membrane. In addition to LC3, which is the best characterized, several Atg8-like proteins exist and are mainly divided into LC3 and Gamma-aminobutyric acid Receptor-Associated Protein (GABARAP) subfamilies. LC3-I conversion to LC3-II is enhanced upon autophagy-inducing conditions, such as nutrient starvation or other stresses. Moreover, an augmented LC3 synthesis after macroautophagy induction has also been described. While LC3 is required for autophagosome maturation, closure, and transport, the GABARAP subfamily seems to be involved in the latest maturation stages (Weidberg *et al*, 2010; Lee & Lee, 2016).

Another factor required not only for the elongation phase but also for phagophore formation is the transmembrane protein ATG9A. ATG9A can localize to different cellular compartments, and it is involved in membrane recruitment (Gómez-Sánchez *et al*, 2021). Under nutrient-rich conditions, ATG9A localizes to the *trans*-Golgi network, where it is clustered in small vesicles (ATG9A-positive vesicles). Upon starvation, it localizes to the phagophores and to the forming autophagosomal membranes, where it dynamically and transiently interacts with other ATG proteins (Orsi *et al*, 2012). The cycling to autophagosomes is ULK1- and PtdIns3K-dependent and can be inhibited by Mitogen-Activated Protein Kinase 14 (MAPK14) (Young *et al*, 2006).

ATG9A interacts with ATG2A for phospholipids transfer from membranes of different sources to the expanding phagophore. ATG2A has been proven to actively transfer lipids between membranes, operating at the ER-phagophore interface

(Maeda *et al*, 2019; Valverde *et al*, 2019). In addition, ATG9A operates as a lipid scramblase to efficiently distribute phospholipids both to the cytoplasmic and the luminal leaflet of the expanding phagophore. The interaction between ATG9A and ATG2A is essential for integrating lipids into the phagophore membrane, promoting its elongation and normal-sized autophagosomes formation (Guardia *et al*, 2020; Matoba & Noda, 2020).

Autophagosome formation and fusion – The exact mechanism that leads to phagophore maturation and closing is still not fully elucidated. After autophagosome completion, microtubules drive it to the endosomal/lysosomal compartment to finally fuse to form the autolysosome. A key protein required for autophagosomes-late endosomes/lysosomes fusion is the RAB7 GTPase (Gutierrez *et al*, 2004; Carroll *et al*, 2013). RAB7 requires a Guanine nucleotide Exchange Factor (GEF) for its activation and to promote the interaction with specific effectors and tethering factors. The GEF involved in RAB7 activation is the MON1-CCZ1 complex, which can be found onto late-endosomes and autophagosomes (Hegedűs *et al*, 2016). The MON1-CCZ1 complex interacts with lysosomal ARL8 and RAB7-interacting lysosomal protein, thus mediating the fusion step (Gao *et al*, 2018). The SNAP receptor (SNARE) machinery components, such as Vacuolar Morphogenesis protein 7 (VAM7), VAM9, or syntaxin 17, have been shown to assemble and participate in the fusion process (Jäger *et al*, 2004; Liang *et al*, 2008; Monastyrska *et al*, 2009). Selected SNAREs are recognized by the Homotypic vacuole fusion and Protein Sorting (HOPS) tethering complex, which bind both RAB7 and SNAREs promoting membrane bridging (Jiang *et al*, 2014).

1.2.2 Macroautophagy regulation

Macroautophagy is primarily involved in extra- and intracellular stress responses. Major regulating events include nutrient deprivation, hypoxia, altered availability of insulin or other growth factors, and Endoplasmic Reticulum (ER) stress. Carbon and nitrogen depletion are sensed by cAMP-dependent Protein Kinase A (PKA) and mTORC1 pathways, respectively. PKA and mTORC1 are negative regulators of autophagy under nutrient-rich conditions (Stephan *et al*, 2010). Specifically, PKA can influence the elongation step through LC3 phosphorylation (Cherra *et al*, 2010). Amino acid availability regulates RAS-related small GTPases (RAG), which in turn activate mTORC1 (Sancak *et al*, 2008). In amino acid-deprived conditions, mTORC1 is inhibited, leading to autophagy induction mainly through mTORC1 substrates dephosphorylation. NRBF2 is a key autophagy regulator, as it binds ATG14-Beclin-1

upon mTORC1 inhibition, promoting ULK1 association and autophagy initiation (Ma *et al*, 2017). It has also been demonstrated that PKA can activate mTORC1, either through direct phosphorylation or through the inactivation of the AMP-activated protein Kinase (AMPK) (Djouder *et al*, 2010). Apart from being a PKA substrate, AMPK is also the major energy-sensing kinase of the cell. It is regulated by the intracellular AMP/ATP levels in the cell. AMP is the primary AMPK activator, indicating low energy levels. As a response, AMPK can phosphorylate and activate the Tuberous Sclerosis Complex 1/2 (TSC1/2), which inactivates mTORC1.

Another AMPK substrate is ULK1, which can be phosphorylated by this kinase for activation (Inoki *et al*, 2003; Kim *et al*, 2011).

Another key regulator, involved both in lysosomal biogenesis and autophagy, is Transcription Factor EB (TFEB). TFEB is involved in the starvation-induced autophagic response in a Mitogen-Activated Protein Kinase (MAPK)–dependent manner (Settembre *et al*, 2011). Under stress conditions, TFEB is translocated to the nucleus to regulate the expression of its target genes (Sardiello *et al*, 2009). TFEB is negatively regulated by mTORC1, which in turn is inhibited by the TFEB-dependent Ras-related GTP-binding protein D (RRAGD) activation. This mechanism provides a feedback response to stabilize the cellular metabolic state (Di Malta *et al*, 2017; Vega-Rubin-de-Celis *et al*, 2017).

An additional important factor that regulates macroautophagy induction is ER stress. ER stress causes [Ca^{2+}] increase in the cytoplasm, resulting in the activation of the calcium/calmodulin-dependent protein kinase kinase beta (CAMKKβ) and autophagy induction (Høyer-Hansen *et al*, 2007). Moreover, ER can also mediate autophagy induction through unfolded protein response (UPR) signaling (Ding *et al*, 2007).

Among other key autophagy-promoting signals, there are hypoxia and unavailability of growth factors. Both factors can suppress mTORC1 activation, also in the presence of favorable nutrient conditions (Lum *et al*, 2005).

1.2.3 Selective macroautophagy

Together with bulk degradation of randomly selected intracellular components, macroautophagy can be highly selective in cargoes recognition. Selective autophagy mediates aggregated proteins and damaged or dysfunctional organelles degradation, as well as the removal of invading pathogens. Specifically targeted cargoes include, but are not limited to, ubiquitinated proteins, ER (ERphagy), mitochondria (mitophagy), ribosomes (ribophagy), nucleus (nucleophagy), and pathogens

(xenophagy). Efficient cargo recognition is mediated by exclusive mechanisms involving Selective Autophagy Receptors (SARs) which specifically drive cargo engulfment within the autophagosomes. The common SARs characteristic is the presence of an LC3 interaction region (LIR) motif, which mediates ATG machinery recruitment to the cargoes and triggers *in situ* autophagosome formation (Noda *et al*, 2008; Alemu *et al*, 2012; Birgisdottir *et al*, 2013). So far, more than 30 SARs have been identified in mammalian cells and can be categorized based on their cargo recognition system in ubiquitin (Ub)-dependent and Ub-independent SARs (Kirkin & Rogov, 2019). Many receptors are able to recruit ULK1 complex to the cargo for autophagosome formation (Smith *et al*, 2018; Ravenhill *et al*, 2019; Turco *et al*, 2019; Vargas *et al*, 2019).

The mammalian SAR p62/SQSTM1 mediates the autophagic degradation of ubiquitinated cargoes such as aggregated and disposable proteins or cytosolic viruses and bacteria (Seibenhener *et al*, 2004; Bjørkøy *et al*, 2005; Pankiv *et al*, 2007; Zheng *et al*, 2009). The architecture of p62 consists of a LIR motif allowing the interaction with LC3, a Ubiquitin-binding domain (UBA) mediating the p62-Ub interaction, and a Phox and Bem1p (PB1) domain that recognizes other proteins and promotes homo-oligomerization. Although the p62 affinity for Ub is not high, oligomerization of p62 increases the relative avidity of the complex. As a result, the binding to the ubiquitinated substrates is stabilized, leading to efficient cargo sequestration within the autophagosomes (Raasi *et al*, 2005; Long *et al*, 2010; Wurzer *et al*, 2015). Ubiquitin stress promotes physical interaction between disposal ubiquitinated cargoes and p62, thus promoting LC3 binding for selective autophagic degradation.

A critical selective pathway is mitophagy, devoted to fine-tuning mitochondrial turnover and maintaining adequate energy metabolism. Dysfunctions in mitochondrial degradation have been associated with various pathological conditions, including cancer, heart and liver diseases, and neurodegenerative pathologies such as Parkinson's disease (Redmann *et al*, 2014). Mitophagy regulatory mechanisms in mammals are complex and can be classified as Ub-dependent or Ub-independent pathways, which are strongly interconnected to each other. The most characterized Ub-dependent pathway is the Phosphatase and tensin homolog (PTEN)-induced kinase 1 (PINK1)–Parkin (PRKN/PARK2) pathway. PINK1 is a Ser/Thr kinase, whereas PRKN is an E3 Ub ligase. The depolarization of the mitochondrial membrane is a major activator of the PINK1/PRKN pathway. Such activation involves a strong interplay of PINK1-mediated phosphorylation of several substrates and Parkin-mediated ubiquitination events on the outer mitochondrial membrane (Koyano *et al*, 2014). As a result of these interactions, the autophagic machinery is recruited and poly-

ubiquitinated mitochondria are recognized by SARs for autophagosomal sequestration. SARs involved in polyubiquitin chains recognition are p62 and Optineurin (OPTN). Mutations involving Parkin and PINK1 genes are strongly associated with an early-onset form of Parkinson's disease (Harper *et al*, 2018; Sekine & Youle, 2018). In addition to the PINK1–PRKN pathway, the outer mitochondrial membrane (OMM) proteins Bcl2 and adenovirus E1B 19-kDa-interacting protein 3 (BNIP3), BNIP3-like (BNIP3L, also known as NIX), and FUN14 domain-containing protein 1 (FUNDC1) have also been described to directly interact with LC3 to drive mitophagy (Guo *et al*, 2001; Shao *et al*, 2020). BNIP3 also exerts death-inducing activity as it can interact with Bcl2 and is required to abolish the antiapoptotic effect of Bcl-X_L (Ray *et al*, 2000). Mitophagy occurs physiologically, ensuring mitochondrial recycling, but it plays a fundamental role in stress conditions, particularly upon starvation or hypoxia (Palikaras *et al*, 2018).

1.3 Autophagy in ischemic stroke

1.3.1 The role of autophagy in ischemic stroke

After an ischemic event, autophagy has been observed in neurons, astrocytes, and endothelial cells in different *in vitro* and *in vivo* models (Adhami *et al*, 2006; Qin *et al*, 2010; Grishchuk *et al*, 2011; Shi *et al*, 2012; Li *et al*, 2013). However, it remains ambiguous whether such activation plays a protective or detrimental role. Indeed, it is common to define autophagy as a *double-edged sword* during brain ischemia development, exerting both protective and detrimental effects.

Autophagic markers such as LC3 and Beclin-1 strongly increase in animal models of stroke. This increase often co-occurs with the expression of the active form of caspase-3 (Rami *et al*, 2008). Moreover, a dramatic increase in autophagosomes has been associated with hippocampal neurons death in neonatal ischemic brains (Koike *et al*, 2008). Altogether these works not only confirm that ischemic injury is followed by autophagy activation but also suggest that autophagy enhancement may represent a death-promoting process. Indeed, there is evidence that autophagy inhibition significantly decreases ischemic volume, brain edema, and motor deficits in the permanent Middle Cerebral Artery Occlusion (pMCAO) model (Wen *et al*, 2008).

On the other hand, some studies described autophagy as a neuroprotective process, helping with the degradation of protein aggregates associated with degeneration (Berezniuk & Fricker, 2010; Balin *et al*, 2011; Medeiros *et al*, 2011). It has been observed that autophagy prevents neuronal death both in *in vitro* and *in*

vivo models of stroke, with Beclin-1 playing an important role in apoptosis control (Carloni *et al*, 2008; Papadakis *et al*, 2013; Wu *et al*, 2017).

The strong crosstalk between autophagy and apoptosis may be a reason for the involvement of autophagy in many pathological conditions. Autophagy may contribute to tissue damage through autophagic cell death or turning cell injury into apoptosis or necrosis. Moreover, lysosomal hydrolases (cathepsins) are also involved in the apoptotic process through caspase activation (Vancompernolle *et al*, 1998; Wen *et al*, 2008; Deng *et al*, 2016).

Interestingly, autophagy plays a differential role during the ischemia and reperfusion phases. Although autophagy is activated in both ischemia and reperfusion, reperfusion is characterized by a different role of autophagy with respect to the early ischemic events. In a myocardial model of I/R, enhancement of autophagy at the same time as reperfusion significantly reduced infarct size and cell death (Xie *et al*, 2021). However, whether autophagy activation during the reperfusion phase may be protective or detrimental is still controversial (Matsui *et al*, 2007; Zhang *et al*, 2013). It must be considered that research works evaluating ischemia and reperfusion as two distinct phases in which autophagy may exert different effects are still limited.

In addition, studies on the role of autophagy in the ischemic context mainly focused on macroautophagy. There is evidence for the activation of CMA after ischemia and hypoxia. Dohi *et* al. investigated ischemia-dependent CMA modulation both *in vitro* and *in* vivo. LAMP2A, a key mediator of CMA, is upregulated in neuronal cells exposed to hypoxic stress. Inhibiting LAMP2A expression enhanced apoptosis after hypoxia regardless of macroautophagy preservation. suggesting that CMA is involved in cell survival during hypoxia and ischemia. In the pMCAO model, LAMP2A positive lysosomes significantly augmented after ischemia (Dohi *et al*, 2012). CMA is also upregulated in the traumatic brain injury animal model (Park *et al*, 2015). However, the exact role of CMA in promoting cell survival or damage is far to be elucidated.

1.3.2 Macroautophagy regulation in ischemic stroke

The major signaling pathways involved in autophagy regulation are also essential to respond to ischemic injury. The AMPK/mTORC1 signaling pathway is strongly activated after ischemia and may provide potential neuroprotective targets for stroke treatment (Balduini *et al*, 2012; Huang *et al*, 2018).

The AMPK signaling pathway is a critical regulator of autophagy after an ischemic event. The increase in [Ca^{2+}] is a major factor promoting AMPK-mediated autophagy, as well as the ATP/AMP ratio decrease due to inadequate energy supply (Meijer & Codogno, 2011; Bootman *et al*, 2018; Sun *et al*, 2018). AMPK is thus activated, inhibiting mTORC1 kinase activity through the TSC1/2 complex, and promoting autophagy (Herzig & Shaw, 2018). mTORC1 inhibition is also promoted by the restricted amino acid and insulin availability after stroke (Menon *et al*, 2014; Tan *et al*, 2017; Hwang *et al*, 2017). Additionally, the reduction of PI3K/Ak strain transforming protein (Akt) pathway activity was also found to consequently decrease mTORC1 activity and promote autophagy (Dutta *et al*, 2015; Mateos *et al*, 2016).

An important factor activated in response to oxygen deprivation is HIF-1. It consists of two main subunits: the oxygen-regulated subunit HIF-1α, and HIF-1β, which is constitutively expressed (Daskalaki *et al*, 2018). When oxygen is abundant HIF-1α is rapidly degraded by the proteasome, while low oxygen levels allow HIF-1α stabilization. Once stabilized, HIF-1α translocates to the nucleus, where it associates with HIF-1β to form the HIF-1 heterodimer (Eales *et al*, 2016). HIF-1α protein levels are reported to increase after ischemia (Althaus *et al*, 2006). Hypoxia response genes include Vascular Endothelial Growth Factor (VEFG) and Erythropoietin (EPO), whose role is to support oxygen distribution to the hypoxic region (Semenza, 2003; Kim *et al*, 2009). Additionally, HIF-1α can also drive autophagy activation by p53 and BNIP3 upregulation (Guo *et al*, 2001). The HIF-1α-mediated upregulation of BNIP3 leads to mitophagy induction, in the attempt to reduce ROS formation, limit oxygen demand, and remove damaged mitochondria. Moreover, upon hypoxic stress or the loss of mitochondrial membrane potential, FUNDC1 is dephosphorylated increasing its affinity for LC3 to drive receptor-mediated mitophagy (Chen *et al*, 2014).

1.3.3 Potential role of autophagy in neuroprotection

Diverse experimental and clinical investigations pointed out that dysfunctional autophagy is involved in several pathological conditions, including cancer and neurodegeneration (Levine & Kroemer, 2008; Mathew *et al*, 2007; Mizushima & Komatsu, 2011; Nixon, 2013). Current research on neuroprotective therapeutics has identified several candidates whose effects were also due to autophagy modulation.

To date, some neuroprotective agents have been reported to modulate autophagy. Among them, statins, which inhibit the 3-hydroxy-3-methylglutaryl co-enzyme A reductase (HMGCR) involved in cholesterol metabolism, influenced autophagy in stroke models. Both Amlodipine and Atorvastatin treatments led to a significant

reduction in LC3-positive cells and a decrease in the infarct volume (Zhang *et al*, 2011). Simvastatin exerted neuroprotective effects after spinal cord injury, partially through the Akt/mTORC1 signaling pathway (Gao *et al*, 2015). Yu *et al.* demonstrated that Ezetimibe, a selective cholesterol absorption inhibitor, prevents neuronal death by promoting AMPK-mediated autophagy activation in the MCAO rat model. The authors reported an increase in a wide range of autophagic markers in treated MCAO neurons, while autophagy inhibition reversed the beneficial effects provided by ezetimibe (Yu *et al*, 2018).

Traditional Chinese drugs have been proven to exert beneficial effects through autophagy regulation. For instance, Puerarin alleviated brain injury after I/R damage by selectively reducing autophagic proteins expression levels in neurons but not in astrocytes (Hongyun *et al*, 2017). Ginsenoside Rb1 reversed mitochondrial dysfunction and up-regulated autophagic markers *in vitro* (Tang *et al*, 2017). Similarly, Triptolide administration decreased apoptosis and enhance autophagy after MCAO (Yang *et al*, 2015).

Another study highlighted Rapamycin neuroprotective potential in both permanent middle cerebral artery ligation (pMCAL) and embolic clot middle cerebral artery occlusion (eMCAO). Results indicated that Rapamycin reduced injury lesions and improved neurological outcomes following ischemia through autophagy and mitophagy induction (Buckley *et al*, 2014; Li *et al*, 2014).

Recently, microRNAs (miRNAs) were also proposed as potential therapeutic targets for stroke. Alteration in miRNA expression in the brain has been associated with ischemic brain injury (Kim *et al*, 2021). Studies evaluating the effect of miRNA-30a upregulation after stroke in the MCAO model revealed that it decreases Beclin-1 levels, thus impairing autophagy. Downregulation of miRNA-30a can promote neuroprotection through the enhancement of Beclin-1-mediated autophagy (Wang *et al*, 2014). Moreover, Wei *et al.* observed that miR-338-3p downregulation in neurons following an ischemic stress targets the Akt/mTORC1 signaling. This leads to autophagy inhibition and contributes to cell survival (Wei *et al*, 2022).

2. AIM OF THE WORK

Brain ischemia is a leading cause of death worldwide in people over 65. To date, therapeutic options are limited to recanalization strategies, which are featured by several limitations in terms of therapeutic window and patient eligibility. It is then imperative to identify alternative effective and long-lasting pharmacological interventions to preserve tissue integrity and functionality.

Small therapeutic molecules able to interfere with the complex series of molecular events that follow brain ischemia represent an exciting area of investigation. Given its homeostatic function both in a physiological and a pathological context, autophagy has been proposed as a promising potential target to foster neuroprotection.

With the present thesis work, I sought to identify potent modulators selectively interfering with the autophagic pathway in stressed conditions. To address this assignment, I worked on three major tasks:

- Firstly, I established a robust Low-Throughput Screening platform to screen a selected bioactive compound library.
- Then I performed the chemical screening, testing drugs under stroke-mimicking conditions.
- I finally validated lead-like compounds by applying a series of stringent tests on different *in vitro* and *in vivo* models.

3. RESULTS

3.1 *In silico*-based virtual screening

The Drug Metabolism and Pharmacokinetics (DMPK) properties of a large compound library provided by Selleckchem were *in silico* predicted using molecular descriptors in comparison to well-characterized bioactive molecules. From the original Selleckchem dataset composed of 6839 compounds, 45 were discarded for the lack of structural information or other errors derived from the software's analysis. Among all the selection criteria provided by the prediction tool, we gave priority to those related to drug-likeness and CNS penetration and activity. We carried out drug-likeness evaluation computing the *QPlogPo/w*, *#stars*, *RuleOfFive*, *RuleOfThree*, *#metab*, and *#rtvFG* parameters (**Figure 5**), while *CNS*, *QPlogBB*, and *QPPMDCK* were selected as CNS-related descriptors (**Figure 6**). Details and ranges used to evaluate the descriptors and properties used for the present study are reported in the Materials and Methods section (**Table 4**).

After the first round of analysis, we identified a subset of 1927 compounds (representing 28.36% of the original dataset) with computed properties falling inside the acceptable range of known drugs. The remaining molecules (71.64%) had at least one computed descriptor falling outside the normal range of known drugs and therefore were excluded from further analyses.

We next prioritized the 1927 candidates performing a second round of *in silico* evaluation. We performed a molecule ranking based on characteristics that should be desirable in screening analyses designed for the identification of CNS-active drugs. We assigned a score to the *CNS*, *QPlogBB*, and *QPPMDCK* values obtained from the first analysis. Each score was then linearly and identically weighted to obtain a final cumulative score for every compound (**Figure 6d**). Using this parameter, we ranked all the compounds, defining a cherry-pick library comprehensive of the first 898 top-scoring ones. Selected compounds obtained a cumulative score greater than 0.367, allowing the exclusion of molecules belonging to the lowest percentile range.

The library was used for the *in vitro* Low-Throughput Screening (LTS) and was heterogeneous in terms of composition. As shown in **Figure 6e**, molecules fall within nineteen different categories. Among them, the most represented ones include *Neuronal Signaling* (17.71%), *Microbiology* (11.58%), and *Metabolism* (5.01%). Additional subsets (accounting for 35.19% of the whole library) include anti-inflammatory compounds, protein kinase modulators, epigenetic regulators, and inhibitors of various receptors and transporters. The 30.51% of the compounds are

categorized as *Others* and comprises intermediates in the production of other chemicals and organic compounds. Of note, more than 350 molecules included in this library are FDA-approved.

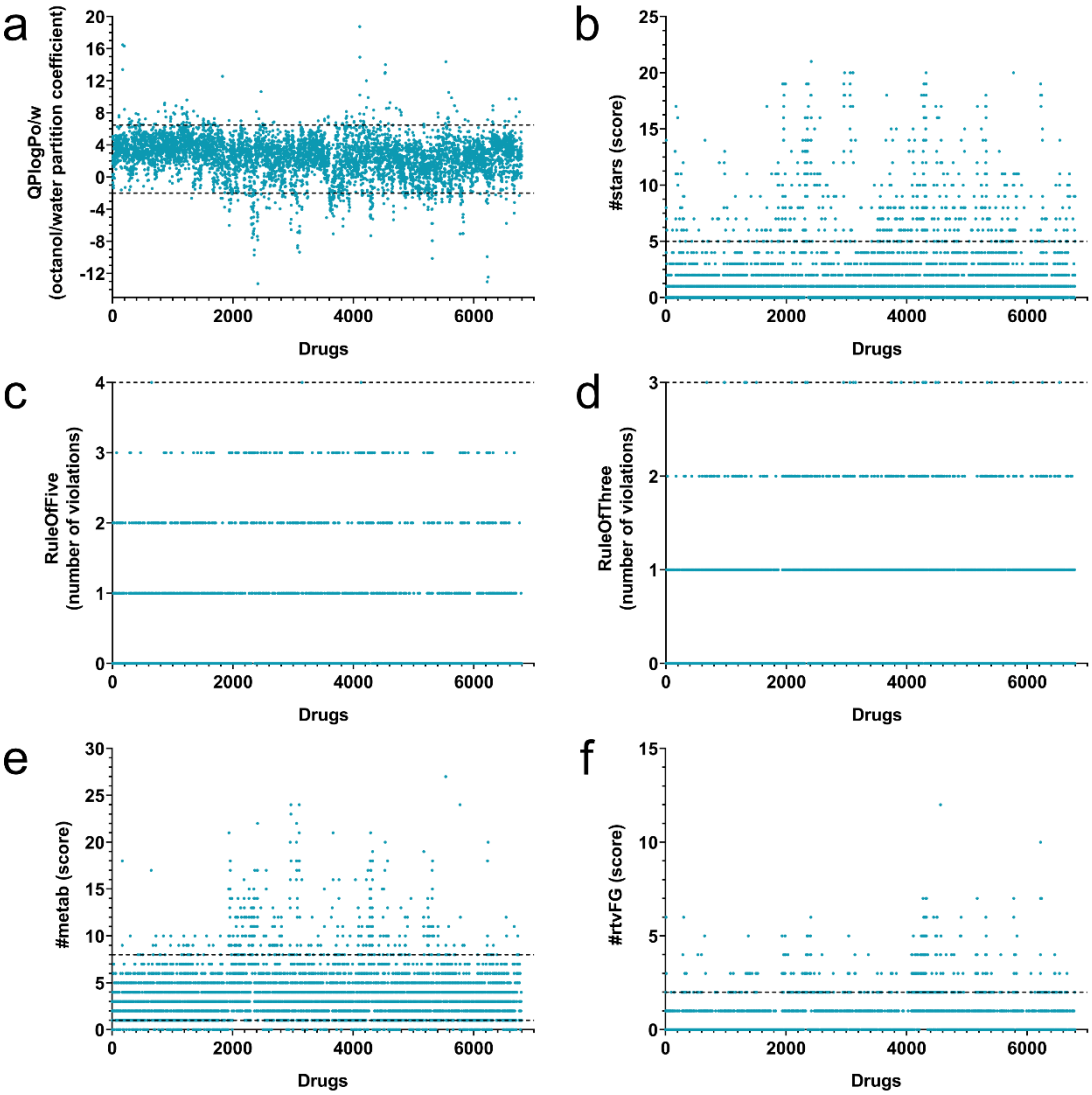

Figure 5 – Graphical representation of drug-like properties for 6794 molecules' dataset. *Graphs reports dispersion of compounds regarding (a) QPlogPo/w, (b) #stars, (c) RuleOfFive, (d) RuleOfThree, (e) #metab, and (f) #rtvFG prediction. Each dot represents a single molecule. Ranges for 95% of known drugs are highlighted by dashed lines.*

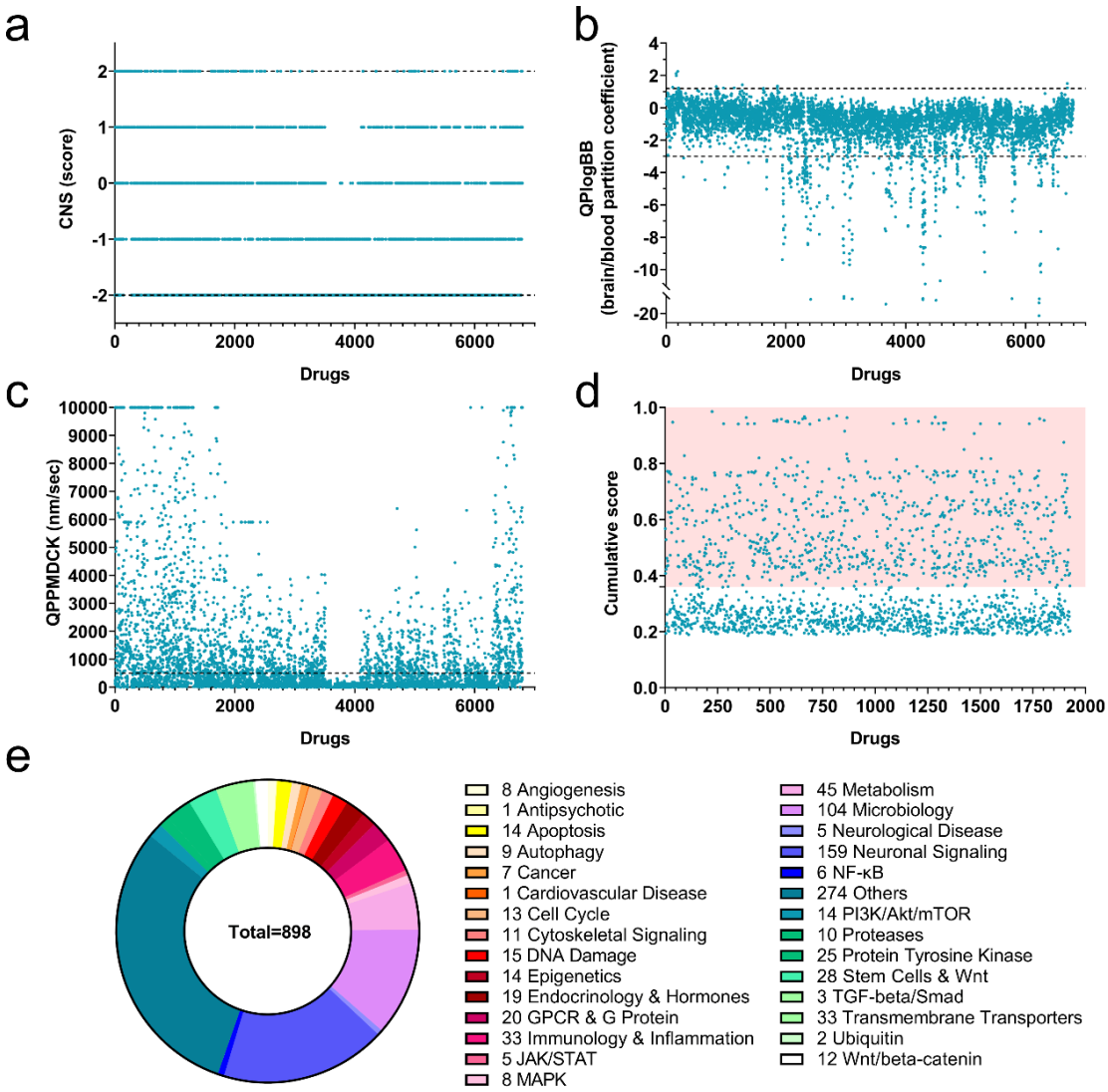

Figure 6 – Graphical representation of CNS-related properties for 6794 molecules' dataset and library definition. *Graphs report dispersion of compounds regarding (a) CNS, (b) QPlogBB, and (c) QPPMDCK prediction. (d) 1927 positive compounds were further ranked based on their CNS activity and penetration properties (cumulative score). The pink box highlights 898 selected compounds. Each dot represents a single molecule. Ranges for 95% of known drugs are highlighted by dashed lines. (e) Graphical representation of library composition based on known major molecular targets.*

3.2 LTS assay development

We next set up screening procedures to test the ability of the compounds to modulate the autophagic process. I monitored LC3 fluctuations using a cell line stably expressing the pHluorin-mKate2-human LC3 (PK-hLC3). This construct takes advantage of the pH-sensitivity of pHluorin, a GFP-variant whose fluorescence is almost completely abolished when the protein is delivered into the acidic lysosomal

compartment (pH 4.5-5.5). Together with pHluorin, the chimeric construct also carries the far-red protein mKate2, which is not pH-sensitive (Tanida *et al*, 2014).

I transfected Neuro-2a cells to establish cell clones constitutively expressing the autophagy sensor. Individual clones were selected applying puromycin selection and isolated following a limiting dilution protocol. Clones were analyzed by fluorescent microscopy, and I ended up selecting the 7B11 cell clone for further validation. I investigated the autophagy-sensing properties of the 7B11 clone using well-known autophagy modulators (**Figure 7**). Specifically, I treated 7B11 cells with Bafilomycin A1 or Torin-1, which inhibit vacuolar H^+-ATPase (V-ATPase) and mTORC1/2, respectively (Thoreen *et al*, 2009; Wang *et al*, 2021b). Dimethyl sulfoxide (DMSO)-treated samples were also included as an experimental control. Cells were fixed and analyzed by confocal microscopy for pHluorin and mKate2. Upon Bafilomycin A1 treatment (200 nM, 6 hours), I observed a substantial increase of green and far-red, double-positive fluorescent puncta within the cytoplasm of these cells. This effect is due to the prevention of lysosomal acidification and the subsequent blockage of the fusion of autophagosomes with lysosomes. Conversely, upon Torin-1 treatment (250 nM, 24 hours), cells showed green-negative but far-red-positive puncta, indicating an enhancement of the autophagic flux (**Figure 7a**).

I next performed western blot (WB) analysis on naïve Neuro-2a and 7B11 cells receiving the same treatments (**Figure 7b**). I assessed the conversion of LC3-I (detectable by SDS-PAGE at approximately 16 kDa) to LC3-II (14 kDa) by measuring the LC3-II levels normalized to β-Actin in each experimental group. In untransfected Neuro-2a cells, Bafilomycin A1 treatment induced a significant LC3-II accumulation compared to DMSO-treated controls, reflecting autophagic flux occurrence at basal conditions. Moreover, I observed an increase in the LC3-II protein levels when treating cells with Torin-1, which was further augmented when Torin-1 and Bafilomycin A1 treatment were combined. On the other hand, in 7B11 cells, I observed faint endogenous LC3 bands, as well as a single band at ~65 kDa, which corresponds to the PK-hLC3 protein (**Figure 7b** and **c**). In 7B11 cells, Bafilomycin A1 treatment resulted in a slight but significant increase in LC3-II protein levels in comparison to DMSO-treated controls, while I observed no more than a trend treating cells with Torin-1. The treatment combining Torin-1 and Bafilomycin A1 increased LC3-II levels, although it did not significantly differ from Bafilomycin A1 alone. These observations suggest that the overexpression of PK-hLC3 may affect the endogenous LC3 turnover in 7B11 cells. Therefore, this tool might not be optimal for the accurate quantification of LC3-II variations by western blot.

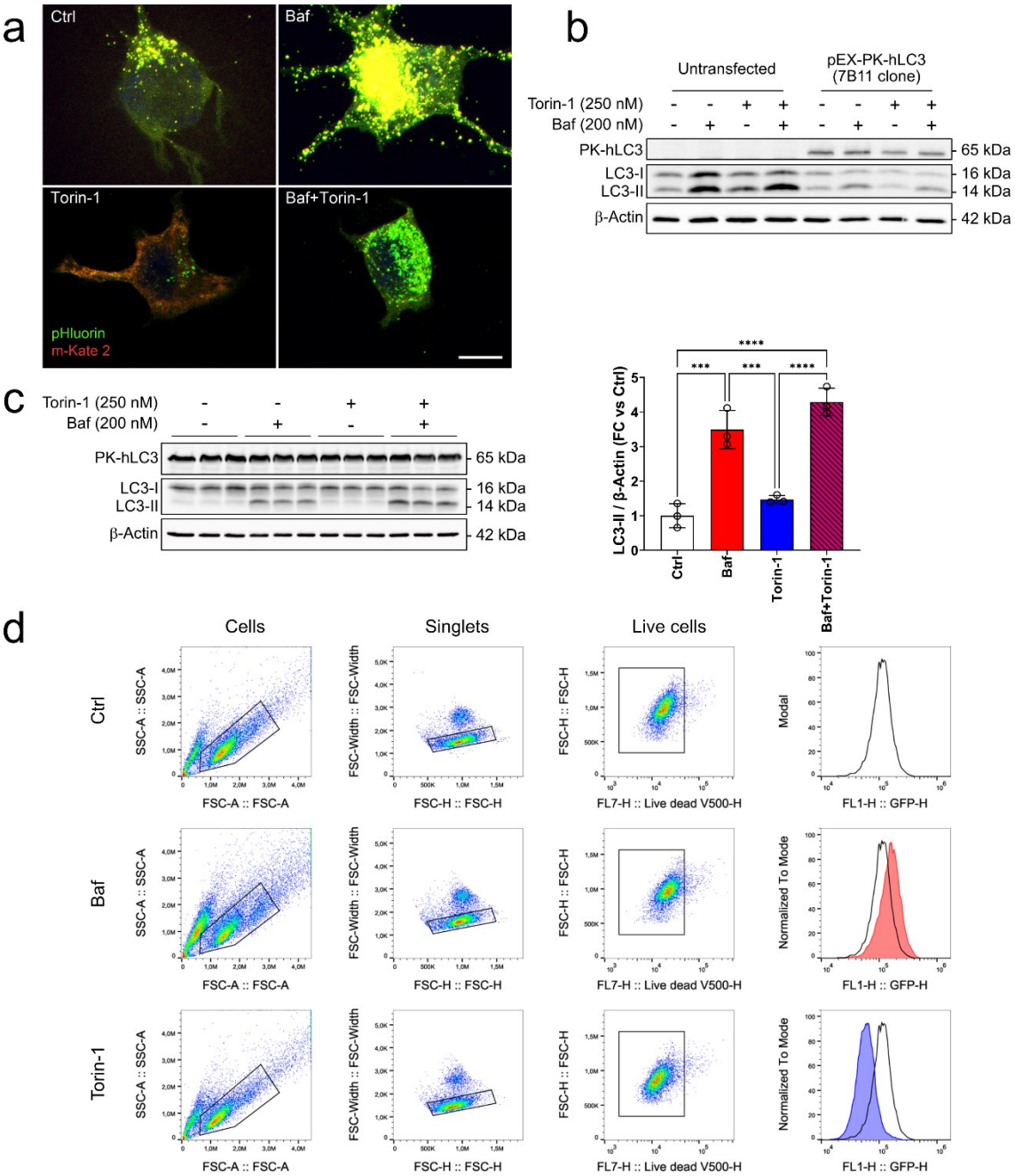

Figure 7 – 7B11 clone as an in vitro cellular model for drug screening. *(a) Maximal projections of confocal stacks of the 7B11 cell clone showing LC3 distribution (n=3 independent samples/condition); green (pHluorin) and far-red (mKate2) fluorescence were monitored in the same field and merged; scale bar 10 µm. (b) Representative WB analysis for LC3 and β-Actin protein levels in protein extracts from untransfected and transfected Neuro-2a cells upon different treatments. (c) Representative WB analysis for LC3 and β-Actin protein levels in protein extracts from 7B11 cell clone; samples were subjected to immunoblotting against LC3B to detect LC3-I/II, and PK-LC3; the histogram shows quantifications (mean ratio ± SD; n=3 independent wells/condition) (d) Representative flow cytometry panels; histograms show pHluorin fluorescence intensity (x-axis) versus events' count normalized to mode (y-axis) (n=3 independent samples/condition). The following treatment conditions were used in all the experiments: DMSO control (Ctrl), Bafilomycin A1 (Baf) 200 nM for 6 hours, and Torin-1 250 nM for 24 hours. One-way ANOVA followed by Tukey's multiple comparison test was used to analyze data from (c); *p<0.05, **p<0.01, ***p<0.001, ****p<0.0001.*

We next planned to use flow cytometry to maximize the time-effectiveness of the chemical screening. Therefore, to finalize the assay set-up, I quantified PK-hLC3 fluctuations by Fluorescence-Activated Cell Sorter (FACS) (Shvets *et al*, 2008). Specifically, I measured pHluorin mean fluorescence intensity (MFI) variation in living 7B11 cells. To provide evidence of the reliability of this approach, I treated cells with Bafilomycin A1 and Torin-1. Upon Bafilomycin A1 treatment, I observed a ~40% MFI increase compared to control, reflecting the PK-hLC3-positive dots accumulation observed by confocal microscopy. On the other hand, Torin-1 led to a ~50% MFI reduction, mirroring the result obtained in previous experiments (**Figure 7d**).

Considering the large signal window offered by the latest described approach, I selected LC3-pHluorin detection by flow cytometry as the best assay read-out. I next performed several confirmatory experiments to validate the accuracy and precision of the assay.

3.2.1 Assay reproducibility assessment

To verify the assay's performances in a throughput setting, I tested the assay's stability and reproducibility. 7B11 cells were treated with Bafilomycin A1 and Torin-1 across different independent experimental replicates. I assessed LC3-pHluorin MFI fluctuation by flow cytometry (**Figure 8**). Bafilomycin A1 treatment resulted in a significantly stable separation band between reference and positive controls. On the other hand, the Torin-1 treatment yielded less stability (**Figure 8a**). After three weeks in culture (experimental replicates 5 and 6), LC3-pHluorin MFI was not consistent with previous measurements. Therefore, I defined a signal stability threshold based on statistical quality control measures, even though data showed overall statistically significant differences (**Figure 8b**).

Using these datasets, I calculated Z'-factor values and the Strictly Standardized Mean Difference (SSMD), two statistical parameters largely applied to validate procedures involving molecular screenings (Zhang *et al*, 1999; Goktug *et al*, 2013). Both measures account for data variability in reference and positive controls. Ranges reflecting general assay performances are reported in the Materials and Methods section (**Table 6**). To get a *very good/excellent* assay, Z'-factor (Z') and SSMD (β) values should meet the following criteria: $0.5 \leq Z' < 1$, and $\beta \geq 4.7$, $\beta \leq -4.7$. In line with MFI analysis, Z' and SSMD values complied with the requirements until the fourth experimental replicate (**Figure 8c**).

Analyzing the generated dataset and comparing Z'-factor and SSMD with reference values, I confirmed the reproducibility of the assay, estimating that 7B11 cells can be used for no more than 14 days.

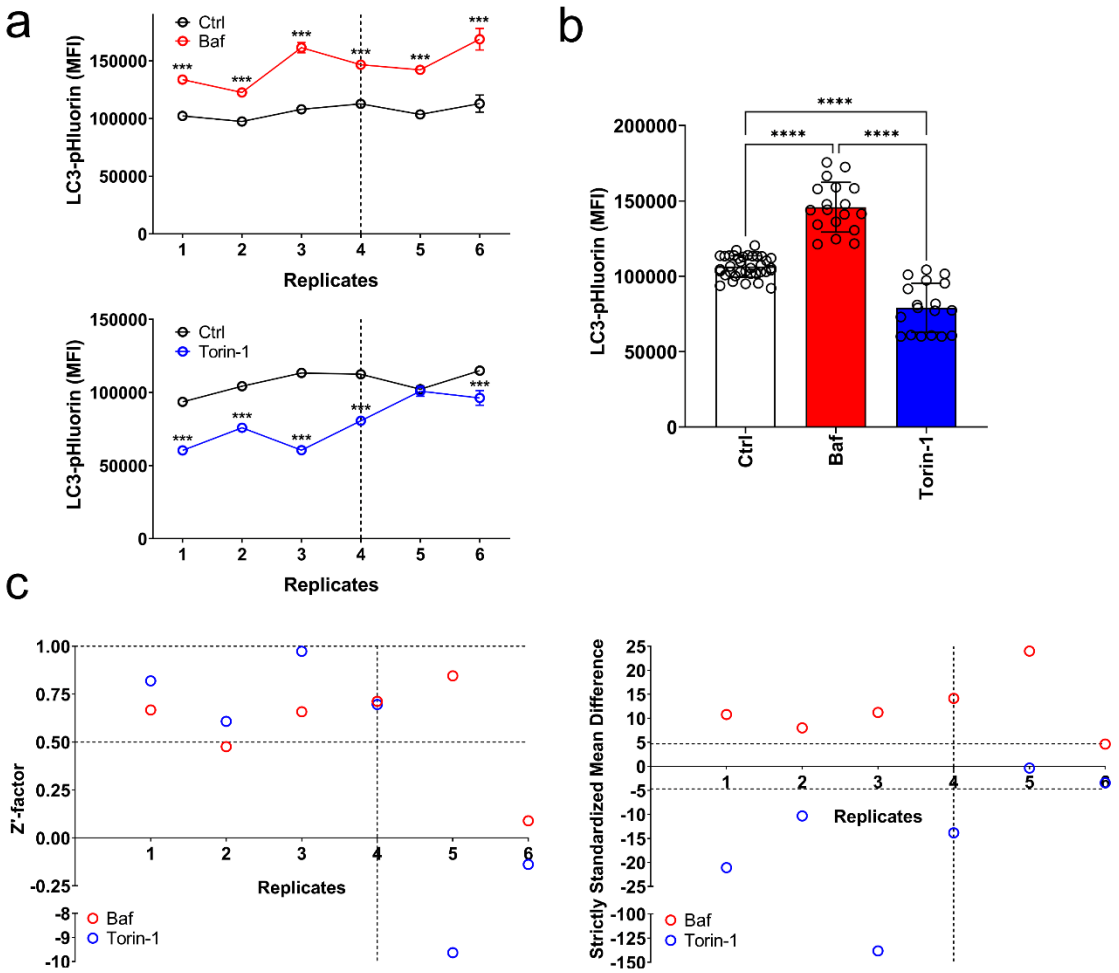

Figure 8 – Assay quality assessment. *(a) Graphs report pHluorin fluorescence intensity (MFI) of 7B11 cells treated with DMSO (Ctrl), Bafilomycin A1 (Baf; 200 nM for 6 hours), or Torin-1 (250 nM for 24 hours), measured by flow cytometry in 6 consecutive experiments (n=3 independent wells/condition); data are reported as mean ± SD. (b) Comprehensive pHluorin fluorescence intensity representation from (a). (c) Z'-factor and SSMD of each experimental replicate reporting the separation band between controls and Baf- or Torin-1-treated samples. Horizontal dashed lines highlight ranges for a very good/excellent assay. Vertical dashed lines indicate the limit for consecutive in vitro cell passages. Two-way ANOVA followed by Šídák's multiple comparisons test was used to analyze data from (a); one-way ANOVA followed by Tukey's multiple comparison test was used to analyze data from (b); *p<0.05, **p<0.01, ***p<0.001, ****p<0.0001.*

3.2.2 Stressor selection

To identify autophagy modulators active in a neuroprotective context, I introduced in the experimental setting a specific stressor that should mimic most of the harmful events occurring in ischemic conditions. Oxygen-Glucose Deprivation (OGD) is a widely used *in vitro* stroke model, reproducing the main stroke features such as cytotoxicity, apoptosis, and autophagy induction (Tasca *et al*, 2015; Zhang *et al*, 2019).

I performed a series of experiments on 7B11 cells, measuring LC3-pHluorin MFI variations in response to OGD treatment (**Figure 9a**). I obtained a linear correlation that linked OGD-exposure with MFI fluctuations. As OGD promotes autophagy activation, these results resembled those obtained upon Torin-1 treatment. I measured a progressive MFI decrease, reaching a 25% reduction after 15 hours of incubation in the OGD environment. To further validate the system, I monitored HIF-1α protein levels by western blot. HIF-1α is a key player in the regulation of oxygen homeostasis, and it is responsible for the transcription of numerous genes, including those related to autophagy modulation (Zhang *et al*, 2008). As expected, after 15 hours of OGD exposure, I observed a strong increase in HIF-1α protein levels with respect to normoxic experimental controls (**Figure 9b**).

In conclusion, with an extensive series of pilot experiments, I developed a robust assay to study the autophagic pathway in living cells. I also introduced a stressor to mimic ischemic conditions *in vitro*. The OGD model is largely used by the scientific community working on ischemic stroke. The OGD exposure time defined with these experiments significantly reduced LC3-pHluorin MFI. However, such reduction is approximately 50% of that induced by Torin-1 treatment. Therefore, the simple OGD treatment is not enough to saturate the system, allowing molecules to further accelerate the autophagic flux.

I also adapted the assay to a semi-automated format (96-well multiple-well plate), dealing with ~70 samples at once and making the acquisition at the cytometer more efficient. Moreover, these preliminary experiments allowed the calculation of the sample size. Specifically, to detect a minimum 10% difference between the experimental and control means, I needed to study three experimental subjects and three control subjects to be able to reject the null hypothesis that the population means of the experimental and control groups are equal with the probability (power) of 0.9. The Type I error probability associated with the test of this null hypothesis is equal to 0.05.

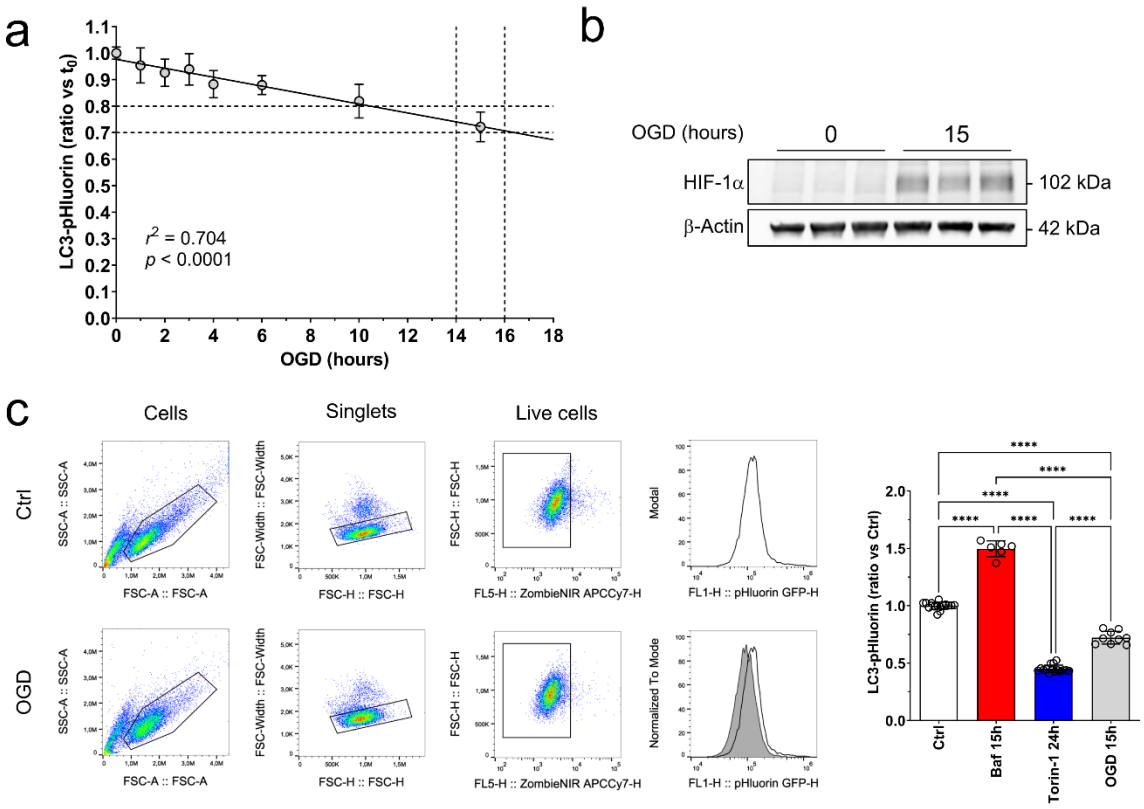

Figure 9 – Oxygen-glucose deprivation as a stressor to mimic ischemic conditions. *(a) Linear correlation between OGD duration (hours) and pHluorin fluorescence intensities normalized to t_0 (n=9 independent wells/condition); data are reported as mean ± SD (r^2=0.704, p<0.0001); dashed lines define the time window for a 25% fluorescence decrease. (b) Representative WB analysis for HIF-1α and β-Actin protein levels in protein extracts from 7B11 cells subjected to 15 hours of OGD (n=3 independent wells/condition). (c) Representative flow cytometry panels; histograms show pHluorin fluorescence intensity (x-axis) versus events' count normalized to mode (y-axis); bar chart shows comprehensive quantification of pHluorin fluorescence intensity normalized to DMSO-treated control (Ctrl); treatments include Bafilomycin A1 (Baf) 200 nM for 15 hours, Torin-1 250 nM for 24 hours, and OGD for 15 hours (n≥6 independent samples/condition). One-way ANOVA followed by Tukey's multiple comparison test was used to analyze data from (b); *p<0.05, **p<0.01, ***p<0.001, ****p<0.0001.*

3.3 LTS revealed modulators of autophagy

To identify novel autophagy modulators, I carried out the primary screening testing the cherry-pick library (898 compounds) in OGD conditions at the single concentration of 1 μM. The basic idea of this assay was to drive the identification of molecules able to prevent the OGD-mediated autophagy induction, but also molecules able to further promote the autophagic flux compared to the OGD stress alone. I selected 1 μM to avoid off-target effects due to higher molecules' concentrations. Each assay was run in triplicate. I received the library in a 384-wells

format, and I aliquoted each plate in a 96-wells format to minimize the impact of freeze-thaw cycles. In each experimental setting, I included Bafilomycin A1- or Torin-1- treated normoxic/high-glucose controls (alternatively used to monitor cells responsiveness to control treatments), vehicle (water or DMSO)-treated normoxic/high-glucose controls, and vehicle-treated OGD controls. I used a viability dye to monitor viability reduction. Controls and samples were not randomized across the plate. For this reason, plates that showed a clear gradient in the fluorescence intensity throughout the acquisition (probably due to non-homogeneous temperature, CO_2, or humidity levels upon acquisition) were discarded, and compounds were subsequently tested in a new experimental setting.

At the end of the primary screening, I checked for the plate-failure rate. I applied a statistical quality-control measure, the Signal-to-Noise ratio (S/N), to compare the level of the OGD signal to the level of untreated samples, considered as background noise. I discarded and repeated all the plates displaying an S/N value lower than 2. Cumulatively, I performed 54 successful experimental runs, and the final S/N distribution for each plate is reported in **Figure 10a**. To further check for screening quality, I analyzed all the experimental controls across all the plates (**Figure 10b**). Controls showed a robust separation, as reported by previously described experiments.

To select candidate molecules, I matched control-based and non-control-based statistical approaches. With the control-based method, I used the unpaired Student's *t*-test to compare the compound's means to OGD-treated controls. With the non-control-based method, I calculated robust Z-score to account for sample activity *per se*. Here the mean and standard deviation are replaced with the median and the Median Absolute Deviation (MAD), respectively, to diminish the outliers' effect on the final analysis. Moreover, this second approach is based on the assumption that most of the samples are inactive, serving as plate's negative controls and allowing true hits identification (Goktug *et al*, 2013). I selected as positive hits all the compounds with a p-value <0.05 and a robust Z-score <-1.96 (autophagy inducers) or >1.96 (autophagy inhibitors) (**Figure 10c**). In summary, crossing these two parameters, 27 out of 898 tested molecules were selected as lead-like candidates to be validated with a secondary screening. Specifically, I identified 16 molecules able to increase LC3-pHluorin MFI and 11 molecules that further reduced fluorescent signals in comparison to OGD controls (**Table 3**). Twelve compounds were excluded from analysis due to their high toxicity in 7B11 cells.

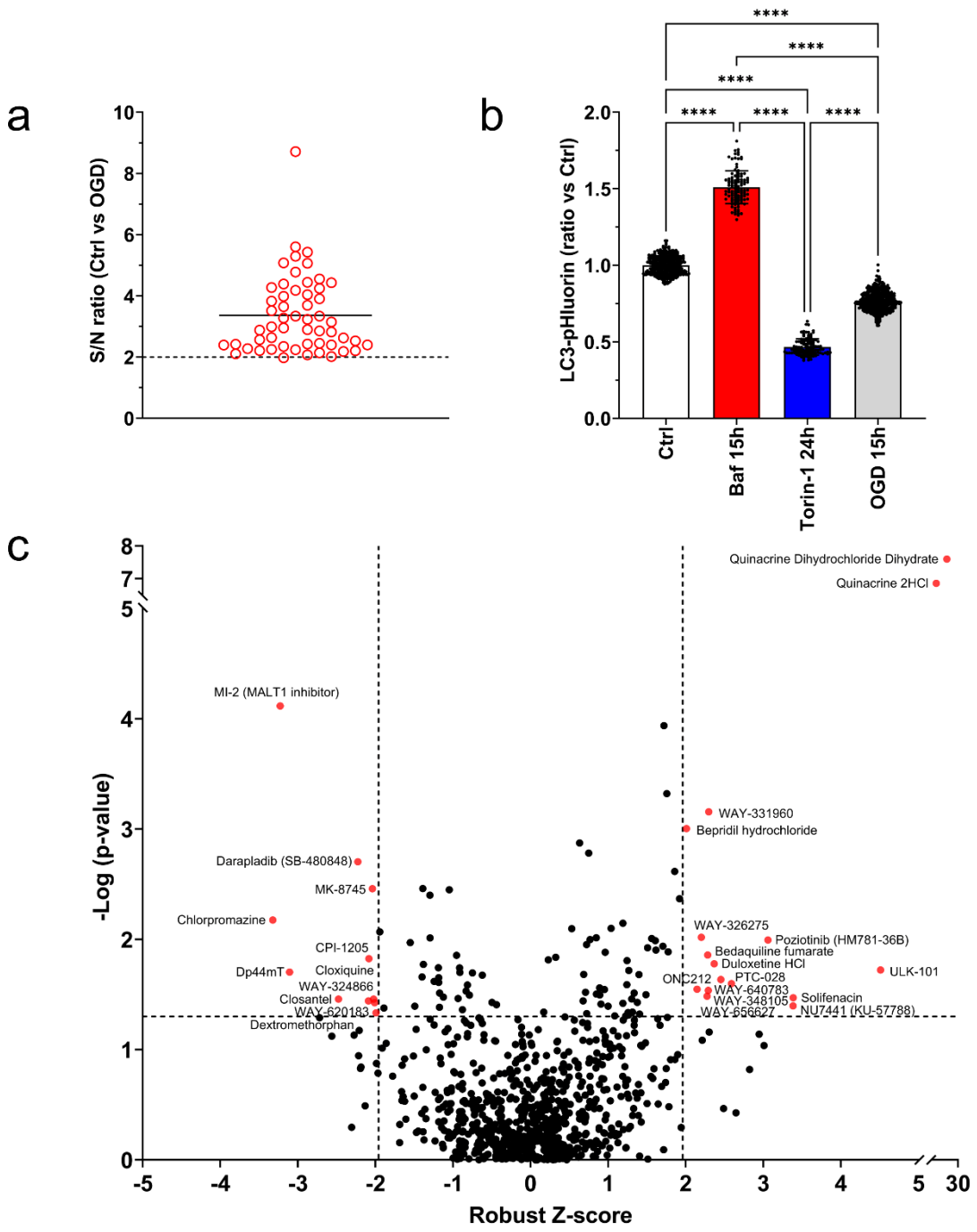

Figure 10 – Primary screening results. *(a) S/N values were calculated for each plate from the primary screening. (b) Comprehensive quantification of pHluorin fluorescence intensity normalized to DMSO-treated control (Ctrl); treatments include: Bafilomycin A1 (Baf) 200 nM for 15 hours, Torin-1 250 nM for 24 hours, and OGD for 15 hours (n≥111 independent samples/condition). (c) Volcano plot displaying -Log(p-value) and Robust Z-score across the whole compound library; 27 lead-like candidates are highlighted in red and labeled; dashed lines indicate selected statistical ranges. One-way ANOVA followed by Tukey's multiple comparison test was used to analyze data from (b); *p<0.05, **p<0.01, ***p<0.001, ****p<0.0001.*

Table 3 – List of lead-like candidates from the primary screening.

Compound name	*S/N plate*	*MFI (x1000)*	*Ratio vs OGD*	*p-value*	*Log p*	*Robust Z-score*
Quinacrine Dihydrochloride Dihydrate	4.443	175.25	1.833	$<10^{7}$	7.60	21.45
Quinacrine 2HCl	3.273	195.23	1.748	$<10^{7}$	6.86	13.20
ULK-101	3.988	107.28	1.111	0.0190	1.72	4.51
Solifenacin	3.518	111.36	1.075	0.0338	1.47	3.39
NU7441 (KU-57788)	4.181	116.21	1.311	0.0401	1.40	3.38
Poziotinib (HM781-36B)	5.293	113.36	1.222	0.0101	1.99	3.06
PTC-028	2.211	100.58	1.121	0.0252	1.60	2.59
ONC212	2.211	99.81	1.113	0.0231	1.64	2.45
Duloxetine HCl	5.079	115.14	1.130	0.0166	1.78	2.37
WAY-331960	2.449	107.67	1.156	0.0007	3.16	2.30
WAY-656627	2.184	99.54	1.142	0.0291	1.54	2.29
Bedaquiline fumarate	3.906	115.80	1.108	0.0139	1.86	2.28
WAY-348105	2.276	108.03	1.089	0.0327	1.49	2.28
WAY-326275	3.696	85.87	1.114	0.0096	2.02	2.20
WAY-640783	2.184	98.70	1.132	0.0283	1.55	2.15
Bepridil hydrochloride	7.475	106.29	1.120	0.0010	3.00	2.01
WAY-620183	3.696	70.60	0.916	0.0464	1.33	-1.99
Dextromethorphan hydrobromide hydrate	4.276	96.95	0.912	0.0375	1.43	-2.01
Cloxiquine	4.276	96.89	0.912	0.0348	1.46	-2.02
MK-8745	2.211	74.34	0.829	0.0035	2.46	-2.04
CPI-1205	2.251	85.25	0.867	0.0150	1.83	-2.08
WAY-324866	2.016	86.93	0.903	0.0361	1.44	-2.09
Darapladib (SB-480848)	7.475	85.19	0.897	0.0020	2.70	-2.23
Closantel	4.387	83.92	0.888	0.0348	1.46	-2.48
Dp44mT	4.245	81.41	0.889	0.0198	1.70	-3.11
MI-2 (MALT1 inhibitor)	4.779	87.59	0.815	0.0001	4.12	-3.23
Chlorpromazine	4.779	87.10	0.811	0.0067	2.18	-3.32

3.4 Validation of putative autophagy modulators

3.4.1 In vitro best hits validation in Neuro-2a cells

With the primary screening, I identified 27 lead-like candidates able to significantly modulate LC3-pHluorin MFI when compared to the OGD treatment alone. A subset of molecules that met the selection criteria was omitted from further analysis because they (1) exerted moderate toxicity (Solifenacin, Dextromethorphan hydrobromide hydrate, Cloxiquine, and CPI-1205), (2) were previously associated with both stroke and autophagy (Quinacrine Dihydrochloride Dihydrate and Quinacrine) (Phillis, 1996; Estevez & Phillis, 1997; Golden *et al*, 2015), (3) were not available in pure form in adequate amounts (WAY-620183 and WAY-324866).

We purchased fresh powder of 19 chemicals (6 inducers and 13 inhibitors) that were assayed in the validation experiments. I selected western blot analysis as the first line of validation. To avoid unintended misinterpretation of the results due to the PK-hLC3 overexpression, I used naïve Neuro-2a cells as a cellular model. I also decided to exclude the OGD treatment from the assay to assess the ability of selected compounds to interfere with the autophagic pathway in basal conditions.

I first set up the assay by performing experiments with control molecules (**Figure 11**). To limit cytotoxicity and to uniform the treatments' timeline, I optimized the final protocol selecting Bafilomycin A1 100 nM for 15 hours and Torin-1 250 nM for 15 hours as control treatments. These treatment conditions were appropriate to observe LC3-II levels variation in naïve Neuro-2a cells.

In the present assay, LC3-II turnover is measured upon the treatment with a selected compound, in both the presence and absence of saturating levels of Bafilomycin A1. As a result, when the compound enhances the autophagic flux, LC3-II levels are higher in the presence of the compound plus Bafilomycin A1, as occurs when Torin-1 and Bafilomycin A1 are combined (**Figure 11a**). This approach allows the identification of autophagy inducers by comparing a selected compound plus Bafilomycin A1 to the compound alone and Bafilomycin A1 alone. Moreover, it is possible to identify putative late-stage inhibitors by comparing a selected molecule to Bafilomycin A1 treatment alone (Mizushima & Yoshimori, 2007; Klionsky *et al*, 2021). I also tested a sequestration inhibitor, 3-Methyladenine (3-MA), to assess the effects of an early-stage inhibitor of autophagy (Seglen & Gordon, 1982). I observed that cells co-treated with 3-MA and Bafilomycin A1 displayed lower LC3-II levels compared to Bafilomycin A1 alone. With this experiment, I confirmed the possibility

to discriminate between early- and late-stage autophagic inhibitors by western blot analysis in Neuro-2a cells (**Figure 11b**).

I tested all the 19 compounds at the single concentration of 1 μM, in the presence or absence of Bafilomycin A1, analyzing LC3-II protein levels normalized to β-Actin. Among the molecules identified from the primary screening as autophagy inhibitors, unexpectedly, none of them increased LC3-II levels in a Bafilomycin-like manner. This suggests that such molecules did not operate as late-stage inhibitors. Based on this observation, I compared the compounds plus Bafilomycin A1 to Bafilomycin A1 alone, and I found that 7 out of 13 putative inhibitors significantly reduced Bafilomycin A1-dependent LC3-II accumulation. I selected NU7441, ONC212, Bedaquiline, WAY-640783 for further validation based on quantitative criteria ($p<0.01$). I also selected Poziotinib and Duloxetine, even though they did not reach statistical significance (**Figure 12**). I excluded from further analysis all the other putative inhibitors (**Figure 13**).

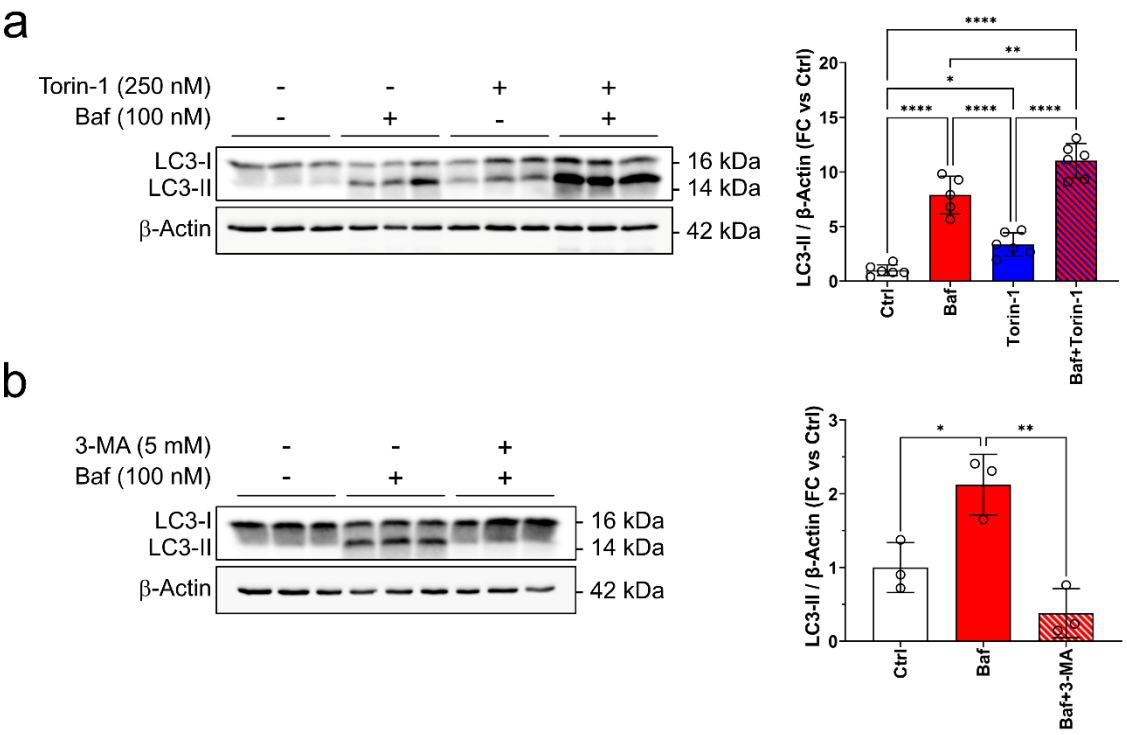

Figure 11 – Set-up of secondary screening assay. *(a) Representative WB analysis for LC3 and β-Actin protein levels in protein extracts from Neuro-2a cells treated with DMSO (Ctrl), Bafilomycin A1 (Baf; 100 nM), or Torin-1 (250 nM) for 15 hours; histograms show quantifications (mean ratio ± SD; n=5-6 independent wells/condition). (b) Representative WB analysis for LC3 and β-Actin protein levels in protein extracts from Neuro-2a cells treated with DMSO (Ctrl), Bafilomycin A1 (Baf; 100 nM), or 3-Methyladenine (3-MA; 5 mM) for 15 hours; histograms show quantifications (mean ratio ± SD; n=3 independent wells/condition). One-way ANOVA followed by Tukey's multiple comparison test was used to analyze data; *p<0.05, **p<0.01, ***p<0.001, ****p<0.0001.*

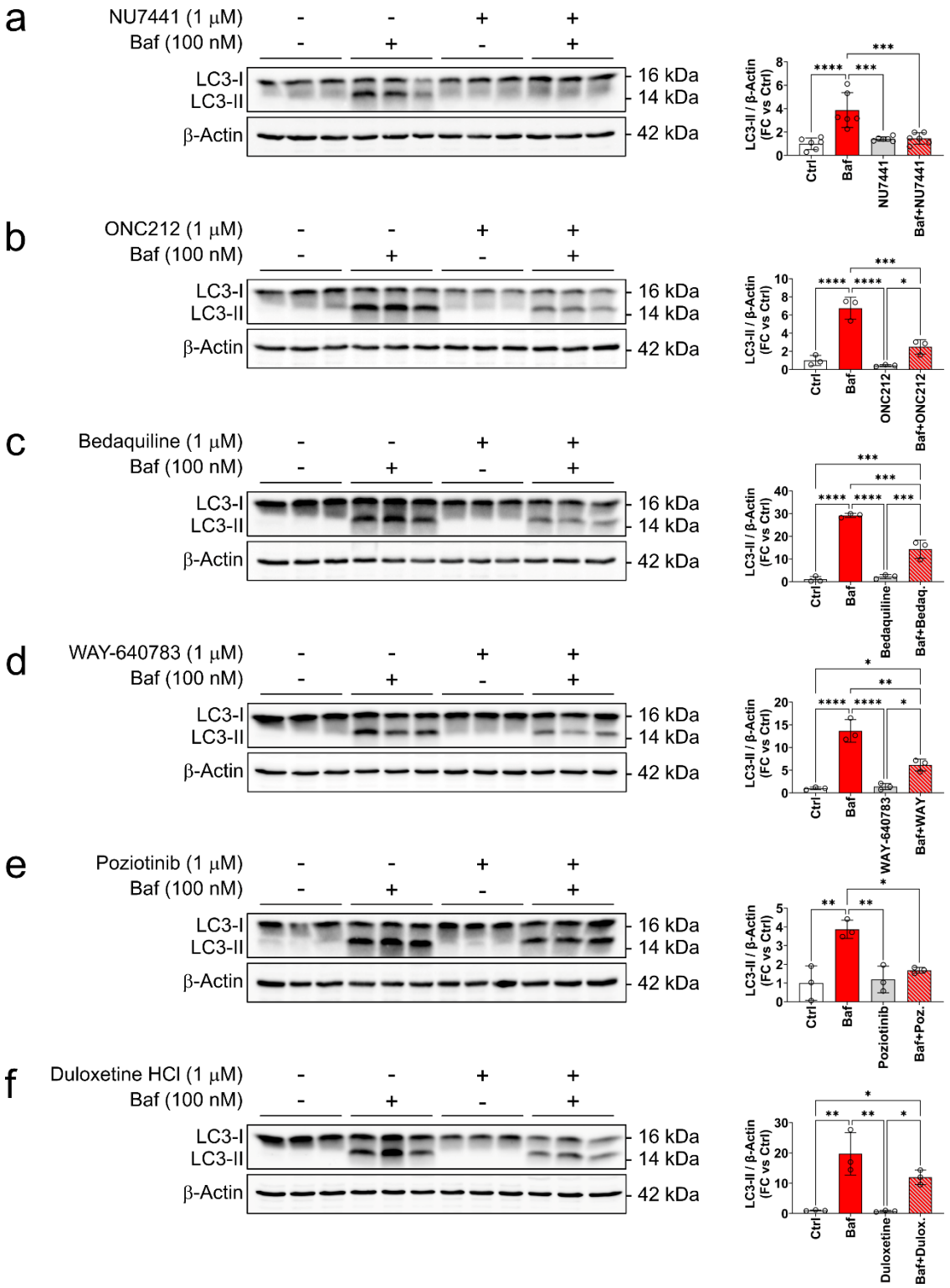

Figure 12 – Selected putative inhibitors. *(a-f) Representative WB analysis for LC3 and β-Actin protein levels in protein extracts from Neuro-2a cells treated with DMSO (Ctrl), Bafilomycin A1 (Baf; 100 nM), or selected compound (1 μM) for 15 hours; histograms show quantifications (mean ratio ± SD; n>3 independent wells/condition). One-way ANOVA followed by Tukey's multiple comparison test was used to analyze data; *p<0.05, **p<0.01, ***p<0.001, ****p<0.0001.*

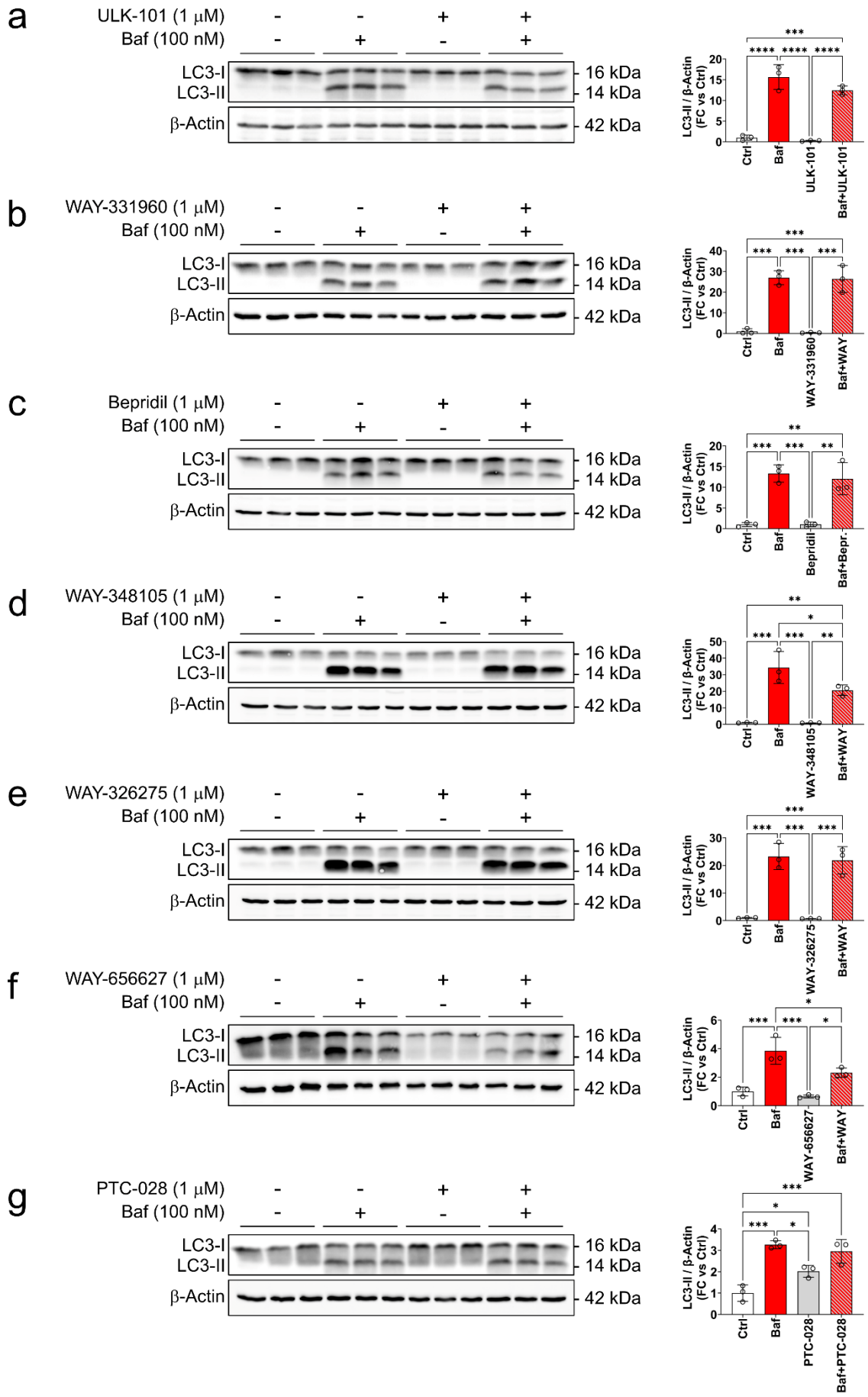
a
ULK-101 (1 μM) - - + +
Baf (100 nM) - + - +
LC3-I
LC3-II
β-Actin
16 kDa
14 kDa
42 kDa
LC3-II / β-Actin (FC vs Ctrl)
Ctrl
Baf
ULK-101
Baf+ULK-101
b
WAY-331960 (1 μM) - - + +
Baf (100 nM) - + - +
WAY-331960
Baf+WAY
c
Bepridil (1 μM) - - + +
Baf (100 nM) - + - +
Bepridil
Baf+Bepr.
d
WAY-348105 (1 μM) - - + +
Baf (100 nM) - + - +
WAY-348105
Baf+WAY
e
WAY-326275 (1 μM) - - + +
Baf (100 nM) - + - +
WAY-326275
Baf+WAY
f
WAY-656627 (1 μM) - - + +
Baf (100 nM) - + - +
WAY-656627
Baf+WAY
g
PTC-028 (1 μM) - - + +
Baf (100 nM) - + - +
PTC-028
Baf+PTC-028

Figure 13 – Excluded putative inhibitors. *(a-g) Representative WB analysis for LC3 and β-Actin protein levels in protein extracts from Neuro-2a cells treated with DMSO (Ctrl), Bafilomycin A1 (Baf; 100 nM), or selected compound (1 μM) for 15 hours; histograms show quantifications (mean ratio ± SD; n>3 independent wells/condition). One-way ANOVA followed by Tukey's multiple comparison test was used to analyze data; *p<0.05, **p<0.01, ***p<0.001, ****p<0.0001.*

On the other hand, among the inducers, I did not observe molecules showing an activity that can overlap that of Torin-1 (**Figure 14**). However, I sorted out a few of them as promising inducers although their performances did not reach statistical significance. I selected Dp44mT for further investigations, as it significantly increased LC3-II protein levels compared to DMSO-treated control (**Figure 14a**). I also selected MK-8745 because it displayed an LC3-II pattern comparable to that of Torin-1, although differences did not reach statistical significance (**Figure 14b**).

3.4.2 Dose-response efficacy properties investigation

As a second line of validation, I evaluated the eight selected molecules over a range of doses (0.1, 1, 10 μM). I further adapted the previous experimental settings differentiating compounds as autophagy inducers or inhibitors. I tested putative inhibitors in the presence of Bafilomycin A1 and compared LC3-II levels to those of Bafilomycin A1 treatment alone (**Figure 15**). On the other hand, when testing a putative inducer, I compared treatments alone to DMSO-treated control (**Figure 16**).

Four out of six tested inhibitors showed a reasonable dose-response effect. ONC212 was also tested at lower concentrations (1 and 10 nM), as at the higher doses the effect in terms of LC3-II reduction was not incremental. I finally selected the following compounds for the next validation assay: NU7441, Poziotinib, Duloxetine, and ONC212 (**Figure 15a**, **b**, **d**, and **e**).

In this experimental setting, neither of the putative inducers modulated autophagy in a dose-dependent manner (**Figure 16**). Except for Dp44mT tested at 1 μM, LC3-II bands were too faint to appreciate autophagy induction upon different treatment conditions. Therefore, I decided to exclude these compounds from further analyses and to consider a different experimental strategy to investigate their effects. Such *in vitro* experiments are currently ongoing.

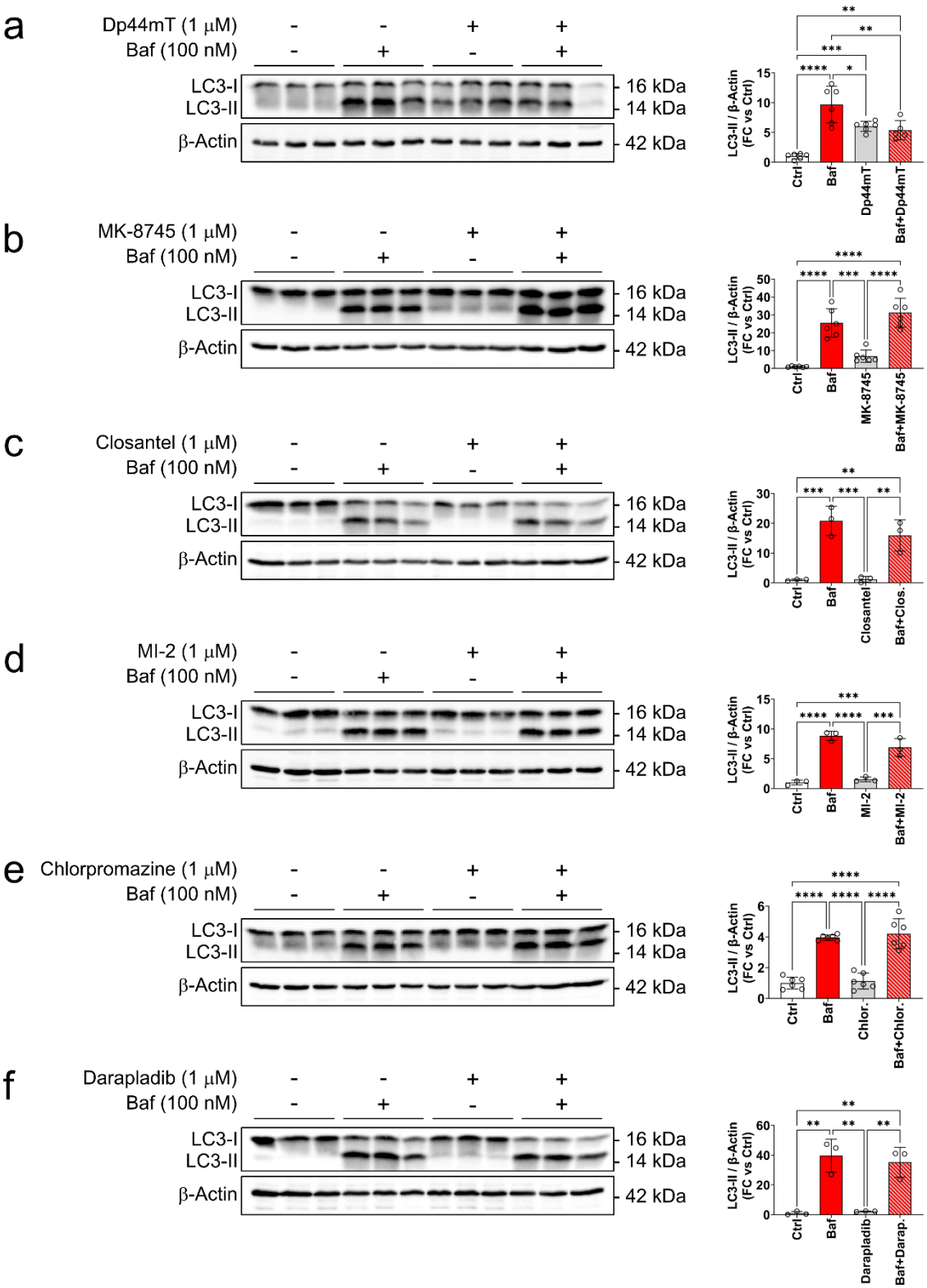

Figure 14 – Validation of putative inducers. *(a-f) Representative WB analysis for LC3 and β-Actin protein levels in protein extracts from Neuro-2a cells treated with DMSO (Ctrl), Bafilomycin A1 (Baf; 100 nM), or selected compound (1 μM) for 15 hours; histograms show quantifications (mean ratio ± SD; n>3 independent wells/condition). One-way ANOVA followed by Tukey's multiple comparison test was used to analyze data; *p<0.05, **p<0.01, ***p<0.001, ****p<0.0001.*

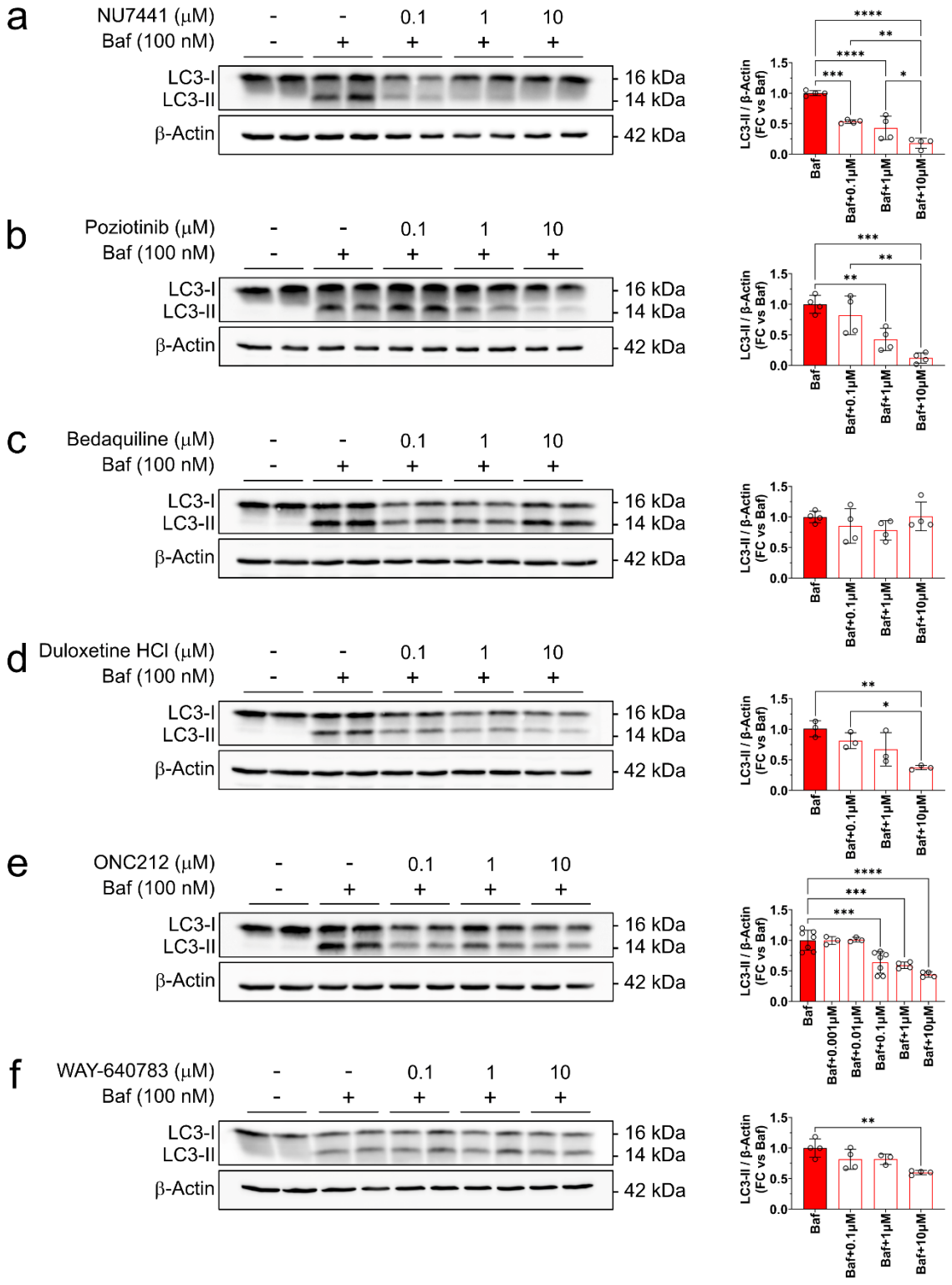

Figure 15 – Dose-response efficacy properties of selected inhibitors. *(a-f) Representative WB analysis for LC3 and β-Actin protein levels in protein extracts from Neuro-2a cells treated with Bafilomycin A1 (Baf; 100 nM), or Baf plus selected compound (0.1, 1, 10 μM) for 15 hours; histograms show quantifications (mean ratio ± SD; n>3 independent wells/condition). One-way ANOVA followed by Tukey's multiple comparison test was used to analyze data; *p<0.05, **p<0.01, ***p<0.001, ****p<0.0001.*

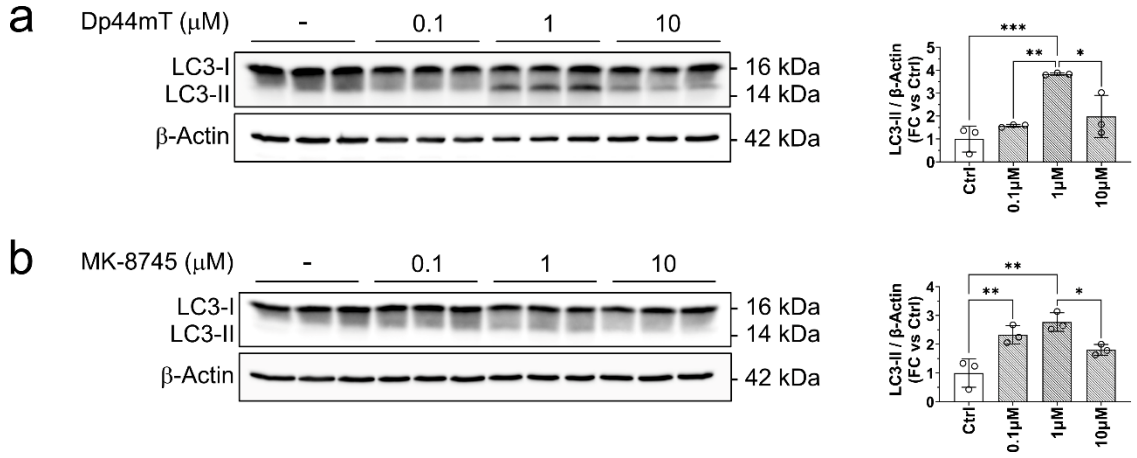

Figure 16 – Dose-response efficacy properties of selected inducers. *(a-b) Representative WB analysis for LC3 and β-Actin protein levels in protein extracts from Neuro-2a cells treated with DMSO (Ctrl), or selected compound (0.1, 1, 10 μM) for 15 hours; histograms show quantifications (mean ratio ± SD; n>3 independent wells/condition). One-way ANOVA followed by Tukey's multiple comparison test was used to analyze data; *p<0.05, **p<0.01, ***p<0.001, ****p<0.0001.*

3.4.3 Electron microscopy analysis of Neuro-2a cells receiving selected compounds

As a third validation experiment on Neuro-2a cells, I analyzed autophagy by Transmission Electron Microscopy (TEM). Neuro-2a cells were treated with DMSO (Ctrl), Bafilomycin A1 (100 nM), and Bafilomycin A1 combined with the sequestration inhibitor 3-MA (5 mM) as control conditions. Selected compounds (NU7441, Duloxetine, ONC212, and Poziotinib) were tested at the single concentration of 10 μM. Compounds were tested in combination with Bafilomycin A1 to investigate their early autophagy inhibition potential.

For this analysis, I quantified autophagic structures, termed Autophagic Vacuoles (AVs), which collectively refer to autophagosomes, amphisomes, and autolysosomes (**Figure 17**). Multivesicular bodies, endosomes, and phagophores were not included in the analysis. I firstly quantified the number of AVs normalized to 100 μm^2 of cytoplasm, and I observed a strong increase of AVs upon Bafilomycin A1 treatment compared to the control, which is in line with all the previous analyses. As an experimental control, I used 3-MA combined with Bafilomycin A1, measuring a significant reduction of AVs with respect to the Bafilomycin A1 treatment alone. Similarly, all the tested compounds significantly reduced the Bafilomycin-induced AVs accumulation, confirming their ability to modulate the early stage of autophagy in

the Neuro-2a model (**Figure 17b**). Notably, NU7441 completely abolished the AVs accumulation induced by Bafilomycin A1.

I next measured the AVs total area per cell profile, to account for the extension of the autophagic compartment (**Figure 17c**). The results partially overlap those obtained by counting the AVs total number. NU7441 and Duloxetine induced a significant reduction of the AVs total area compared to the Bafilomycin A1 treatment alone. On the contrary, ONC212 and Poziotinib did not induce any significant variation, suggesting that although the total number of AVs is reduced upon the compound treatment, the vesicles are proportionally bigger than those present in the Bafilomycin control.

In conclusion, I performed three different validation experiments on naïve Neuro-2a. Among the 19 compounds selected from those identified from the primary screening, I selected NU7441, Duloxetine, ONC212, and Poziotinib for further analyses. All these four compounds operate as early autophagy inhibitors in this *in vitro* model.

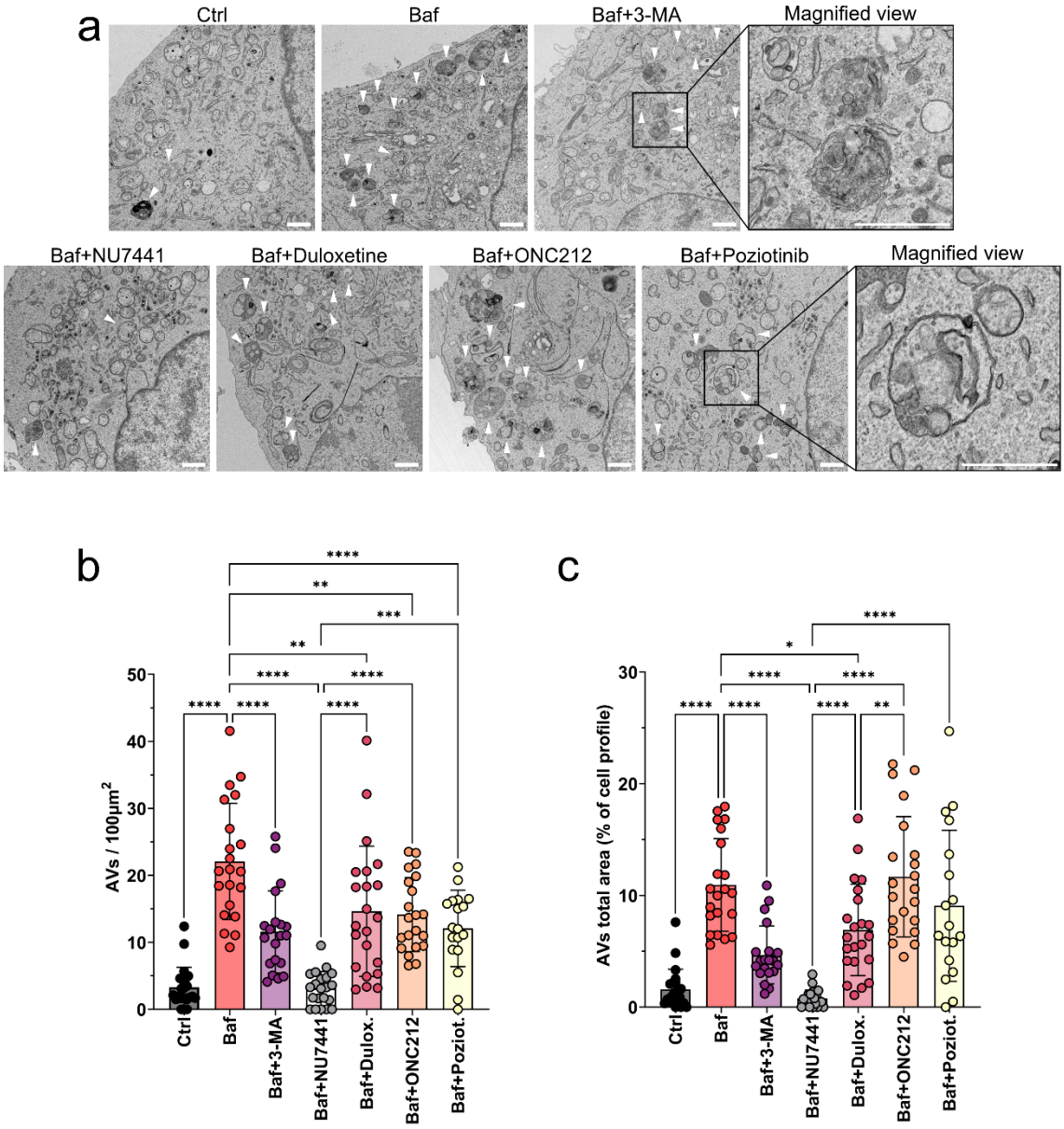

Figure 17 – Transmission electron microscopy analysis of autophagic vacuoles. *(a) Representative electron micrographs of Neuro-2a cells treated with DMSO (Ctrl), Bafilomycin A1 (Baf; 100 nM), and Baf plus 3-Methyladenine (3-MA; 5 mM) or selected compound (10 µM) for 15 hours; autophagic vacuoles (AVs) are highlighted by arrows (scale bar 1 µm); (b) histogram shows quantifications of AVs total number normalized to 100 µm² (mean ratio ± SD; n≥18 micrographs/condition); (c) histogram shows quantifications of AVs total area per cell profile (mean ratio ± SD; n≥18 micrographs/condition). One-way ANOVA followed by Tukey's multiple comparison test was used to analyze data; *p<0.05, **p<0.01, ***p<0.001, ****p<0.0001.*

3.4.4 In vitro best hits validation in ad hoc stressed primary neuronal cultures

All the previous experiments relied on Neuro-2a cells, a murine neuroblastoma cell line. Although these cells were instrumental to set up and perform the molecular screening, I next moved to primary neuronal cultures.

Before performing validation experiments, cellular cultures were characterized by immunolabeling against major neuronal and astrocytic markers: neuron-specific class III beta-tubulin (TUJ1) to stain neuronal processes, Microtubule-Associated Protein 2 (MAP2) as a more mature neuronal marker than TUJ1, and Glial Fibrillary Acidic Protein (GFAP) as astrocyte-specific protein. For these confirmatory experiments, I used cells at Day *In Vitro* (DIV) 7. At this stage, cultured neurons are young and not fully mature, as they express both TUJ1 and MAP2 markers. Moreover, neurons are the predominant cell type in culture, whereas the GFAP staining also revealed a moderate number of astrocytes (**Figure 18**).

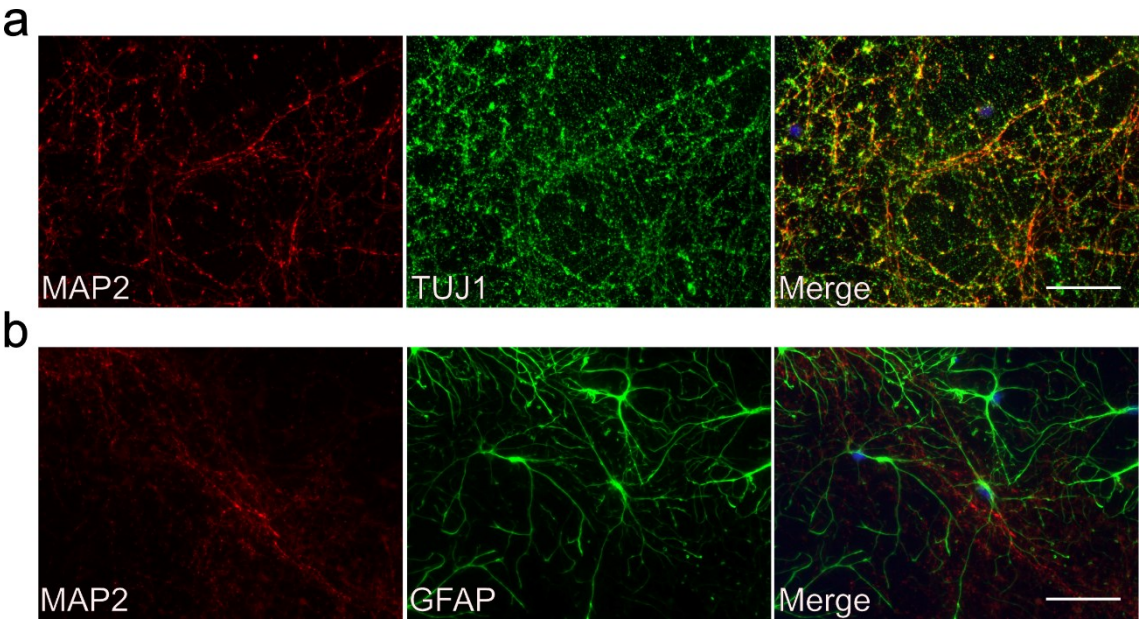

Figure 18 – Characterization of primary cortical neuronal cultures. *Representative panel showing primary cortical murine cultures at DIV7 (n=3 independent sample/condition); cells were immunolabeled for (a) MAP2 (red; neurons) and TUJ1 (green; neuron-specific class III beta-tubulin), and (b) MAP2 (red; neurons) and GFAP (green; astrocytes). Scale bar 100 µm.*

To modulate autophagy, I first tested Bafilomycin A1 as a control at different concentrations (20, 60, and 180 nM) (**Figure 19a**). I observed a significant increase of LC3-II protein levels at all concentrations. Moreover, I took advantage of a stressor mimicking stroke-mediated autophagy induction, adapting a previously published protocol (Young *et al*, 2009). Specifically, I exposed neurons to a nutrient-limited medium (DMEM without B27 supplementation) for different timepoints (4, 8, and 15 hours). Ideally, this procedure should induce a mTORC1-dependent autophagic activation. All the tested conditions increased LC3-II levels by at least 50% compared to control (nutrient-rich medium) (**Figure 19b**). In line with all the previous experimental settings, I selected a time window of 15 hours for the present assay.

I next tested the four best hits (NU7441, Duloxetine, ONC212, and Poziotinib) in nutrient-deprived neurons at the concentration of 10 μM (**Figure 20**). I compared the LC3-II levels of the compound plus nutrient deprivation (ND) to those of nutrient deprivation alone. As in previous validation assays, NU7441 strongly abolished nutrient deprivation-induced LC3-II increase, supporting the early-inhibitory properties of this compound (**Figure 20a**). On the contrary, Duloxetine and ONC212 increased LC3-II levels by 100% and 50%, respectively, when compared to cells receiving nutrient deprivation alone (**Figure 20b** and **c**). Poziotinib did not alter LC3-II protein levels (**Figure 20d**), suggesting that the effect observed on Neuro-2a might be restricted to proliferating cells.

Given all the results obtained so far, I selected NU7441, Duloxetine, and ONC212 for *in vivo* validation, taking advantage of a well-established experimental stroke model.

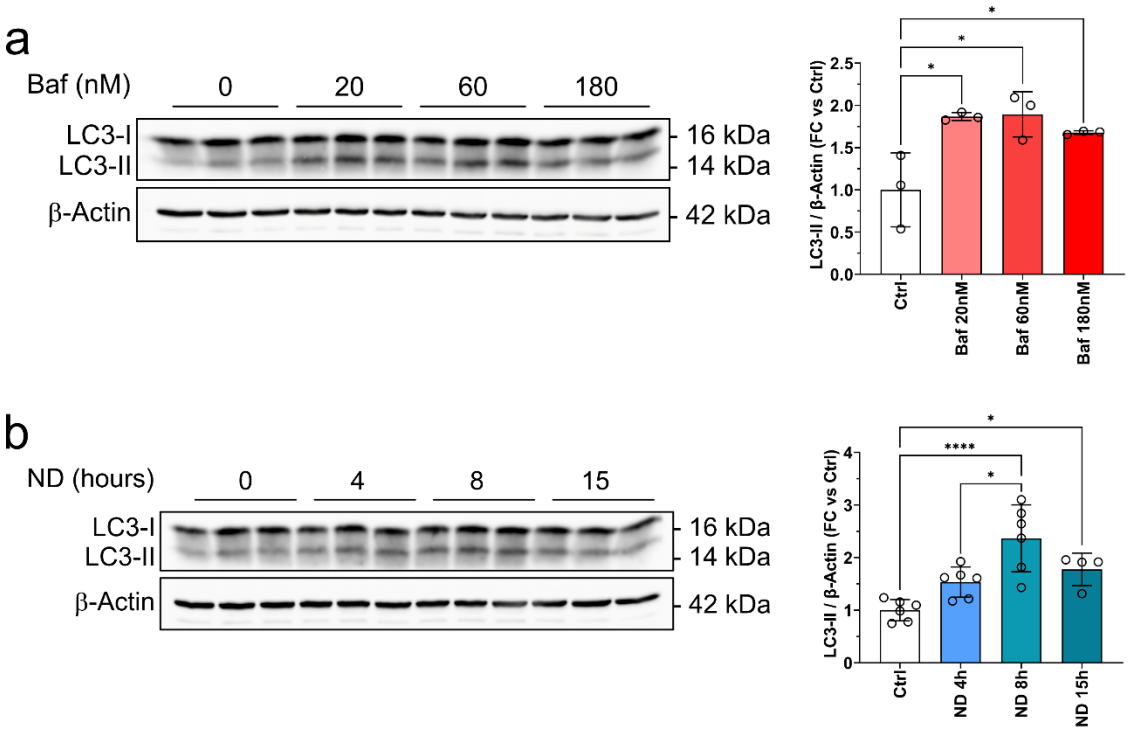

Figure 19 – Bafilomycin A1 and nutrient deprivation efficiently modulate autophagy in mouse cortical neurons. *(a) Representative WB analysis for LC3 and β-Actin protein levels in protein extracts from mouse cortical neurons treated with DMSO or Bafilomycin A1 (Baf; 20, 60, 180 nM) for 15 hours. (b) Representative WB analysis for LC3 and β-Actin protein levels in protein extracts from mouse cortical neurons treated with nutrient-rich medium (Ctrl) or nutrient-deprived medium (ND; 0, 4, 8, 15 hours); histograms show quantifications (mean ratio ± SD; n=3 independent wells/condition). One-way ANOVA followed by Tukey's multiple comparison test was used to analyze data; *p<0.05, **p<0.01, ***p<0.001, ****p<0.0001.*

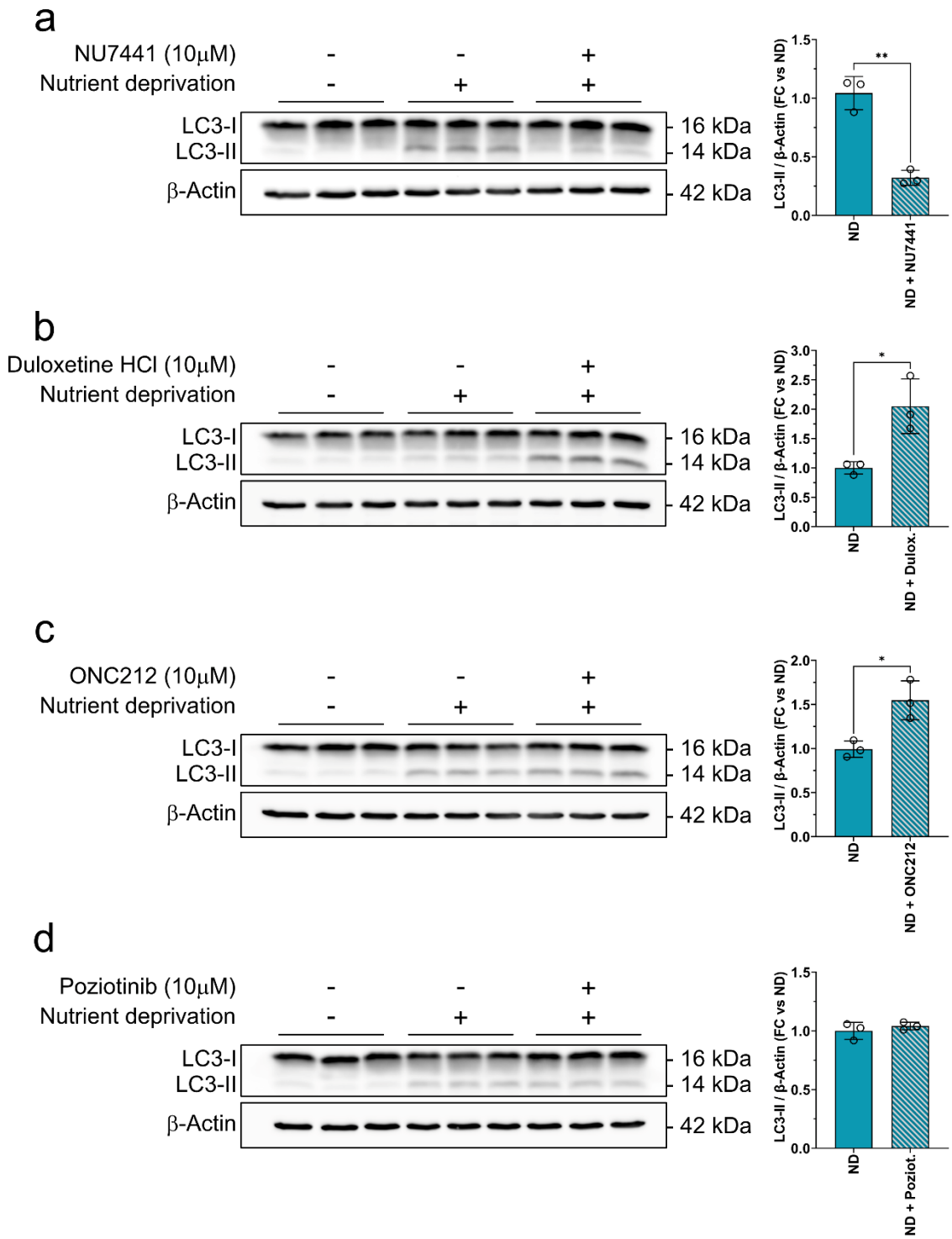

Figure 20 – Neuronal validation of lead-like compounds. *(a-d) Representative WB analysis for LC3 and β-Actin protein levels in protein extracts from mouse cortical neurons treated with nutrient deprivation in the presence or absence of selected compound (10 μM for 15 hours); histograms show quantifications (mean ratio ± SD; n=3 independent wells/condition). Unpaired Student's t-test was used to analyze data; *p<0.05, **p<0.01, ***p<0.001, ****p<0.0001.*

3.4.5 Experimental stroke model for in vivo validation

The transient Middle Cerebral Artery Occlusion (tMCAO) is a widely used animal model of ischemic stroke, mainly employed to study pathophysiology and neuroprotection. In our laboratory, we adapted a well-established occlusion protocol, performing a transient forty-five minutes left MCAO on adult male mice (Hata *et al*, 2000; Hermann *et al*, 2001; Bacigaluppi *et al*, 2009). Firstly, I measured MCAO-mediated autophagy induction as reported by the recent literature (Li *et al*, 2021; Liu *et al*, 2021; Yao *et al*, 2021). I measured LC3-II protein levels in both lesioned (ipsilateral) and control (contralateral) hemispheres 48 hours after MCAO induction (I/R48h) or sham operation (Sham). I observed a significant increase (70%) of the total LC3-II levels in the stroked hemisphere of I/R mice compared to Sham (**Figure 21a**), while I did not observe any differences analyzing samples from the contralateral hemispheres (**Figure 21b**).

I also extended the analysis to other markers involved in the autophagic pathway: p62, to account for autophagosome's substrates degradation, and (p-)p70S6K, to check for mTORC1-mediated autophagy modulation (**Figure 21c** and **d**). I measured a ~30% reduction in p-p70S6K/p70S6K ratio in protein extracts from the ipsilateral hemispheres of I/R mice compared to Sham. However, analyzing the same samples, I did not observe any significant difference in p62 protein levels. Moreover, I did not observe any differences in protein levels when I assayed the contralateral samples, indicating that the MCAO model can selectively induce autophagy in the hemisphere ipsilateral to the occlusion.

I selected Duloxetine as the first compound to be tested in the MCAO mouse model. Adapting the Toda's protocol, mice were subjected to forty-five minutes MCAO, and we administered Duloxetine (10 mg/kg, *i.p.*) every 12 hours, starting just before reperfusion. Experimental groups (n=5 mice per group) included: Sham vehicle-treated, I/R vehicle-treated, and I/R Duloxetine-treated mice. It must be reported that two mice from the sham group died for reasons not related to the experimental procedure.

We sacrificed mice at 48 hours after I/R, separately collecting ipsilateral and contralateral hemispheres. To validate the potential autophagy-modulating properties of Duloxetine, I firstly analyzed LC3-II protein levels, normalizing data to the housekeeping β-Actin (**Figure 22**). As observed in previous measurements, I/R alone can efficiently induce autophagy in the ipsilateral hemisphere (**Figure 22a**). However, in this experimental setting, a similar induction was also detectable in the contralateral hemispheres of the I/R vehicle-treated mice (**Figure 22b**).

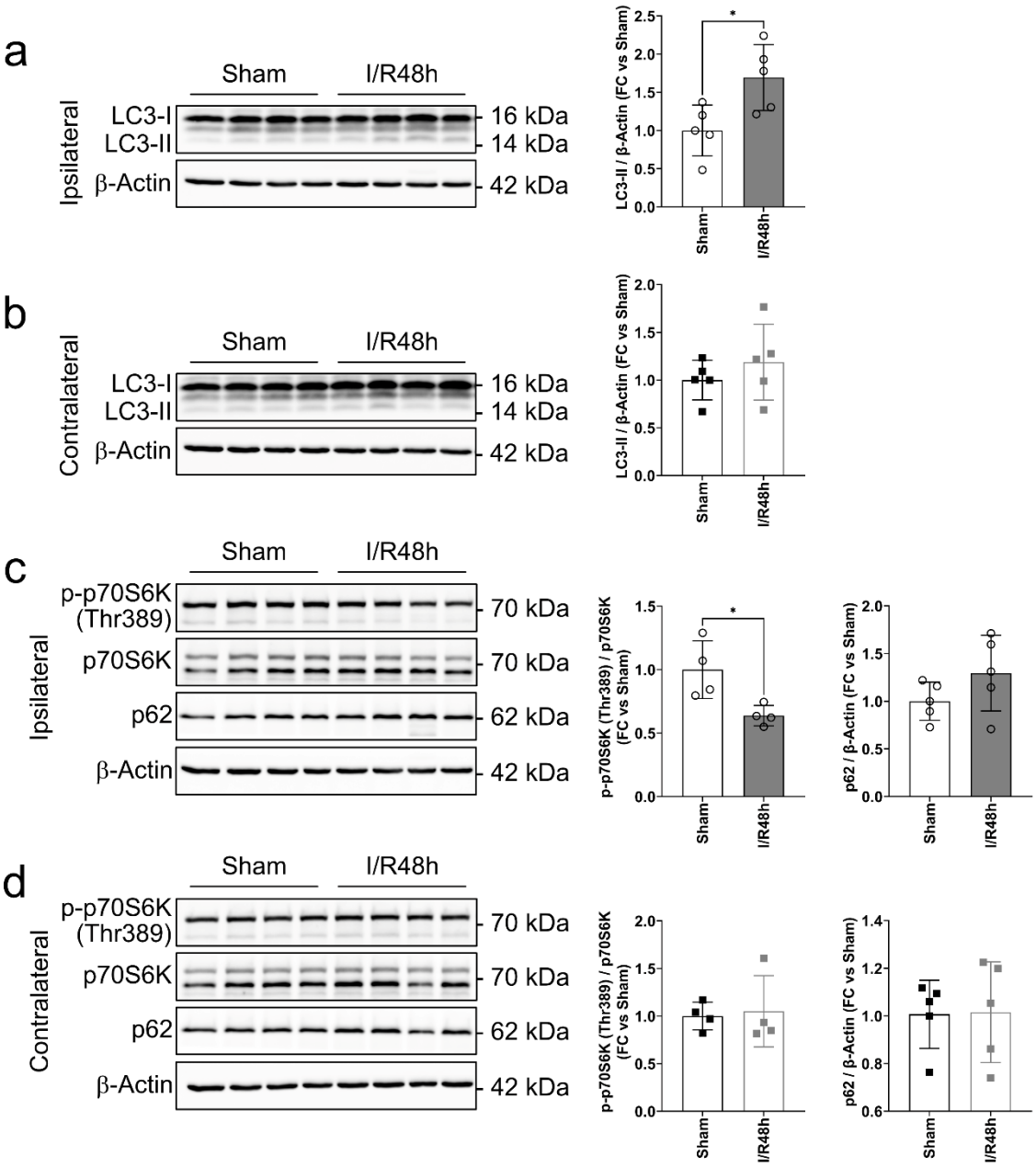

Figure 21 – Autophagy is induced in the ipsilateral hemisphere in the MCAO mouse model. *Representative WB analysis for different autophagic markers in protein extracts from ischemic (ipsilateral) or contralateral hemisphere 48 hours after sham operation (Sham) or ischemia induction (I/R48h); samples were subjected to immunoblotting against (a-b) LC3, (c-d) p-p70S6K (Thr389), p70S6K, p62, and β-Actin; histograms show quantification (mean ratio ± SD; n=5 mouse/condition). Unpaired Student's t-test was used to analyze data; *p<0.05, **p<0.01, ***p<0.001, ****p<0.0001.*

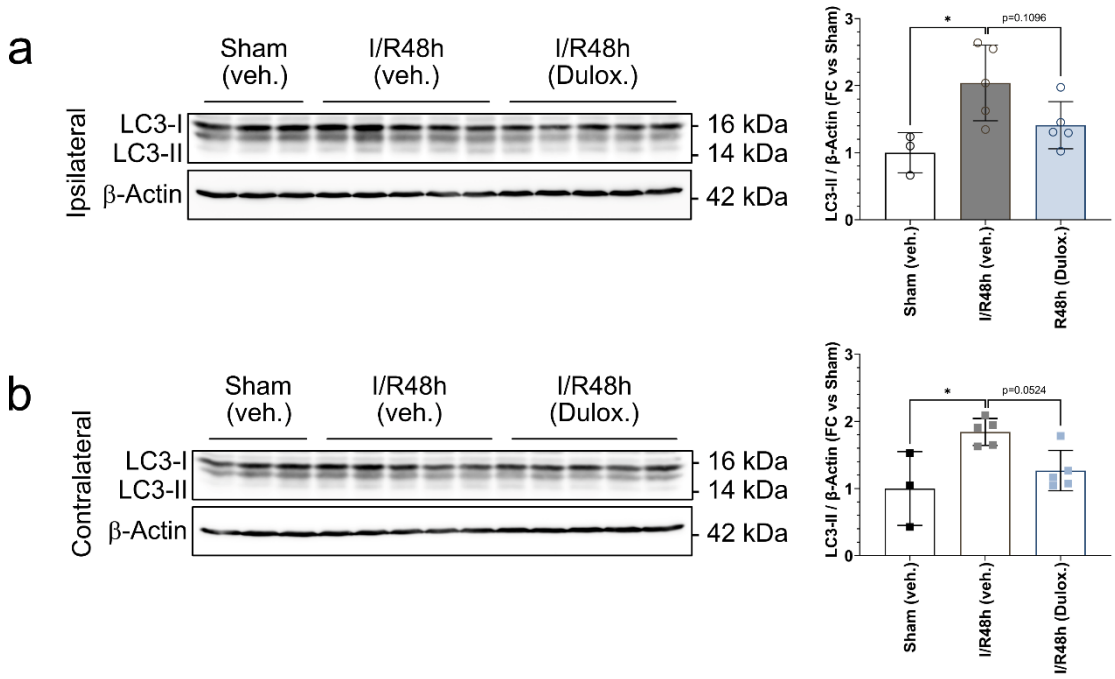

Figure 22 – Duloxetine effect on LC3-II levels in vivo. *Representative WB analysis for LC3 and β-Actin in protein extracts from ischemic (ipsilateral) or contralateral hemisphere 48 hours after sham operation (Sham) or ischemia induction (I/R48h); histograms show quantification (mean ratio ± SD; n≥3 mouse/condition). One-way ANOVA followed by Tukey's multiple comparison test was used to analyze data; *p<0.05, **p<0.01, ***p<0.001, ****p<0.0001.*

I detected a slight but not significant decrease in LC3-II protein levels comparing the Duloxetine-treated I/R group to the vehicle-treated I/R group. This reduction was observed analyzing data from both the ipsi- and contralateral hemispheres. I also analyzed p62 protein levels in all the experimental groups (**Figure 23**). Neither I/R alone nor Duloxetine modified p62 protein levels in both the ipsilateral and the contralateral hemispheres.

Considering the present *in vivo* experiments, I am currently unable to confirm Duloxetine as a true autophagy modulator. Therefore, further analyses are needed to clarify the potential effect of this compound *in vivo* and to optimize drug concentrations.

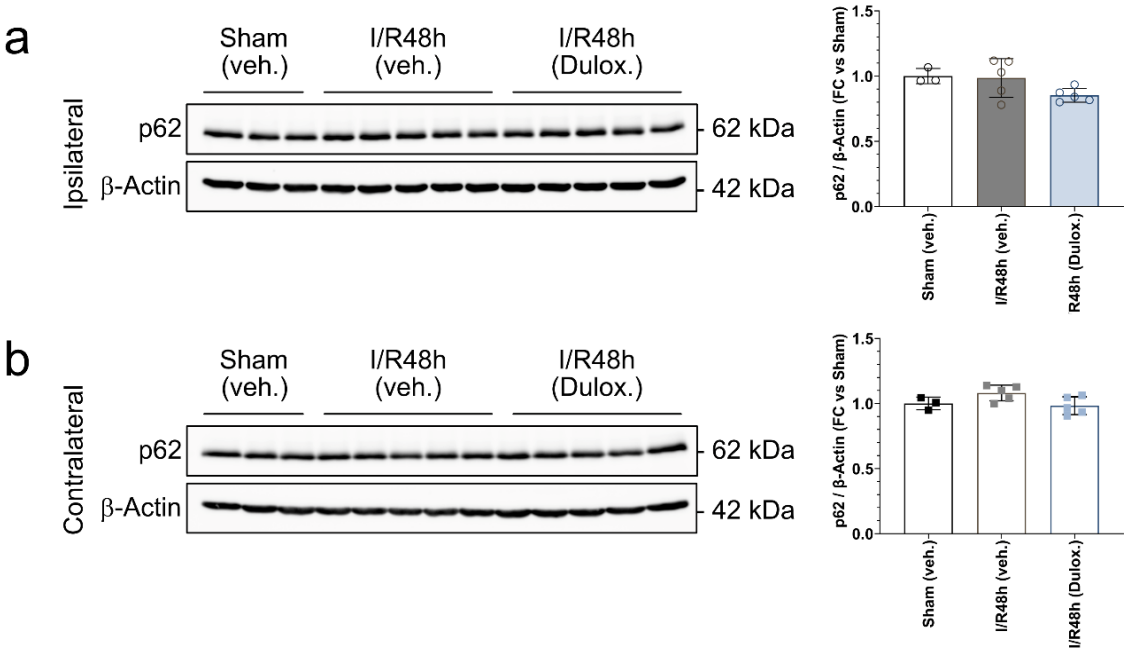

Figure 23 – p62 levels are not affected by Duloxetine treatment in the MCAO mouse model. *Representative WB analysis for p62 and β-Actin in protein extracts from ischemic (ipsilateral) or contralateral hemisphere 48 hours after sham operation (Sham) or ischemia induction (I/R48h); histograms show quantification (mean ratio ± SD; n≥3 mouse/condition). One-way ANOVA followed by Tukey's multiple comparison test was used to analyze data; *p<0.05, **p<0.01, ***p<0.001, ****p<0.0001.*

4. DISCUSSION

Therapeutic options for ischemic stroke treatment are still limited to recanalization strategies. Therefore, novel neuroprotective agents are a general need in the field. Increasing evidence supports autophagy involvement in various pathological contexts, including ischemic stroke (Wang *et al*, 2018). Autophagy has been proposed as a promising neuroprotective target, although its exact role in promoting cell survival or death after stroke is still controversial (Gunn *et al*, 2018). Therefore, novel drugs targeting the autophagic machinery are required.

Chemical screenings provide a powerful strategy to accelerate hits identification for clinical application, as well as to deepen the role of autophagy in stroke pathophysiology. In the present work, I set out and developed an iterative drug screening pipeline to identify novel and specific autophagy modulators that can be active in the ischemic brain. We started with a preliminary *in silico*-based screening to select a restrained list of putative lead-like compounds. Using this approach, we not only reduced the original library from 6839 to 898 bioactive compounds, but we also selected the best candidates based on predicted drug-like properties and CNS activity, thus maximizing time- and cost-effectiveness. In parallel, I set up a robust fluorescence-based LTS assay to discriminate between autophagy inducers and inhibitors. To mimic ischemic conditions *in vitro,* I introduced OGD in the experimental setting as it is widely used as an ischemic stroke model, promoting autophagy activation. Thus, with this strategy, I identified a subset of molecules either limiting or further strengthening OGD-dependent autophagy induction.

Selected lead-like compounds underwent a series of confirmatory assays to account for false positives, and to validate the autophagy-modulating potential of the best hits. I initially applied an experimental paradigm to measure autophagic flux in Neuro-2a cells in response to different treatments. Each compound was tested in the presence or absence of saturating levels of a late-stage autophagy inhibitor, a common procedure that is largely used in autophagy studies (Klionsky *et al*, 2021). Subsequently, I investigated the dose-response efficacy properties of selected compounds using the same cellular model. I concluded these confirmatory assays on Neuro-2a cells validating four potential autophagy inhibitors.

In basal conditions, Neuro-2a cells display a relatively modest autophagic flux, which is reflected by the poorly detectable LC3-II protein levels. Thus, the *in vitro* validation of putative autophagy inducers is still ongoing as I defined a different experimental strategy to assess autophagy induction and to increase the assay

sensitivity. A successful approach to study autophagy inducers could be based on exposing Neuro-2a cells to autophagy-activating stressors (*e.g.,* OGD or starvation). This should concur to set a baseline level of LC3-II that is instrumental for the accurate quantification of autophagy modulation. Alternatively, I could optimize the experimental design working with non-saturating levels of Bafilomycin A1.

I next tested putative inhibitors for neuronal validation, as this is a fundamental step to reach the preclinical setting. Following the same principle as for the primary screening campaign, I reintroduced in the experimental setting an autophagy-enhancing stressor, which should mimic brain ischemia. I am aware that nutrient deprivation is only one of the different features of an ischemic insult. However, I adapted the nutrient deprivation protocol published by Young *et al.,* which induces a robust autophagy activation in primary neurons. In this manuscript, the authors demonstrated that insulin is the key autophagy-driving factor, reducing mTORC1 phosphorylation (Young *et al*, 2009). I efficiently replicated the protocol, observing a significant LC3-I to LC3-II conversion enhancement upon nutrient and insulin deprivation. I tested the four selected compounds using this paradigm. Among them, NU7441, ONC212, and Duloxetine modulated LC3-II protein levels, thus confirming results I obtained in Neuro-2a cells. Unfortunately, I did not observe any substantial LC3-II variations upon Poziotinib treatment.

NU7441 (KU-57788) is a potent and selective DNA-dependent protein kinase (DNA-PK) inhibitor (IC_{50} = 14 nM) (Leahy *et al*, 2004). DNA-PK plays an essential role in genome stability maintenance and DNA-damage response, ensuring an effective double-strand break repair through non-homologous end-joining and homologous recombination (Shrivastav *et al*, 2008). More recently, it has been proposed that DNA-PK influences cell survival through p53 activity upregulation (Ma *et al*, 2018; Chen *et al*, 2021), and its role in autophagy modulation has also been observed. A recent manuscript published in 2020 by Puustinen *et al*. demonstrated that the inhibition of DNA-PK catalytic subunit in cancer cell lines leads to efficient negative regulation of AMPK. This modulation results in autophagy inhibition, which can be observed in basal conditions, as well as upon a stressor administration (Puustinen *et al*, 2020). My observations are in line with their published results and demonstrate that the compound's efficacy is achievable also in terminally differentiated cells.

ONC212 is an antitumor agent, belonging to the impiridones family. It is an activator of the G Protein-Coupled Receptor 132 (GPR132) and Gq alpha subunit (Gαq) signaling, leading to apoptosis induction (Lin & Ye, 2003; Nii *et al*, 2019). A recent publication linked G protein-coupled receptors with Gαq to mediate autophagy

regulation, highlighting a key role of the Gαq subunit in mTORC1 modulation. Indeed, Gαq stimulation leads to mTORC1 activation, inhibiting autophagy (Cabezudo *et al*, 2021). Experiments conducted on cancer cell lines also demonstrated that ONC212 disrupts the mitochondrial unfoldase-peptidase ClpXP complex, leading to oxidative phosphorylation impairment, with a consequent decrease in energy production (Ferrarini *et al*, 2021). The caseinolytic protease P (ClpP) is a mitochondrial protease, similar to the cytoplasmic proteasome. It complexes with ClpX, which functions as a AAA ATPase chaperone. The ClpPX complex plays a fundamental role in the maintenance of the respiratory chain and it is typically overexpressed in tumors (Cole *et al*, 2015; Seo *et al*, 2016). ONC212 induces the hyperactivation of ClpP and mediates ClpX dissociation and downregulation in a concentration-dependent manner. ClpP hyperactivation strongly downregulates respiratory chain complexes, impairing mitochondrial bioenergetics, and inducing AMPK phosphorylation (Ishizawa *et al*, 2019). The present results on Neuro-2a and primary neurons support the idea that ONC212 can affect autophagy. However, I observed different outcomes when I compared the effect of ONC212 in proliferating and post-mitotic cells. Results deriving from Neuro-2a are in line with previously published data that assayed Gαq subunit stimulation. On the other hand, ONC212 enhanced nutrient deprivation-induced autophagy in primary neurons. I can speculate that the effect exerted by ONC212 on primary neurons might be due to the neuronal reliance on mitochondrial respiration. Therefore, neurons could be more sensitive to ONC212-dependent ClpP hyperactivation than Neuro-2a cells. Further analyses are needed to clarify the mechanism of action of ONC212 and the importance of its targets' stimulation in different experimental models.

Poziotinib (HM781-36B) is a potent and irreversible pan-HER inhibitor, with a strong inhibitory effect on the Epidermal Growth factor Receptor (EGFR, also known as HER1) and Human Epidermal growth factor Receptor 2 (HER2) (Nam *et al*, 2011). Inhibition of EGFR inhibits a series of downstream signaling cascades, including those involved in autophagy regulation. However, given the complexity of the EGFR signaling pathway, the exact role of EGFR modulators in mediating autophagy induction or inhibition is still controversial and appears to be context-dependent (Wu & Zhang, 2020). My results on Neuro-2a cells suggest that Poziotinib operates as an early autophagy inhibitor. Unfortunately, these results were not confirmed by the validation experiments performed on primary cultures. EGFR protein is mainly expressed by epithelial cells and it plays a key role during brain development, especially during astrocyte maturation (Burrows *et al*, 1997). However, the expression of EGFR decreases during adulthood, as shown in rat brains (Quirion *et*

al, 1988). Studies relying on immunostaining showed that EGFR is also expressed in the brain of adult and aged rats, prominently in cerebral cortical neurons (layers IV and V), in the hippocampus, and in the periventricular germinal zones, while EGFR signal is weak or absent in post-natal astrocytes (Gómez-Pinilla *et al*, 1988; Ferrer *et al*, 1996). Another study describes that EGFR is upregulated in activated astrocytes after neural injury (Liu *et al*, 2006). I can conclude that EGFR levels in post-natal neurons are generally low. Therefore, the lack of autophagy modulation in Poziotinib-treated neurons could derive from the limited expression of EGFR. Although this result is not conclusive, further analysis in cell populations involved in stroke pathophysiology could reveal a field of application of Poziotinib.

Duloxetine is a serotonin-norepinephrine reuptake inhibitor, widely used for depression, anxiety, and neuropathic pain treatment (Bouhassira *et al*, 2014; Hsu *et al*, 2014). *In vitro* studies on cultured neurons propose Duloxetine as a protective molecule against oxidative stress and Ca^{2+} overload, identifying Transient Receptor Potential Melastatin 2 (TRPM2) as the main mediator of its protective effects (Akpinar *et al*, 2014; Demirdaş *et al*, 2017). Interestingly, TRPM2 has recently emerged as a novel therapeutic target for ischemic stroke treatment (Wang *et al*, 2021a). Moreover, Duloxetine might also inhibit autophagy through the down-regulation of AMPK phosphorylation (Zinnah & Park, 2019). In the herein described experimental setting Duloxetine confirmed its ability to modulate autophagy, although I observed different responses to the treatment between mitotically active and post-mitotic cells. As stated above, it is not surprising to find differences in autophagic responses when mitotically active cancer cells and terminally differentiated neuronal cultures are compared. Such a differential response might derive from metabolic changes that often occur during tumorigenesis (Aminzadeh *et al*, 2015). Indeed, dysregulation of AMPK/mTORC1 signaling is reported to be a common feature that can be observed in different cancer cells (Wu *et al*, 2013; Cairns *et al*, 2020).

The recent literature points out Duloxetine as a protective drug against ischemic brain damage (Toda *et al*, 2019), therefore I decided to test this molecule in the tMCAO mouse model. As a first step, I decided to assess whether the autophagic markers could be easily detectable in protein extracts from MCAO mice. This experiment was instrumental to explore the ability of the drug to modulate autophagy *in vivo*. After performing these experiments, confirming the impact of tMCAO on the autophagic pathway, I introduced Duloxetine as pharmacological treatment. Although I did not reach statistical significance, I observed a trend showing that Duloxetine can limit the I/R-induced LC3-II accumulation. However, further studies are needed to deepen the Duloxetine effect *in vivo* and, above all, to optimize drug concentration

in our model for autophagy investigation. We will also consider introducing in our *in vivo* experimental settings a lysosomal degradation inhibitor (*i.e.*, Chloroquine). Such experimental control might be of use to estimate LC3-II digestion rate, as well as to gain sensitivity for *in vivo* drug validation experiments.

In conclusion, with the present work, I designed and developed a chemical screening platform to identify potential autophagy modulators. Through different *in vitro* assays, I selected the three best candidates for preclinical validation. Given the amount of time and resources demanded by the screening, I initially focused the attention on the monitoring of LC3 as a reliable parameter for autophagy assessment. However, further validations are needed to propose selected candidates as true autophagy modulators. Therefore, I plan to implement the characterization of each compound, integrating the strategy with different approaches and additional markers (*e.g.,* p62, Beclin-1, and p70S6K). To do so, I will monitor autophagy induction and inhibition exploiting an array of different techniques, including live-cell imaging and electron microscopy, to assess drug performances under basal and stressed conditions. Moreover, I plan to investigate the mechanism of action (MOA) of each selected compound, which is of paramount importance in the roadmap that drives a small molecule from the bench to the pharmacy shelf.

Overall, this work provides a new perspective on autophagy in brain ischemia. In addition, it shed new light on methods and approaches that can be exploited to identify molecules active in complex disorders. Protocols involving mitotically active cell lines are useful for screening procedures. However, they can only provide approximate predictions for neurological disorders, highlighting the need for further validations in more suitable experimental models.

Future studies should also consider the significant changes that occur with aging. Aging is a major risk factor for stroke and it is accompanied by a plethora of changes, including increased oxidative stress and dysregulated hormone response (Cuervo *et al*, 2005), that lead to macroautophagy dysregulation. Such modifications can affect protein and organelles homeostasis, a condition that is further impaired upon an ischemic insult. Therefore, it will be crucial to describe the effects of autophagy modulators also in aging brain models.

5. MATERIALS AND METHODS

5.1 Reagents

Torin-1 (Cat. No. 4247) and Bafilomycin A1 (Cat. No. 1334) were purchased from Tocris Bioscience. Puromycin (Cat. No. P8833) and 3-Methyladenine (Cat. No. M9281) were purchased from Sigma. Bepridil hydrochloride (Cat. No. HY-16952A), Darapladib (Cat. No. HY-10521), ULK-101 (Cat. No. HY-114490), ONC212 (Cat. No. HY-111343), Duloxetine HCl (Cat. No. HY-B0161A), Bedaquiline fumarate (Cat. No. HY-14881A), Closantel (Cat. No. HY-17596), and Dp44mT (Cat. No. HY-18973) for *in vitro* validation were purchased from MedChemExpress. WAY-331960 (Cat. No. P-425440429), WAY-326275 (Cat. No. P-34884134), WAY-656627 (Cat. No. P-6984125), WAY-348105 (Cat. No. P-605854424), WAY-640783 (Cat. No. P-486113558), and PTC-028 (Cat. No. P-608273002) for *in vitro* validation were purchased from Mcule. NU7441 (Cat. No. S2638), Chlorpromazine (Cat. No. S5749), MK-8745 (Cat. No. S7065), Poziotinib (Cat. No. S7358), and MI-2 (Cat. No. S7429) for *in vitro* validation were purchased from Selleckchem. Duloxetine HCl (Cat. No. S2084) for *in vivo* validation was purchased from Selleckchem.

5.2 Cell culture

Neuro-2a cell line was obtained from the American Type Culture Collection (CCL-131™). Cells were plated on culture dishes or plates and maintained in Dulbecco's Modified Eagle Medium (DMEM; Gibco, Cat. No. 11965084) supplemented with 10% FBS (Corning) and 1% penicillin/streptomycin (Gibco). Cells were grown in a humidified 5% CO_2 atmosphere at 37°C.

5.3 Generation of Neuro-2a cell line stably expressing PK-hLC3

In order to generate a stable cell line allowing the monitoring of the autophagic flux, Neuro-2a cells were transfected with the pEX-PK-hLC3 plasmid (Addgene, Cat. No. 61458) following Lipofectamine LTX (Invitrogen, Cat. No. A12621) manufacturer's protocol. Twenty-four hours post-transfection, cells underwent antibiotic selection using 4.5 µg/ml puromycin. The culture medium was refreshed every 2-3 days. After a week, the resistant bulk culture was seeded in a 96-well plate, following a limiting dilution protocol. Single clones were grown in a selection medium for 14 days and periodically inspected for morphology and fluorescence

intensity. Selected clones were expanded and cryopreserved for further analysis. Clone 7B11 was selected and used for the primary screening.

5.4 *In silico* preliminary screening

Bioactive Compound Library-I (Selleckchem, Cat. No. L1700) was *in silico* analyzed and screened according to a specific set of functional parameters. *In silico* analysis was conducted using the QikProp Absorption, Distribution, Metabolism, and Excretion (ADME) prediction tool (Schrödinger, LLC, New York), which uses an algorithm based on the correlation between experimentally determined properties and Monte Carlo simulations. Molecules underwent a first prioritization round based on pharmaceutically relevant Drug Metabolism and Pharmacokinetics (DMPK) properties listed in **Table 4**. After the first analysis, 1927 molecules underwent a second prioritization round. Compounds' ranking was performed using a linear function to assign a score to the most relevant properties identically weighted. CNS, QPPMDCK, and QPlogBB descriptors were selected to rank the compounds.

Table 4 – In silico DMPK parameters used in the present study.

Property or Descriptor	*Range (for 95% of known drugs)*	*Description*
CNS	-2 to +2	Predicted CNS activity
QPPMDCK	<25 poor >500 great	Predicted apparent MDCK cells permeability in nm/sec. MDCK cells are a good mimic for the BBB
QPlogBB	-3.0 to 1.2	Predicted brain/blood partition coefficient
QPlogPo/w	-2.0 to 6.5	Predicted octanol/water partition coefficient
#stars	0 to 5	Number of property or descriptor values that fall outside the 95% range of similar values for known drugs
RuleOfFive	Maximum is 4	Number of violations of Lipinski's rule of five

Property or Descriptor	*Range (for 95% of known drugs)*	*Description*
RuleOfThree	Maximum is 3	Number of violations of Jorgensen's rule of three
#metab	1 to 8	Number of likely metabolic reactions
#rtvFG	0 to 2	Number of reactive functional groups

5.5 Low-throughput autophagy screening assay and OGD treatment

Cherry Pick Library (384-well, Cat. No. L2000-Z382759-30µl) was purchased from Selleckchem and included 898 compounds. PK-hLC3-expressing Neuro-2a cells (7B11 clone) were used to screen the compounds library. Cells were plated in complete DMEM supplemented with 4.5 µg/ml puromycin, at a density of 1.2 x 10^5 cells/well in 12-well multiple-well plates (Costar) and grown for 24 hours. To induce OGD, the complete medium was replaced by deoxygenated, serum-free, glucose-free DMEM (Sigma, Cat. No. D5030) supplemented with 3.7 g/L $NaHCO_3$ and 1% penicillin/streptomycin, and cells were exposed to a hypoxic atmosphere (1% O_2, 5% CO_2, 94% N_2) in a controlled-oxygen workstation (SCI-tive, Baker Ruskinn). Each drug was tested in OGD conditions at a final concentration of 1 µM, for 15 hours. Depending on the diluent used to resuspend individual drugs, I established controls incubating cells with DMSO or water. Torin-1 and Bafilomycin A1-treated controls were alternatively included in each experiment. For screening purposes, cells were maintained in culture for no more than four *in vitro* passages.

5.6 Flow cytometry

Flow cytometry analysis was performed on samples derived from OGD conditions. They were processed in normoxic conditions, for the time needed to prepare the experimental setting. Briefly, living cells were detached with 0.05% Trypsin-EDTA (Gibco), transferred to a 96-well multiple-well plate (V-bottom), centrifuged at 300 x *g* for 5 minutes at 4°C, and washed with cold 1x PBS. After washing, cells were stained with Zombie NIR Fixable Viability kit (Biolegend, Cat. No. 43105) for 20

minutes at 4°C. Fluorescence was acquired on Cytoflex S flow cytometer (Beckman Coulter), in a semi-automated format. Upon acquisition, events were gated on single and viable cells by excluding dead cells with the live/dead staining, as detailed in the gating strategy (**Figure 24**). For each sample, 1 x 10^7 living cells were acquired and analyzed with FlowJo software (BD Biosciences).

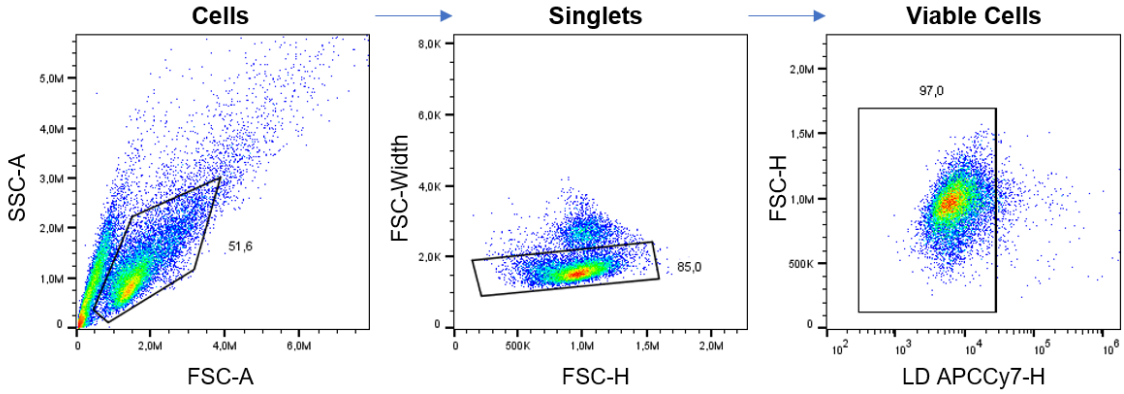

Figure 24 – Representative panel showing the flow cytometry gating strategy used in this work.

5.7 Primary neuronal cultures

Primary cortical neurons were prepared from the brains of E17.5 mouse embryos and used at DIV7. Embryonic brains were dissected under sterile conditions in cold Hanks' Balanced Salt Solution (HBSS; Sigma, Cat. No. 55037C) supplemented with 0.6% D-(+)-glucose (Sigma, Cat. No. G8270) and 5 mM Hepes (Gibco, Cat. No. 15630080). After dissection, single cortices were gently triturated to loosen up the tissue. Cells were mechanically dissociated and resuspended in the dissection medium, followed by centrifugation at 100 x *g* for 5 minutes. Cells were plated on cell culture treated multiple-well plates or HNO_3-treated glass coverslips, both coated with 0.2 mg/ml poly-L-lysine (Sigma, Cat. No. P2636) and 10 µg/ml mouse laminin (Sigma, Cat. No. L2020).

Cells were maintained in Neurobasal-A medium (Gibco, Cat. No. A2477501) supplemented with 2% B-27 (Gibco, Cat. No. 17504), 1% L-glutamine, 0.6% D-glucose, and 5 mM Hepes. Twenty-five percent of the culture media was refreshed every 2-3 days, and cells were kept at 37°C with 5% CO_2 until DIV7.

5.8 Nutrient deprivation and treatments on cortical neurons

Nutrient deprivation induction on primary neuronal cultures was adapted from a previously described protocol (Young *et al*, 2009). Briefly, primary cortical neurons from E17.5 embryos were plated in the complete Neurobasal-A medium at a density of 2.2 x 10^5 cells/well in 12-well multiple-well plates (Costar). At DIV7, the complete medium was replaced with nutrient-limited media (DMEM alone). For autophagy modulation studies, neurons were cultured for 15 hours in the presence or absence of selected compounds at a final concentration of 10 μM.

5.9 Mice

Experiments were performed using male C57BL/6N and female CD1 mice (Charles River Laboratories). Mice were maintained at San Raffaele Hospital mouse facility (Milan, Italy) under specific pathogen-free conditions and a standard 12-hour light-dark cycle with food and water *ad libitum*.

Experimental procedures were approved by the Institutional Animal Care and Use Committee (IACUC No. 692, 798, and 1198), and all efforts were made to minimize animal suffering and to reduce the number of mice used, in accordance with the European Communities Council Directive of 24 November 1986 (86/609/EEC).

5.10 Transient focal ischemia model and drug injection *in vivo*

Stroke was induced on seven weeks-old male C57BL/6N mice through tMCAO (Hata *et al*, 2000; Hermann *et al*, 2001; Bacigaluppi *et al*, 2009). Animals were anesthetized with 1-1.5% isoflurane (Merial, Assago, Italy) in 30% O_2. Focal cerebral ischemia of the left Middle Cerebral Artery (MCA) was induced with a 7-0 silicon-coated filament (Doccol, Cat. No. 702034PK5Re). The temperature was maintained between 36.0 and 36.5°C during the procedure, and Cerebral Blood Flow (CBF) was monitored in the cerebral cortex ipsilateral to the occluded MCA with a Laser Doppler Flowmeter (LDF) (PeriFlux System 5000, Perimed). Animals that stably reached a CBF below 30% of their initial baseline were included in the study. Animals that experienced bleeding during surgery were excluded from the experiment. In our model, the filament was removed after 45 minutes, and animals were sacrificed after 48 hours from reperfusion.

In order to test selected drugs *in vivo*, compounds were dissolved in DMSO at the final concentration of 10 mM. Animals intraperitoneally received vehicle or treatment (10 mg/Kg) just before and 12, 24, and 36 hours from reperfusion. On the day of sacrifice, mice received an overdose of anesthetic drug (avertine), and they were perfused with a saline solution containing 0.2% EDTA 0.5 M. Brains were rapidly isolated, and ~4 mm-thick coronal sections of the stroked (left, ipsilateral) and contralateral (right) hemispheres (bregma=0; from +2 to -2) were separately snap-frozen by immersion in liquid nitrogen and stored at -80°C before processing.

5.11 Transmission Electron Microscopy

Naïve Neuro-2a cells were plated in complete DMEM, at a density of 2.5 x 10^5 cells/well in 6-well multiple-well plates (Costar) and grown for 24 hours. Cells were cultured for 15 hours in the presence of selected compounds at the final concentration of 10 μM, in combination with 100 nM BafA1.

Cells were fixed in 2.5% glutaraldehyde (Sigma, Cat. No. G5882) solution for 1 hour at room temperature. After fixation cells were rinsed with 0.1 M sodium cacodylate (Sigma, Cat. No. C4945) buffer (pH 7.4), 3 times for 5 minutes at room temperature. Cells were post-fixed in a solution containing: 1% OsO_4 (Sigma, Cat. No. 75632), 1.5% $K_4Fe(CN)_6$ (Sigma, Cat. No. 702587), and 0.1 M sodium cacodylate for 1 hour at 4°C protected from light. After fixation samples were washed 3 times for 5 minutes with 0.1 M sodium cacodylate buffer and washed 5 times with distilled water. Samples were then stained with 0.5% uranyl acetate at 4°C overnight, protected from light. After 5 washing steps with distilled water, samples were dehydrated using the following increasing concentration of ethanol (5 minutes per step): 30%, 50%, 70%, 80%, 90%, and 96%. Then, samples were incubated 3 times for 5 minutes in 100% ethanol. After dehydration, samples were covered with a mixture of ethanol and epoxy resin (1:1) and left for 2 hours on a shaker at room temperature. After two changes of pure epoxy resin (1 hour per change) at room temperature, samples were finally embedded in fresh epoxy resin and polymerized overnight at 45°C and then incubated at 60°C for 24 hours.

Ultrathin sectioning (70 nm) was performed on a Leica EM UC6 ultramicrotome. Sections were picked up and positioned on a 300 mesh squares grid. Thin sections were contrasted with 2% aqueous uranyl acetate for 5 minutes, followed by three washes in filtered distilled water (1 minute each). Subsequently, grids were placed in a drop of Sato lead stain and incubated for 2 minutes, rinsed 3 times with pure

water, and dried with Whatman filter paper. Images were collected using a FEI Tecnai-12 transmission electron microscope.

5.12 Immunoblotting

For protein extraction, cells were washed with cold 1x PBS and lysed in buffer containing the following: 50 mM Tris-HCl pH 7.4, 150 mM NaCl, 1% Triton X-100, 0.5% sodium deoxycholate, 1 mM EDTA, 10 mM NaF, 1 mM DTT, 1 mM EGTA. For cell lysates, lysis buffer was supplemented with a 1x protease inhibitor cocktail (Sigma, Cat. No. P2714).

For tissue samples, brain hemispheres were homogenized in the above-described lysis buffer supplemented with 1x protease and phosphatase inhibitor cocktail (Sigma, Cat. No. PPC1010) using the Precellys CK14 lysing kit (Bertin corp., Cat. No. P000933-LYSK0-A). Homogenates were then centrifuged at 12000 rpm for 10 minutes at 4°C (Eppendorf, Centrifuge 5424). Supernatants were collected and aliquoted in fresh tubes, and stored at -80°C.

Total protein concentration was measured with the Bicinchronic Acid (BCA) assay kit (Thermo Scientific, Cat. No. 23225). Equal aliquots of protein (20-30 µg) were subjected to SDS-PAGE (7.5%, 10%, or 15% polyacrylamide gels), transferred to a nitrocellulose membrane using the Trans-Blot® Turbo™ Transfer System (Bio-Rad). Membranes were blocked with 5% non-fat dry milk or BSA (PBST 0.1%) and processed for incubation with primary and secondary HRP-conjugated antibodies (**Table 5**). After incubations, membranes were washed and reacted with enhanced chemiluminescence (ECL) reagent (Bio-Rad, Cat. No. 1705061). Images were acquired on Bio-Rad ChemiDoc Imager, and quantifications were done using the Image Lab 6.0.1 software (Bio-Rad).

5.13 Fluorescence microscopy

Cells seeded on *ad hoc*-coated glass coverslips were washed with 1x PBS, fixed with 2-4% paraformaldehyde for 10 minutes, and incubated with 0.1 M glycine for 10 minutes. For LC3 puncta imaging, PK-hLC3-expressing Neuro-2a cells were directly imaged by confocal microscopy (Leica TCS SP5) equipped with an HCX PL APO lambda blue 63.0x1.40 OIL UV objective. Stacks (1024X1024) were post-processed to generate maximal projections of Z-stacks (acquired with a 0.3 µm step).

For primary cultures characterization, cortical neurons were permeabilized with 0.1% Triton X-100 (in 1x PBS) for 10 minutes, blocked in a solution composed of 1x PBS, 0.1% Triton X-100, 10% donkey serum (Sigma) for 1.5 hours at room temperature, and then stained with specific primary antibodies (**Table 5**) diluted in 1x PBS, 0.1% Triton X-100, 0.1% donkey serum overnight at 4°C. The next day, samples were incubated in donkey secondary antibodies Alexa 488, Alexa 555, and Alexa 546 (**Table 5**). Samples were incubated with Hoechst 33342 (Sigma) for nuclei counterstaining. Images were acquired using Olympus BX52 microscope with x40 and x63 objectives, equipped with Leica CCD Microscope DFC3000G and DMC2900 cameras to obtain 16-bit light and fluorescence images (1296x966 pixels).

5.14 Antibodies

Table 5 – List of antibodies used in the present study and suppliers.

	Brand	*Cat. No.*	*Dilution*	*Application*
Primary antibodies				
LC3B	Novus Bio	NB100-2220	1:1000	WB
P62/SQSTM1 (2C11)	Novus Bio	H00008878-M01	1:1000	WB
HIF-1α (D2U3T)	Cell Signalling	14179	1:1000	WB
p70 S6 Kinase	Cell Signalling	9202	1:1000	WB
Phospho-p70 S6 Kinase (Thr389)	Cell Signalling	9205	1:1000	WB
β-Actin	Sigma	A1978	1:20000	WB
MAP2	Millipore	AB5622	1:250	IF
MAP2	Millipore	MAB3418	1:250	IF
TUJ1	BioLegend	801202	1:100	IF

	Brand	*Cat. No.*	*Dilution*	*Application*
GFAP	Agilent	Z0334	1:500	IF
Secondary antibodies				
Goat Anti-Rabbit IgG-HRP Conjugated	Bio-Rad	1706515	1:3000	WB
Goat Anti-Mouse IgG-HRP Conjugated	Bio-Rad	1706516	1:3000	WB
Goat Anti-Mouse IgG, Alexa Fluor 488	Thermo Fisher	a21202	1:500	IF
Goat Anti-Mouse IgG, Alexa Fluor488	Thermo Fisher	a21206	1:500	IF
Donkey Anti-Rabbit IgG, Alexa Fluor 555	Thermo Fisher	a31572	1:500	IF
Donkey Anti-Mouse IgG, Alexa Fluor 546	Immunological Sciences	IS20305	1:500	IF

5.15 Statistical analysis

Statistical analyses were performed using GraphPad Prism 9 software (GraphPad Software, LLC). Results are expressed as the mean value ± the standard deviation of the mean (SD). Comparisons were made using the following statistical tests: unpaired Student's *t*-test, one-way or two-way Analysis of Variance (ANOVA), followed by Tukey's or Šídák's multiple comparison tests. *p* values lower than 0.05 were considered statistically significant.

Mathematical formulae of statistical measures used for the screening assay development and validation are herein reported. Values include means (μ), and standard deviations (σ).

$$Z'\text{-}factor = 1 - \frac{3\,(\sigma_{samples} + \sigma_{controls})}{|\mu_{samples} - \mu_{controls}|}$$

$$SSMD = \frac{\mu_{samples} - \mu_{controls}}{\sqrt{{\sigma_{samples}}^2 + {\sigma_{controls}}^2}}$$

$$S/N = \frac{\mu(C_{pos}) - \mu(C_{neg})}{\sqrt{\sigma(C_{pos})^2 + \sigma(C_{neg})^2}}$$

$$Robust\ Z\text{-}score = \frac{S_i - median(S_{all})}{MAD(S_{all})}$$

$$MAD(S_{all}) = 1.4826 \times median(|S_i - median(S_{all})|)$$

Table 6 – Ranges for statistical parameters used to assess assay quality.

Statistical parameter	*Assay quality*	*Range*
Z'-factor	Very good	0.5 ≤ Z' < 1
	Acceptable	0 ≤ Z' < 0.5
	Unacceptable	Z' < 0
Strictly Standardized Mean Difference	Excellent	β ≥ 4.7; β ≤ -4.7
	Good	3 > β ≥ 4.7; -4.7 < β ≤ -3
	Inferior	2 > β ≥ 3; -3 < β ≤ -2
	Poor	β ≥ 2; β ≤ -2

Table 7 – Ranges for statistical parameters used for lead-like compounds selection.

Robust Z-score	*p-value*	*Confidence level*
< -1.65 or > 1.65	< 0.1	90%
< -1.96 or > 1.96	< 0.05	95%
< -2.58 or > 2.58	< 0.01	99%

6. REFERENCES

Adams HP, Bendixen BH, Kappelle LJ, Biller J, Love BB, Gordon DL & Marsh EE (1993) Classification of subtype of acute ischemic stroke. Definitions for use in a multicenter clinical trial. TOAST. Trial of Org 10172 in Acute Stroke Treatment. *Stroke* 24: 35–41

Adhami F, Liao G, Morozov YM, Schloemer A, Schmithorst VJ, Lorenz JN, Dunn RS, Vorhees CV, Wills-Karp M, Degen JL, *et al* (2006) Cerebral Ischemia-Hypoxia Induces Intravascular Coagulation and Autophagy. *Am J Pathol* 169: 566–583

Akpinar A, Uğuz AC & Nazıroğlu M (2014) Agomelatine and Duloxetine Synergistically Modulates Apoptotic Pathway by Inhibiting Oxidative Stress Triggered Intracellular Calcium Entry in Neuronal PC12 Cells: Role of TRPM2 and Voltage-Gated Calcium Channels. *J Membr Biol* 247: 451–459

Alemu EA, Lamark T, Torgersen KM, Birgisdottir AB, Larsen KB, Jain A, Olsvik H, Øvervatn A, Kirkin V & Johansen T (2012) ATG8 Family Proteins Act as Scaffolds for Assembly of the ULK Complex: SEQUENCE REQUIREMENTS FOR LC3-INTERACTING REGION (LIR) MOTIFS *. *J Biol Chem* 287: 39275–39290

Althaus J, Bernaudin M, Petit E, Toutain J, Touzani O & Rami A (2006) Expression of the gene encoding the pro-apoptotic BNIP3 protein and stimulation of hypoxia-inducible factor-1alpha (HIF-1alpha) protein following focal cerebral ischemia in rats. *Neurochem Int* 48: 687–695

Amarenco P, Bogousslavsky J, Caplan LR, Donnan GA & Hennerici MG (2009) Classification of stroke subtypes. *Cerebrovasc Dis Basel Switz* 27: 493–501

Aminzadeh S, Vidali S, Sperl W, Kofler B & Feichtinger RG (2015) Energy metabolism in neuroblastoma and Wilms tumor. *Transl Pediatr* 4: 202–232

Axe EL, Walker SA, Manifava M, Chandra P, Roderick HL, Habermann A, Griffiths G & Ktistakis NT (2008) Autophagosome formation from membrane compartments enriched in phosphatidylinositol 3-phosphate and dynamically connected to the endoplasmic reticulum. *J Cell Biol* 182: 685–701

Ay H, Benner T, Arsava EM, Furie KL, Singhal AB, Jensen MB, Ayata C, Towfighi A, Smith EE, Chong JY, *et al* (2007) A computerized algorithm for etiologic classification of ischemic stroke: the Causative Classification of Stroke System. *Stroke* 38: 2979–2984

Bach A (2017) Targeting Oxidative Stress in Stroke. In *Neuroprotective Therapy for Stroke and Ischemic Disease*, Lapchak PA & Zhang JH (eds) pp 203–250. Springer International Publishing

Bacigaluppi M, Pluchino S, Peruzzotti-Jametti L, Jametti LP, Kilic E, Kilic U, Salani G, Brambilla E, West MJ, Comi G, *et al* (2009) Delayed post-ischaemic neuroprotection following systemic neural stem cell transplantation involves multiple mechanisms. *Brain J Neurol* 132: 2239–2251

Balduini W, Carloni S & Buonocore G (2012) Autophagy in hypoxia-ischemia induced brain injury. *J Matern-Fetal Neonatal Med Off J Eur Assoc Perinat Med Fed Asia Ocean Perinat Soc Int Soc Perinat Obstet* 25 Suppl 1: 30–34

Balin B, Abrams JT & Schrogie J (2011) Toward a Unifying Hypothesis in the Development of Alzheimer's Disease. *CNS Neurosci Ther* 17: 587–589

Bar-Peled L & Sabatini DM (2014) Regulation of mTORC1 by amino acids. *Trends Cell Biol* 24: 400–406

Beghi E, Binder H, Birle C, Bornstein N, Diserens K, Groppa S, Homberg V, Lisnic V, Pugliatti M, Randall G, *et al* (2021) European Academy of Neurology and European Federation of Neurorehabilitation Societies guideline on pharmacological support in early motor rehabilitation after acute ischaemic stroke. *Eur J Neurol* 28: 2831–2845

Berardelli A & Cruccu G (2015) La Neurologia della Sapienza Società Editrice Esculapio, Roma

Berezniuk I & Fricker LD (2010) A defect in cytosolic carboxypeptidase 1 (Nna1) causes autophagy in Purkinje cell degeneration mouse brain. *Autophagy* 6: 558–559

Birgisdottir ÅB, Lamark T & Johansen T (2013) The LIR motif - crucial for selective autophagy. *J Cell Sci* 126: 3237–3247

Bjørkøy G, Lamark T, Brech A, Outzen H, Perander M, Øvervatn A, Stenmark H & Johansen T (2005) p62/SQSTM1 forms protein aggregates degraded by autophagy and has a protective effect on huntingtin-induced cell death. *J Cell Biol* 171: 603–614

Bootman MD, Chehab T, Bultynck G, Parys JB & Rietdorf K (2018) The regulation of autophagy by calcium signals: Do we have a consensus? *Cell Calcium* 70: 32–46

Bouhassira D, Wilhelm S, Schacht A, Perrot S, Kosek E, Cruccu G, Freynhagen R, Tesfaye S, Lledó A, Choy E, *et al* (2014) Neuropathic pain phenotyping as a predictor of treatment response in painful diabetic neuropathy: Data from the randomized, double-blind, COMBO-DN study. *PAIN* 155: 2171–2179

Bourdenx M, Martín-Segura A, Scrivo A, Rodriguez-Navarro JA, Kaushik S, Tasset I, Diaz A, Storm NJ, Xin Q, Juste YR, *et al* (2021) Chaperone-mediated autophagy prevents collapse of the neuronal metastable proteome. *Cell* 184: 2696-2714.e25

Braeuninger S & Kleinschnitz C (2009) Rodent models of focal cerebral ischemia: procedural pitfalls and translational problems. *Exp Transl Stroke Med* 1: 8

Buckley KM, Hess DL, Sazonova IY, Periyasamy-Thandavan S, Barrett JR, Kirks R, Grace H, Kondrikova G, Johnson MH, Hess DC, *et al* (2014) Rapamycin up-regulation of autophagy reduces infarct size and improves outcomes in both permanent MCAL, and embolic MCAO, murine models of stroke. *Exp Transl Stroke Med* 6: 8

Burrows RC, Wancio D, Levitt P & Lillien L (1997) Response diversity and the timing of progenitor cell maturation are regulated by developmental changes in EGFR expression in the cortex. *Neuron* 19: 251–267

Cabezudo S, Sanz-Flores M, Caballero A, Tasset I, Rebollo E, Diaz A, Aragay AM, Cuervo AM, Mayor F & Ribas C (2021) Gαq activation modulates autophagy by promoting mTORC1 signaling. *Nat Commun* 12: 4540

Cairns J, Ly RC, Niu N, Kalari KR, Carlson EE & Wang L (2020) CDC25B partners with PP2A to induce AMPK activation and tumor suppression in triple negative breast cancer. *NAR Cancer* 2: zcaa039

Candelario-Jalil E, González-Falcón A, García-Cabrera M, León OS & Fiebich BL (2007) Post-ischaemic treatment with the cyclooxygenase-2 inhibitor nimesulide reduces blood-brain barrier disruption and leukocyte infiltration following transient focal cerebral ischaemia in rats. *J Neurochem* 100: 1108–1120

Carloni S, Buonocore G & Balduini W (2008) Protective role of autophagy in neonatal hypoxia-ischemia induced brain injury. *Neurobiol Dis* 32: 329–339

Carroll B, Mohd-Naim N, Maximiano F, Frasa MA, McCormack J, Finelli M, Thoresen SB, Perdios L, Daigaku R, Francis RE, *et al* (2013) The TBC/RabGAP Armus Coordinates Rac1 and Rab7 Functions during Autophagy. *Dev Cell* 25: 15–28

Chen G, Han Z, Feng D, Chen Y, Chen L, Wu H, Huang L, Zhou C, Cai X, Fu C, *et al* (2014) A regulatory signaling loop comprising the PGAM5 phosphatase and CK2 controls receptor-mediated mitophagy. *Mol Cell* 54: 362–377

Chen T-Y, Huang B-M, Tang TK, Chao Y-Y, Xiao X-Y, Lee P-R, Yang L-Y & Wang C-Y (2021) Genotoxic stress-activated DNA-PK-p53 cascade and autophagy cooperatively induce ciliogenesis to maintain the DNA damage response. *Cell Death Differ* 28: 1865–1879

Cherra SJ, Kulich SM, Uechi G, Balasubramani M, Mountzouris J, Day BW & Chu CT (2010) Regulation of the autophagy protein LC3 by phosphorylation. *J Cell Biol* 190: 533–539

Choi DW & Rothman SM (1990) The Role of Glutamate Neurotoxicity in Hypoxic-Ischemic Neuronal Death. *Annu Rev Neurosci* 13: 171–182

Cole A, Wang Z, Coyaud E, Voisin V, Gronda M, Jitkova Y, Mattson R, Hurren R, Babovic S, Maclean N, *et al* (2015) Inhibition of the Mitochondrial Protease ClpP as a Therapeutic Strategy for Human Acute Myeloid Leukemia. *Cancer Cell* 27: 864–876

Cuervo AM (2004) Autophagy: many paths to the same end. *Mol Cell Biochem* 263: 55–72

Cuervo AM, Bergamini E, Brunk UT, Dröge W, Ffrench M & Terman A (2005) Autophagy and Aging: The Importance of Maintaining 'Clean' Cells. *Autophagy* 1: 131–140

Cuervo AM & Dice JF (1996) A receptor for the selective uptake and degradation of proteins by lysosomes. *Science* 273: 501–503

Daskalaki I, Gkikas I & Tavernarakis N (2018) Hypoxia and Selective Autophagy in Cancer Development and Therapy. *Front Cell Dev Biol* 6: 104

Demirdaş A, Nazıroğlu M & Övey İS (2017) Duloxetine Reduces Oxidative Stress, Apoptosis, and Ca2+ Entry Through Modulation of TRPM2 and TRPV1 Channels in the Hippocampus and Dorsal Root Ganglion of Rats. *Mol Neurobiol* 54: 4683–4695

Deng Y, He H, Yang L & Zhang P (2016) Dynamic changes in neuronal autophagy and apoptosis in the ischemic penumbra following permanent ischemic stroke. *Neural Regen Res* 11: 1108–1114

Di Malta C, Siciliano D, Calcagni A, Monfregola J, Punzi S, Pastore N, Eastes AN, Davis O, De Cegli R, Zampelli A, *et al* (2017) Transcriptional activation of RagD GTPase controls mTORC1 and promotes cancer growth. *Science* 356: 1188–1192

Dikic I & Elazar Z (2018) Mechanism and medical implications of mammalian autophagy. *Nat Rev Mol Cell Biol* 19: 349–364

Ding W-X, Ni H-M, Gao W, Hou Y-F, Melan MA, Chen X, Stolz DB, Shao Z-M & Yin X-M (2007) Differential effects of endoplasmic reticulum stress-induced autophagy on cell survival. *J Biol Chem* 282: 4702–4710

Djouder N, Tuerk RD, Suter M, Salvioni P, Thali RF, Scholz R, Vaahtomeri K, Auchli Y, Rechsteiner H, Brunisholz RA, *et al* (2010) PKA phosphorylates and inactivates AMPKalpha to promote efficient lipolysis. *EMBO J* 29: 469–481

Dohi E, Tanaka S, Seki T, Miyagi T, Hide I, Takahashi T, Matsumoto M & Sakai N (2012) Hypoxic stress activates chaperone-mediated autophagy and modulates neuronal cell survival. *Neurochem Int* 60: 431–442

Dutta S, Rutkai I, Katakam PVG & Busija DW (2015) The mechanistic target of rapamycin (mTOR) pathway and S6 Kinase mediate diazoxide preconditioning in primary rat cortical neurons. *J Neurochem* 134: 845–856

Eales KL, Hollinshead KER & Tennant DA (2016) Hypoxia and metabolic adaptation of cancer cells. *Oncogenesis* 5: e190

Estevez AY & Phillis JW (1997) The phospholipase A2 inhibitor, quinacrine, reduces infarct size in rats after transient middle cerebral artery occlusion. *Brain Res* 752: 203–208

Ferrarini I, Louie A, Zhou L & El-Deiry WS (2021) ONC212 is a Novel Mitocan Acting Synergistically with Glycolysis Inhibition in Pancreatic Cancer. *Mol Cancer Ther* 20: 1572–1583

Ferrer I, Alcántara S, Ballabriga J, Olivé M, Blanco R, Rivera R, Carmona M, Berruezo M, Pitarch S & Planas AM (1996) Transforming growth factor-alpha (TGF-alpha) and epidermal growth factor-receptor (EGF-R) immunoreactivity in normal and pathologic brain. *Prog Neurobiol* 49: 99–123

Fitridge R & Thompson M eds. (2011) Mechanisms of Vascular Disease: A Reference Book for Vascular Specialists Adelaide (AU): University of Adelaide Press

Förstermann U (2010) Nitric oxide and oxidative stress in vascular disease. *Pflugers Arch* 459: 923–939

Gao J, Langemeyer L, Kümmel D, Reggiori F & Ungermann C (2018) Molecular mechanism to target the endosomal Mon1-Ccz1 GEF complex to the pre-autophagosomal structure. *eLife* 7: e31145

Gao K, Wang G, Wang Y, Han D, Bi J, Yuan Y, Yao T, Wan Z, Li H & Mei X (2015) Neuroprotective Effect of Simvastatin via Inducing the Autophagy on Spinal Cord Injury in the Rat Model. *BioMed Res Int* 2015: e260161

GBD 2019 Stroke Collaborators (2021) Global, regional, and national burden of stroke and its risk factors, 1990–2019: a systematic analysis for the Global Burden of Disease Study 2019 - The Lancet Neurology. *The Lancet*

Ge L, Melville D, Zhang M & Schekman R (2013) The ER–Golgi intermediate compartment is a key membrane source for the LC3 lipidation step of autophagosome biogenesis. *eLife* 2: e00947

Geng J & Klionsky DJ (2008) The Atg8 and Atg12 ubiquitin-like conjugation systems in macroautophagy. 'Protein modifications: beyond the usual suspects' review series. *EMBO Rep* 9: 859–864

Girouard H, Wang G, Gallo EF, Anrather J, Zhou P, Pickel VM & Iadecola C (2009) NMDA Receptor Activation Increases Free Radical Production through Nitric Oxide and NOX2. *J Neurosci* 29: 2545–2552

Gogela SL, Abruzzo TA & Zuccarello M (2017) Modern Endovascular Treatment of Ischemic Disease. In *Neuroprotective Therapy for Stroke and Ischemic Disease*, Lapchak PA & Zhang JH (eds) pp 501–526. Springer International Publishing

Goktug AN, Chai SC & Chen T (2013) Data Analysis Approaches in High Throughput Screening IntechOpen

Golden EB, Cho H-Y, Hofman FM, Louie SG, Schönthal AH & Chen TC (2015) Quinoline-based antimalarial drugs: a novel class of autophagy inhibitors. *Neurosurg Focus* 38: E12

Goldstein LB, Adams R, Alberts MJ, Appel LJ, Brass LM, Bushnell CD, Culebras A, Degraba TJ, Gorelick PB, Guyton JR, *et al* (2006) Primary prevention of ischemic stroke: a guideline from the American Heart Association/American Stroke Association Stroke Council: cosponsored by the Atherosclerotic Peripheral Vascular Disease Interdisciplinary Working Group; Cardiovascular Nursing Council; Clinical Cardiology Council; Nutrition, Physical Activity, and Metabolism Council; and the Quality of Care and Outcomes Research Interdisciplinary Working Group: the

American Academy of Neurology affirms the value of this guideline. *Stroke* 37: 1583–1633

Gómez-Pinilla F, Knauer DJ & Nieto-Sampedro M (1988) Epidermal growth factor receptor immunoreactivity in rat brain. Development and cellular localization. *Brain Res* 438: 385–390

Gómez-Sánchez R, Tooze SA & Reggiori F (2021) Membrane supply and remodeling during autophagosome biogenesis. *Curr Opin Cell Biol* 71: 112–119

González A & Hall MN (2017) Nutrient sensing and TOR signaling in yeast and mammals. *EMBO J* 36: 397–408

Grishchuk Y, Ginet V, Truttmann AC, Clarke PGH & Puyal J (2011) Beclin 1-independent autophagy contributes to apoptosis in cortical neurons. *Autophagy* 7: 1115–1131

Guardia CM, Tan X-F, Lian T, Rana MS, Zhou W, Christenson ET, Lowry AJ, Faraldo-Gómez JD, Bonifacino JS, Jiang J, *et al* (2020) Structure of Human ATG9A, the Only Transmembrane Protein of the Core Autophagy Machinery. *Cell Rep* 31: 107837

Gunn A, Singh A, Diao3 A & Chen R (2018) Pharmacological Modulation of Autophagy for Neuroprotection in Ischaemic Stroke. *J Exp Stroke Transl Med* 11: 1–10

Guo K, Searfoss G, Krolikowski D, Pagnoni M, Franks C, Clark K, Yu KT, Jaye M & Ivashchenko Y (2001) Hypoxia induces the expression of the pro-apoptotic gene BNIP3. *Cell Death Differ* 8: 367–376

Gutierrez MG, Munafó DB, Berón W & Colombo MI (2004) Rab7 is required for the normal progression of the autophagic pathway in mammalian cells. *J Cell Sci* 117: 2687–2697

Hamasaki M, Furuta N, Matsuda A, Nezu A, Yamamoto A, Fujita N, Oomori H, Noda T, Haraguchi T, Hiraoka Y, *et al* (2013) Autophagosomes form at ER–mitochondria contact sites. *Nature* 495: 389–393

Hara T, Takamura A, Kishi C, Iemura S-I, Natsume T, Guan J-L & Mizushima N (2008) FIP200, a ULK-interacting protein, is required for autophagosome formation in mammalian cells. *J Cell Biol* 181: 497–510

Harper JW, Ordureau A & Heo J-M (2018) Building and decoding ubiquitin chains for mitophagy. *Nat Rev Mol Cell Biol* 19: 93–108

Hata R, Maeda K, Hermann D, Mies G & Hossmann KA (2000) Evolution of brain infarction after transient focal cerebral ischemia in mice. *J Cereb Blood Flow Metab Off J Int Soc Cereb Blood Flow Metab* 20: 937–946

Haugaard-Kedström LM, Fernandes EFA & Strømgaard K (2017) Targeting PSD-95 as a Novel Approach in the Treatment of Stroke. In *Neuroprotective Therapy for Stroke and Ischemic Disease*, Lapchak PA & Zhang JH (eds) pp 157–184. Cham: Springer International Publishing

Hegedűs K, Takáts S, Boda A, Jipa A, Nagy P, Varga K, Kovács AL & Juhász G (2016) The Ccz1-Mon1-Rab7 module and Rab5 control distinct steps of autophagy. *Mol Biol Cell* 27: 3132–3142

Heiss W-D (2011) The ischemic penumbra: correlates in imaging and implications for treatment of ischemic stroke. The Johann Jacob Wepfer award 2011. *Cerebrovasc Dis Basel Switz* 32: 307–320

Hermann DM, Kilic E, Hata R, Hossmann KA & Mies G (2001) Relationship between metabolic dysfunctions, gene responses and delayed cell death after mild focal cerebral ischemia in mice. *Neuroscience* 104: 947–955

Herzig S & Shaw RJ (2018) AMPK: guardian of metabolism and mitochondrial homeostasis. *Nat Rev Mol Cell Biol* 19: 121–135

Hill MD, Goyal M, Menon BK, Nogueira RG, McTaggart RA, Demchuk AM, Poppe AY, Buck BH, Field TS, Dowlatshahi D, *et al* (2020) Efficacy and safety of nerinetide for the treatment of acute ischaemic stroke (ESCAPE-NA1): a multicentre, double-blind, randomised controlled trial. *Lancet Lond Engl* 395: 878–887

Hong JM, Choi MH, Sohn S-I, Hwang Y-H, Ahn SH, Lee Y-B, Shin D-I, Chamorro Á, Choi DW, Hong JM, *et al* (2018) Safety and Optimal Neuroprotection of neu2000 in acute Ischemic stroke with reCanalization: study protocol for a randomized, double-blinded, placebo-controlled, phase-II trial. *Trials* 19: 375

Hongyun H, Tao G, Pengyue Z, Liqiang Y & Yihao D (2017) Puerarin provides a neuroprotection against transient cerebral ischemia by attenuating autophagy at the ischemic penumbra in neurons but not in astrocytes. *Neurosci Lett* 643: 45–51

Høyer-Hansen M, Bastholm L, Szyniarowski P, Campanella M, Szabadkai G, Farkas T, Bianchi K, Fehrenbacher N, Elling F, Rizzuto R, *et al* (2007) Control of macroautophagy by calcium, calmodulin-dependent kinase kinase-beta, and Bcl-2. *Mol Cell* 25: 193–205

Hsu C-C, Chang C-W, Peng C-H & Liang C-S (2014) Rapid Management of Trigeminal Neuralgia and Comorbid Major Depressive Disorder With Duloxetine. *Ann Pharmacother* 48: 1090–1092

Huang L, Chen C, Zhang X, Li X, Chen Z, Yang C, Liang X, Zhu G & Xu Z (2018) Neuroprotective Effect of Curcumin Against Cerebral Ischemia-Reperfusion Via Mediating Autophagy and Inflammation. *J Mol Neurosci MN* 64: 129–139

Hwang J-Y, Gertner M, Pontarelli F, Court-Vazquez B, Bennett MVL, Ofengeim D & Zukin RS (2017) Global ischemia induces lysosomal-mediated degradation of mTOR and activation of autophagy in hippocampal neurons destined to die. *Cell Death Differ* 24: 317–329

Ichimura Y, Kirisako T, Takao T, Satomi Y, Shimonishi Y, Ishihara N, Mizushima N, Tanida I, Kominami E, Ohsumi M, *et al* (2000) A ubiquitin-like system mediates protein lipidation. *Nature* 408: 488–492

Inoki K, Zhu T & Guan K-L (2003) TSC2 mediates cellular energy response to control cell growth and survival. *Cell* 115: 577–590

Ishizawa J, Zarabi SF, Davis RE, Halgas O, Nii T, Jitkova Y, Zhao R, St-Germain J, Heese LE, Egan G, *et al* (2019) Mitochondrial ClpP-Mediated Proteolysis Induces Selective Cancer Cell Lethality. *Cancer Cell* 35: 721-737.e9

Itakura E & Mizushima N (2010) Characterization of autophagosome formation site by a hierarchical analysis of mammalian Atg proteins. *Autophagy* 6: 764–776

Jäger S, Bucci C, Tanida I, Ueno T, Kominami E, Saftig P & Eskelinen E-L (2004) Role for Rab7 in maturation of late autophagic vacuoles. *J Cell Sci* 117: 4837–4848

Jiang P, Nishimura T, Sakamaki Y, Itakura E, Hatta T, Natsume T & Mizushima N (2014) The HOPS complex mediates autophagosome–lysosome fusion through interaction with syntaxin 17. *Mol Biol Cell* 25: 1327–1337

Jung CH, Jun CB, Ro S-H, Kim Y-M, Otto NM, Cao J, Kundu M & Kim D-H (2009) ULK-Atg13-FIP200 complexes mediate mTOR signaling to the autophagy machinery. *Mol Biol Cell* 20: 1992–2003

Kaushik S & Cuervo AM (2018) The coming of age of chaperone-mediated autophagy. *Nat Rev Mol Cell Biol* 19: 365–381

Kelmanson IV, Shokhina AG, Kotova DA, Pochechuev MS, Ivanova AD, Kostyuk AI, Panova AS, Borodinova AA, Solotenkov MA, Stepanov EA, *et al* (2021) In vivo

dynamics of acidosis and oxidative stress in the acute phase of an ischemic stroke in a rodent model. *Redox Biol* 48: 102178

Kim HA, Mahato RI & Lee M (2009) Hypoxia-specific gene expression for ischemic disease gene therapy. *Adv Drug Deliv Rev* 61: 614–622

Kim J, Kundu M, Viollet B & Guan K-L (2011) AMPK and mTOR regulate autophagy through direct phosphorylation of Ulk1. *Nat Cell Biol* 13: 132–141

Kim J-M, Byun J-S, Kim J, Park M-S, Hong SA, Nam T-K, Choi HH, Hong S, Han S-H, Jeong H-B, *et al* (2021) Analysis of microRNA signatures in ischemic stroke thrombus. *J NeuroInterventional Surg*

Kirkin V & Rogov VV (2019) A Diversity of Selective Autophagy Receptors Determines the Specificity of the Autophagy Pathway. *Mol Cell* 76: 268–285

Klionsky DJ, Abdel-Aziz AK, Abdelfatah S, Abdellatif M, Abdoli A, Abel S, Abeliovich H, Abildgaard MH, Abudu YP, Acevedo-Arozena A, *et al* (2021) Guidelines for the use and interpretation of assays for monitoring autophagy (4th edition)1. *Autophagy* 17: 1–382

Koike M, Shibata M, Tadakoshi M, Gotoh K, Komatsu M, Waguri S, Kawahara N, Kuida K, Nagata S, Kominami E, *et al* (2008) Inhibition of autophagy prevents hippocampal pyramidal neuron death after hypoxic-ischemic injury. *Am J Pathol* 172: 454–469

Koyano F, Okatsu K, Kosako H, Tamura Y, Go E, Kimura M, Kimura Y, Tsuchiya H, Yoshihara H, Hirokawa T, *et al* (2014) Ubiquitin is phosphorylated by PINK1 to activate parkin. *Nature* 510: 162–166

Krick R, Muehe Y, Prick T, Bremer S, Schlotterhose P, Eskelinen E-L, Millen J, Goldfarb DS & Thumm M (2008) Piecemeal Microautophagy of the Nucleus Requires the Core Macroautophagy Genes. *Mol Biol Cell* 19: 4492–4505

Lapchak PA & Boitano PD (2017) Reflections on Neuroprotection Research and the Path Toward Clinical Success. In *Neuroprotective Therapy for Stroke and Ischemic Disease*, Lapchak PA & Zhang JH (eds) pp 3–71. Springer International Publishing

Leahy JJJ, Golding BT, Griffin RJ, Hardcastle IR, Richardson C, Rigoreau L & Smith GCM (2004) Identification of a highly potent and selective DNA-dependent protein kinase (DNA-PK) inhibitor (NU7441) by screening of chromenone libraries. *Bioorg Med Chem Lett* 14: 6083–6087

Lee Y-K & Lee J-A (2016) Role of the mammalian ATG8/LC3 family in autophagy: differential and compensatory roles in the spatiotemporal regulation of autophagy. *BMB Rep* 49: 424–430

Levine B & Kroemer G (2008) Autophagy in the pathogenesis of disease. *Cell* 132: 27–42

Li H, Peng D, Zhang S-J, Zhang Y, Wang Q & Guan L (2021) Buyang Huanwu Decoction promotes neurogenesis via sirtuin 1/autophagy pathway in a cerebral ischemia model. *Mol Med Rep* 24: 791

Li Q, Zhang T, Wang J, Zhang Z, Zhai Y, Yang G-Y & Sun X (2014) Rapamycin attenuates mitochondrial dysfunction via activation of mitophagy in experimental ischemic stroke. *Biochem Biophys Res Commun* 444: 182–188

Li W-L, Yu SP, Chen D, Yu SS, Jiang Y-J, Genetta T & Wei L (2013) The regulatory role of NF-κB in autophagy-like cell death after focal cerebral ischemia in mice. *Neuroscience* 244: 16–30

Liang C, Feng P, Ku B, Dotan I, Canaani D, Oh B-H & Jung JU (2006) Autophagic and tumour suppressor activity of a novel Beclin1-binding protein UVRAG. *Nat Cell Biol* 8: 688–699

Liang C, Lee J, Inn K, Gack MU, Li Q, Roberts EA, Vergne I, Deretic V, Feng P, Akazawa C, *et al* (2008) Beclin1-binding UVRAG targets the class C Vps complex to coordinate autophagosome maturation and endocytic trafficking. *Nat Cell Biol* 10: 776–787

Lin P & Ye RD (2003) The lysophospholipid receptor G2A activates a specific combination of G proteins and promotes apoptosis. *J Biol Chem* 278: 14379–14386

Liu B, Chen H, Johns TG & Neufeld AH (2006) Epidermal growth factor receptor activation: an upstream signal for transition of quiescent astrocytes into reactive astrocytes after neural injury. *J Neurosci Off J Soc Neurosci* 26: 7532–7540

Liu N, Peng A, Sun H, Zhuang Y, Yu M, Wang Q & Wang J (2021) LncRNA AC136007.2 alleviates cerebral ischemic-reperfusion injury by suppressing autophagy. *Aging* 13: 19587–19597

Liu RR & Murphy TH (2009) Reversible cyclosporin A-sensitive mitochondrial depolarization occurs within minutes of stroke onset in mouse somatosensory cortex in vivo: a two-photon imaging study. *J Biol Chem* 284: 36109–36117

Long J, Garner TP, Pandya MJ, Craven CJ, Chen P, Shaw B, Williamson MP, Layfield R & Searle MS (2010) Dimerisation of the UBA domain of p62 inhibits ubiquitin binding and regulates NF-kappaB signalling. *J Mol Biol* 396: 178–194

Longatti A, Lamb CA, Razi M, Yoshimura S, Barr FA & Tooze SA (2012) TBC1D14 regulates autophagosome formation via Rab11- and ULK1-positive recycling endosomes. *J Cell Biol* 197: 659–675

Lu J, He L, Behrends C, Araki M, Araki K, Jun Wang Q, Catanzaro JM, Friedman SL, Zong W-X, Fiel MI, *et al* (2014) NRBF2 regulates autophagy and prevents liver injury by modulating Atg14L-linked phosphatidylinositol-3 kinase III activity. *Nat Commun* 5: 3920

Lum JJ, Bauer DE, Kong M, Harris MH, Li C, Lindsten T & Thompson CB (2005) Growth factor regulation of autophagy and cell survival in the absence of apoptosis. *Cell* 120: 237–248

Ma D, Chen X, Zhang P-Y, Zhang H, Wei L-J, Hu S, Tang J-Z, Zhou M-T, Xie C, Ou R, *et al* (2018) Upregulation of the ALDOA/DNA-PK/p53 pathway by dietary restriction suppresses tumor growth. *Oncogene* 37: 1041–1048

Ma X, Zhang S, He L, Rong Y, Brier LW, Sun Q, Liu R, Fan W, Chen S, Yue Z, *et al* (2017) MTORC1-mediated NRBF2 phosphorylation functions as a switch for the class III PtdIns3K and autophagy. *Autophagy* 13: 592–607

Macdonald RL & Stoodley M (1998) Pathophysiology of cerebral ischemia. *Neurol Med Chir (Tokyo)* 38: 1–11

Maeda S, Otomo C & Otomo T (2019) The autophagic membrane tether ATG2A transfers lipids between membranes. *eLife* 8: e45777

Malik R, Chauhan G, Traylor M, Sargurupremraj M, Okada Y, Mishra A, Rutten-Jacobs L, Giese A-K, van der Laan SW, Gretarsdottir S, *et al* (2018) Multiancestry genome-wide association study of 520,000 subjects identifies 32 loci associated with stroke and stroke subtypes. *Nat Genet* 50: 524–537

Mateos L, Perez-Alvarez MJ & Wandosell F (2016) Angiotensin II type-2 receptor stimulation induces neuronal VEGF synthesis after cerebral ischemia. *Biochim Biophys Acta* 1862: 1297–1308

Mathew R, Karantza-Wadsworth V & White E (2007) Role of autophagy in cancer. *Nat Rev Cancer* 7: 961–967

Matoba K & Noda NN (2020) Secret of Atg9: lipid scramblase activity drives de novo autophagosome biogenesis. *Cell Death Differ* 27: 3386–3388

Matsui Y, Takagi H, Qu X, Abdellatif M, Sakoda H, Asano T, Levine B & Sadoshima J (2007) Distinct roles of autophagy in the heart during ischemia and reperfusion: roles of AMP-activated protein kinase and Beclin 1 in mediating autophagy. *Circ Res* 100: 914–922

Medeiros R, Baglietto-Vargas D & LaFerla FM (2011) The role of tau in Alzheimer's disease and related disorders. *CNS Neurosci Ther* 17: 514–524

Meijer AJ & Codogno P (2011) Autophagy: regulation by energy sensing. *Curr Biol CB* 21: R227-229

Mejlvang J, Olsvik H, Svenning S, Bruun J-A, Abudu YP, Larsen KB, Brech A, Hansen TE, Brenne H, Hansen T, *et al* (2018) Starvation induces rapid degradation of selective autophagy receptors by endosomal microautophagy. *J Cell Biol* 217: 3640–3655

Menon S, Dibble CC, Talbott G, Hoxhaj G, Valvezan AJ, Takahashi H, Cantley LC & Manning BD (2014) Spatial control of the TSC complex integrates insulin and nutrient regulation of mTORC1 at the lysosome. *Cell* 156: 771–785

Mergenthaler P, Dirnagl U & Kunz A (2016) Ischemic Stroke: Basic Pathophysiology and Clinical Implication. In *Neuroscience in the 21st Century: From Basic to Clinical*, Pfaff DW & Volkow ND (eds) pp 3385–3405. New York, NY: Springer

Mizushima N & Komatsu M (2011) Autophagy: renovation of cells and tissues. *Cell* 147: 728–741

Mizushima N & Yoshimori T (2007) How to interpret LC3 immunoblotting. *Autophagy* 3: 542–545

Mizushima N, Yoshimori T & Ohsumi Y (2011) The role of Atg proteins in autophagosome formation. *Annu Rev Cell Dev Biol* 27: 107–132

Monastyrska I, Rieter E, Klionsky DJ & Reggiori F (2009) Multiple roles of the cytoskeleton in autophagy. *Biol Rev Camb Philos Soc* 84: 431–448

Morshed S, Tasnin MN & Ushimaru T (2020) ESCRT machinery plays a role in microautophagy in yeast. *BMC Mol Cell Biol* 21: 70

Nam H-J, Kim H-P, Yoon Y-K, Hur H-S, Song S-H, Kim M-S, Lee G-S, Han S-W, Im S-A, Kim T-Y, *et al* (2011) Antitumor activity of HM781-36B, an irreversible Pan-

HER inhibitor, alone or in combination with cytotoxic chemotherapeutic agents in gastric cancer. *Cancer Lett* 302: 155–165

National Institute of Neurological Disorders and Stroke rt-PA Stroke Study Group (1995) Tissue plasminogen activator for acute ischemic stroke. *N Engl J Med* 333: 1581–1587

Nii T, Prabhu VV, Ruvolo V, Madhukar N, Zhao R, Mu H, Heese L, Nishida Y, Kojima K, Garnett MJ, *et al* (2019) Imipridone ONC212 activates orphan G protein-coupled receptor GPR132 and integrated stress response in acute myeloid leukemia. *Leukemia* 33: 2805–2816

Nixon RA (2013) The role of autophagy in neurodegenerative disease. *Nat Med* 19: 983–997

Noda NN, Kumeta H, Nakatogawa H, Satoo K, Adachi W, Ishii J, Fujioka Y, Ohsumi Y & Inagaki F (2008) Structural basis of target recognition by Atg8/LC3 during selective autophagy. *Genes Cells Devoted Mol Cell Mech* 13: 1211–1218

O'Collins VE, Macleod MR, Donnan GA, Horky LL, van der Worp BH & Howells DW (2006) 1,026 experimental treatments in acute stroke. *Ann Neurol* 59: 467–477

Ohashi Y, Soler N, García Ortegón M, Zhang L, Kirsten ML, Perisic O, Masson GR, Burke JE, Jakobi AJ, Apostolakis AA, *et al* (2016) Characterization of Atg38 and NRBF2, a fifth subunit of the autophagic Vps34/PIK3C3 complex. *Autophagy* 12: 2129–2144

Orsi A, Razi M, Dooley HC, Robinson D, Weston AE, Collinson LM & Tooze SA (2012) Dynamic and transient interactions of Atg9 with autophagosomes, but not membrane integration, are required for autophagy. *Mol Biol Cell* 23: 1860–1873

Palikaras K, Lionaki E & Tavernarakis N (2018) Mechanisms of mitophagy in cellular homeostasis, physiology and pathology. *Nat Cell Biol* 20: 1013–1022

Pankiv S, Clausen TH, Lamark T, Brech A, Bruun J-A, Outzen H, Øvervatn A, Bjørkøy G & Johansen T (2007) p62/SQSTM1 binds directly to Atg8/LC3 to facilitate degradation of ubiquitinated protein aggregates by autophagy. *J Biol Chem* 282: 24131–24145

Paoni NF, Peale F, Wang F, Errett-Baroncini C, Steinmetz H, Toy K, Bai W, Williams PM, Bunting S, Gerritsen ME, *et al* (2002) Time course of skeletal muscle repair and gene expression following acute hind limb ischemia in mice. *Physiol Genomics* 11: 263–272

Papadakis M, Hadley G, Xilouri M, Hoyte LC, Nagel S, McMenamin MM, Tsaknakis G, Watt SM, Drakesmith CW, Chen R, *et al* (2013) Tsc1 (hamartin) confers neuroprotection against ischemia by inducing autophagy. *Nat Med* 19: 351–357

Park Y, Liu C, Luo T, Dietrich WD, Bramlett H & Hu B (2015) Chaperone-Mediated Autophagy after Traumatic Brain Injury. *J Neurotrauma* 32: 1449–1457

Parzych KR & Klionsky DJ (2014) An overview of autophagy: morphology, mechanism, and regulation. *Antioxid Redox Signal* 20: 460–473

Paul S & Candelario-Jalil E (2021) Emerging neuroprotective strategies for the treatment of ischemic stroke: An overview of clinical and preclinical studies. *Exp Neurol* 335: 113518

Peng PL, Zhong X, Tu W, Soundarapandian MM, Molner P, Zhu D, Lau L, Liu S, Liu F & Lu Y (2006) ADAR2-dependent RNA editing of AMPA receptor subunit GluR2 determines vulnerability of neurons in forebrain ischemia. *Neuron* 49: 719–733

Phillis JW (1996) Cerebroprotective action of the phospholipase inhibitor quinacrine in the ischemia/reperfused gerbil hippocampus. *Life Sci* 58: PL97-101

Powers WJ, Grubb RL & Raichle ME (1984) Physiological responses to focal cerebral ischemia in humans. *Ann Neurol* 16: 546–552

Powers WJ, Rabinstein AA, Ackerson T, Adeoye OM, Bambakidis NC, Becker K, Biller J, Brown M, Demaerschalk BM, Hoh B, *et al* (2019) Guidelines for the Early Management of Patients With Acute Ischemic Stroke: 2019 Update to the 2018 Guidelines for the Early Management of Acute Ischemic Stroke: A Guideline for Healthcare Professionals From the American Heart Association/American Stroke Association. *Stroke* 50: e344–e418

Proikas-Cezanne T, Takacs Z, Dönnes P & Kohlbacher O (2015) WIPI proteins: essential PtdIns3P effectors at the nascent autophagosome. *J Cell Sci* 128: 207–217

Puka-Sundvall M, Gajkowska B, Cholewinski M, Blomgren K, Lazarewicz JW & Hagberg H (2000) Subcellular distribution of calcium and ultrastructural changes after cerebral hypoxia-ischemia in immature rats. *Brain Res Dev Brain Res* 125: 31–41

Puustinen P, Keldsbo A, Corcelle-Termeau E, Ngoei K, Sønder SL, Farkas T, Kaae Andersen K, Oakhill JS & Jäättelä M (2020) DNA-dependent protein kinase

regulates lysosomal AMP-dependent protein kinase activation and autophagy. *Autophagy* 16: 1871–1888

Qin A-P, Liu C-F, Qin Y-Y, Hong L-Z, Xu M, Yang L, Liu J, Qin Z-H & Zhang H-L (2010) Autophagy was activated in injured astrocytes and mildly decreased cell survival following glucose and oxygen deprivation and focal cerebral ischemia. *Autophagy* 6: 738–753

Quirion R, Araujo D, Nair NPV & Chabot J-G (1988) Visualization of growth factor receptor sites in rat forebrain. *Synapse* 2: 212–218

Raasi S, Varadan R, Fushman D & Pickart CM (2005) Diverse polyubiquitin interaction properties of ubiquitin-associated domains. *Nat Struct Mol Biol* 12: 708–714

Rabinstein AA (2017) Treatment of Acute Ischemic Stroke. *Contin Lifelong Learn Neurol* 23: 62

Rami A, Langhagen A & Steiger S (2008) Focal cerebral ischemia induces upregulation of Beclin 1 and autophagy-like cell death. *Neurobiol Dis* 29: 132–141

Ravenhill BJ, Boyle KB, von Muhlinen N, Ellison CJ, Masson GR, Otten EG, Foeglein A, Williams R & Randow F (2019) The Cargo Receptor NDP52 Initiates Selective Autophagy by Recruiting the ULK Complex to Cytosol-Invading Bacteria. *Mol Cell* 74: 320-329.e6

Ravikumar B, Moreau K, Jahreiss L, Puri C & Rubinsztein DC (2010) Plasma membrane contributes to the formation of pre-autophagosomal structures. *Nat Cell Biol* 12: 747–757

Ray R, Chen G, Velde CV, Cizeau J, Park JH, Reed JC, Gietz RD & Greenberg AH (2000) BNIP3 Heterodimerizes with Bcl-2/Bcl-XL and Induces Cell Death Independent of a Bcl-2 Homology 3 (BH3) Domain at Both Mitochondrial and Nonmitochondrial Sites *. *J Biol Chem* 275: 1439–1448

Redmann M, Dodson M, Boyer-Guittaut M, Darley-Usmar V & Zhang J (2014) Mitophagy mechanisms and role in human diseases. *Int J Biochem Cell Biol* 53: 127–133

Ren J, Liang R, Wang W, Zhang D, Yu L & Feng W (2020) Multi-site-mediated entwining of the linear WIR-motif around WIPI β-propellers for autophagy. *Nat Commun* 11: 2702

Roth GA, Abate D, Abate KH, Abay SM, Abbafati C, Abbasi N, Abbastabar H, Abd-Allah F, Abdela J, Abdelalim A, *et al* (2018) Global, regional, and national age-sex-

specific mortality for 282 causes of death in 195 countries and territories, 1980–2017: a systematic analysis for the Global Burden of Disease Study 2017. *The Lancet* 392: 1736–1788

Sacchetti ML (2008) Is It Time to Definitely Abandon Neuroprotection in Acute Ischemic Stroke? *Stroke* 39: 1659–1660

Sacco RL, Kasner SE, Broderick JP, Caplan LR, Connors JJB, Culebras A, Elkind MSV, George MG, Hamdan AD, Higashida RT, *et al* (2013) An updated definition of stroke for the 21st century: a statement for healthcare professionals from the American Heart Association/American Stroke Association. *Stroke* 44: 2064–2089

Safronova O & Morita I (2010) Transcriptome remodeling in hypoxic inflammation. *J Dent Res* 89: 430–444

Sahu R, Kaushik S, Clement CC, Cannizzo ES, Scharf B, Follenzi A, Potolicchio I, Nieves E, Cuervo AM & Santambrogio L (2011) Microautophagy of cytosolic proteins by late endosomes. *Dev Cell* 20: 131–139

Sancak Y, Peterson TR, Shaul YD, Lindquist RA, Thoreen CC, Bar-Peled L & Sabatini DM (2008) The Rag GTPases bind raptor and mediate amino acid signaling to mTORC1. *Science* 320: 1496–1501

Sardiello M, Palmieri M, di Ronza A, Medina DL, Valenza M, Gennarino VA, Di Malta C, Donaudy F, Embrione V, Polishchuk RS, *et al* (2009) A gene network regulating lysosomal biogenesis and function. *Science* 325: 473–477

Saxton RA & Sabatini DM (2017) mTOR Signaling in Growth, Metabolism, and Disease. *Cell* 168: 960–976

Schuck S (2020) Microautophagy – distinct molecular mechanisms handle cargoes of many sizes. *J Cell Sci* 133: jcs246322

Seglen PO & Gordon PB (1982) 3-Methyladenine: specific inhibitor of autophagic/lysosomal protein degradation in isolated rat hepatocytes. *Proc Natl Acad Sci U S A* 79: 1889–1892

Seibenhener ML, Babu JR, Geetha T, Wong HC, Krishna NR & Wooten MW (2004) Sequestosome 1/p62 Is a Polyubiquitin Chain Binding Protein Involved in Ubiquitin Proteasome Degradation. *Mol Cell Biol* 24: 8055–8068

Sekine S & Youle RJ (2018) PINK1 import regulation; a fine system to convey mitochondrial stress to the cytosol. *BMC Biol* 16: 2

Semenza GL (2003) Targeting HIF-1 for cancer therapy. *Nat Rev Cancer* 3: 721–732

Seo JH, Rivadeneira DB, Caino MC, Chae YC, Speicher DW, Tang H-Y, Vaira V, Bosari S, Palleschi A, Rampini P, *et al* (2016) The Mitochondrial Unfoldase-Peptidase Complex ClpXP Controls Bioenergetics Stress and Metastasis. *PLoS Biol* 14: e1002507

Settembre C, Malta CD, Polito VA, Arencibia MG, Vetrini F, Erdin S, Erdin SU, Huynh T, Medina D, Colella P, *et al* (2011) TFEB Links Autophagy to Lysosomal Biogenesis. *Science*

Shakir R (2018) The struggle for stroke reclassification. *Nat Rev Neurol* 14: 447–448

Shao Z, Dou S, Zhu J, Wang H, Xu D, Wang C, Cheng B & Bai B (2020) The Role of Mitophagy in Ischemic Stroke. *Front Neurol* 11

Shi R, Weng J, Zhao L, Li X-M, Gao T-M & Kong J (2012) Excessive autophagy contributes to neuron death in cerebral ischemia. *CNS Neurosci Ther* 18: 250–260

Shrivastav M, De Haro LP & Nickoloff JA (2008) Regulation of DNA double-strand break repair pathway choice. *Cell Res* 18: 134–147

Shvets E, Fass E & Elazar Z (2008) Utilizing flow cytometry to monitor autophagy in living mammalian cells. *Autophagy* 4: 621–628

Siesjö BK & Bengtsson F (1989) Calcium fluxes, calcium antagonists, and calcium-related pathology in brain ischemia, hypoglycemia, and spreading depression: a unifying hypothesis. *J Cereb Blood Flow Metab Off J Int Soc Cereb Blood Flow Metab* 9: 127–140

Smith MD, Harley ME, Kemp AJ, Wills J, Lee M, Arends M, von Kriegsheim A, Behrends C & Wilkinson S (2018) CCPG1 Is a Non-canonical Autophagy Cargo Receptor Essential for ER-Phagy and Pancreatic ER Proteostasis. *Dev Cell* 44: 217-232.e11

Stephan JS, Yeh Y-Y, Ramachandran V, Deminoff SJ & Herman PK (2010) The Tor and cAMP-dependent protein kinase signaling pathways coordinately control autophagy in Saccharomyces cerevisiae. *Autophagy* 6: 294–295

Strilciuc S, Vécsei L, Boering D, Pražnikar A, Kaut O, Riederer P & Battistin L (2021) Safety of Cerebrolysin for Neurorecovery after Acute Ischemic Stroke: A Systematic Review and Meta-Analysis of Twelve Randomized-Controlled Trials. *Pharm Basel Switz* 14: 1297

Sun B, Ou H, Ren F, Huan Y, Zhong T, Gao M & Cai H (2018) Propofol inhibited autophagy through Ca2+/CaMKKβ/AMPK/mTOR pathway in OGD/R-induced neuron injury. *Mol Med Camb Mass* 24: 58

Suzuki K, Kirisako T, Kamada Y, Mizushima N, Noda T & Ohsumi Y (2001) The pre-autophagosomal structure organized by concerted functions of APG genes is essential for autophagosome formation. *EMBO J* 20: 5971–5981

Takahashi Y, Coppola D, Matsushita N, Cualing HD, Sun M, Sato Y, Liang C, Jung JU, Cheng JQ, Mulé JJ, *et al* (2007) Bif-1 interacts with Beclin 1 through UVRAG and regulates autophagy and tumorigenesis. *Nat Cell Biol* 9: 1142–1151

Takeshige K, Baba M, Tsuboi S, Noda T & Ohsumi Y (1992) Autophagy in yeast demonstrated with proteinase-deficient mutants and conditions for its induction. *J Cell Biol* 119: 301–311

Tan HWS, Sim AYL & Long YC (2017) Glutamine metabolism regulates autophagy-dependent mTORC1 reactivation during amino acid starvation. *Nat Commun* 8: 338

Tang X, Chen N & Long X (2017) Ginsenoside Rg1 improves ischemic brain injury by balancing mitochondrial biogenesis and mitophagy. *Trop J Pharm Res* 16: 2469–2475

Tanida I, Ueno T & Uchiyama Y (2014) A Super-Ecliptic, pHluorin-mKate2, Tandem Fluorescent Protein-Tagged Human LC3 for the Monitoring of Mammalian Autophagy. *PLOS ONE* 9: e110600

Tasca CI, Dal-Cim T & Cimarosti H (2015) In vitro oxygen-glucose deprivation to study ischemic cell death. *Methods Mol Biol Clifton NJ* 1254: 197–210

Thoreen CC, Kang SA, Chang JW, Liu Q, Zhang J, Gao Y, Reichling LJ, Sim T, Sabatini DM & Gray NS (2009) An ATP-competitive Mammalian Target of Rapamycin Inhibitor Reveals Rapamycin-resistant Functions of mTORC1 *. *J Biol Chem* 284: 8023–8032

Toda T, Yamamoto S, Umehara N, Mori Y, Wakamori M & Shimizu S (2019) Protective Effects of Duloxetine against Cerebral Ischemia-Reperfusion Injury via Transient Receptor Potential Melastatin 2 Inhibition. *J Pharmacol Exp Ther* 368: 246–254

Tsukada M & Ohsumi Y (1993) Isolation and characterization of autophagy-defective mutants of Saccharomyces cerevisiae. *FEBS Lett* 333: 169–174

Turco E, Witt M, Abert C, Bock-Bierbaum T, Su M-Y, Trapannone R, Sztacho M, Danieli A, Shi X, Zaffagnini G, *et al* (2019) FIP200 Claw Domain Binding to p62 Promotes Autophagosome Formation at Ubiquitin Condensates. *Mol Cell* 74: 330-346.e11

Valverde DP, Yu S, Boggavarapu V, Kumar N, Lees JA, Walz T, Reinisch KM & Melia TJ (2019) ATG2 transports lipids to promote autophagosome biogenesis. *J Cell Biol* 218: 1787–1798

Vancompernolle K, Van Herreweghe F, Pynaert G, Van de Craen M, De Vos K, Totty N, Sterling A, Fiers W, Vandenabeele P & Grooten J (1998) Atractyloside-induced release of cathepsin B, a protease with caspase-processing activity. *FEBS Lett* 438: 150–158

Vargas JNS, Wang C, Bunker E, Hao L, Maric D, Schiavo G, Randow F & Youle RJ (2019) Spatiotemporal Control of ULK1 Activation by NDP52 and TBK1 during Selective Autophagy. *Mol Cell* 74: 347-362.e6

Vega-Rubin-de-Celis S, Peña-Llopis S, Konda M & Brugarolas J (2017) Multistep regulation of TFEB by MTORC1. *Autophagy* 13: 464–472

Velikkakath AKG, Nishimura T, Oita E, Ishihara N & Mizushima N (2012) Mammalian Atg2 proteins are essential for autophagosome formation and important for regulation of size and distribution of lipid droplets. *Mol Biol Cell* 23: 896–909

Virani SS, Alonso A, Aparicio HJ, Benjamin EJ, Bittencourt MS, Callaway CW, Carson AP, Chamberlain AM, Cheng S, Delling FN, *et al* (2021) Heart Disease and Stroke Statistics-2021 Update: A Report From the American Heart Association. *Circulation* 143: e254–e743

Vos T, Lim SS, Abbafati C, Abbas KM, Abbasi M, Abbasifard M, Abbasi-Kangevari M, Abbastabar H, Abd-Allah F, Abdelalim A, *et al* (2020) Global burden of 369 diseases and injuries in 204 countries and territories, 1990–2019: a systematic analysis for the Global Burden of Disease Study 2019. *The Lancet* 396: 1204–1222

Wang P, Liang J, Li Y, Li J, Yang X, Zhang X, Han S, Li S & Li J (2014) Down-Regulation of miRNA-30a Alleviates Cerebral Ischemic Injury Through Enhancing Beclin 1-Mediated Autophagy. *Neurochem Res* 39: 1279–1291

Wang P, Shao B-Z, Deng Z, Chen S, Yue Z & Miao C-Y (2018) Autophagy in ischemic stroke. *Prog Neurobiol* 163–164: 98–117

Wang Q, Liu N, Ni Y-S, Yang J-M, Ma L, Lan X-B, Wu J, Niu J-G & Yu J-Q (2021a) TRPM2 in ischemic stroke: Structure, molecular mechanisms, and drug intervention. *Channels* 15: 136–154

Wang R, Wang J, Hassan A, Lee C-H, Xie X-S & Li X (2021b) Molecular basis of V-ATPase inhibition by bafilomycin A1. *Nat Commun* 12: 1782

Wei H, Peng Z, Guo J, Chen L & Shao K (2022) Downregulation of miR-338-3p alleviates neuronal ischemic injury by decreasing cPKCγ-Mediated autophagy through the Akt/mTOR pathway. *Neurochem Int* 154: 105279

Weidberg H, Shvets E & Elazar Z (2011) Biogenesis and cargo selectivity of autophagosomes. *Annu Rev Biochem* 80: 125–156

Weidberg H, Shvets E, Shpilka T, Shimron F, Shinder V & Elazar Z (2010) LC3 and GATE-16/GABARAP subfamilies are both essential yet act differently in autophagosome biogenesis. *EMBO J* 29: 1792–1802

Wen Y-D, Sheng R, Zhang L-S, Han R, Zhang X, Zhang X-D, Han F, Fukunaga K & Qin Z-H (2008) Neuronal injury in rat model of permanent focal cerebral ischemia is associated with activation of autophagic and lysosomal pathways. *Autophagy* 4: 762–769

Wu B, Luo H, Zhou X, Cheng C-Y, Lin L, Liu B-L, Liu K, Li P & Yang H (2017) Succinate-induced neuronal mitochondrial fission and hexokinase II malfunction in ischemic stroke: Therapeutical effects of kaempferol. *Biochim Biophys Acta Mol Basis Dis* 1863: 2307–2318

Wu CL, Qiang L, Han W, Ming M, Viollet B & He YY (2013) Role of AMPK in UVB-induced DNA damage repair and growth control. *Oncogene* 32: 2682–2689

Wu H, Chen S, Ammar A-B, Xu J, Wu Q, Pan K, Zhang J & Hong Y (2015) Crosstalk Between Macroautophagy and Chaperone-Mediated Autophagy: Implications for the Treatment of Neurological Diseases. *Mol Neurobiol* 52: 1284–1296

Wu M & Zhang P (2020) EGFR-mediated autophagy in tumourigenesis and therapeutic resistance. *Cancer Lett* 469: 207–216

Wurzer B, Zaffagnini G, Fracchiolla D, Turco E, Abert C, Romanov J & Martens S (2015) Oligomerization of p62 allows for selection of ubiquitinated cargo and isolation membrane during selective autophagy. *eLife* 4: e08941

Xie M, Cho GW, Kong Y, Li DL, Altamirano F, Luo X, Morales CR, Jiang N, Schiattarella GG, May HI, *et al* (2021) Activation of Autophagic Flux Blunts Cardiac Ischemia/Reperfusion Injury. *Circ Res* 129: 435–450

Yang Y, Gao K, Hu Z, Li W, Davies H, Ling S, Rudd JA & Fang M (2015) Autophagy Upregulation and Apoptosis Downregulation in DAHP and Triptolide Treated Cerebral Ischemia. *Mediators Inflamm* 2015: e120198

Yang Y & Rosenberg GA (2011) Blood-brain barrier breakdown in acute and chronic cerebrovascular disease. *Stroke* 42: 3323–3328

Yao Y, Ji Y, Ren J, Liu H, Khanna R & Sun L (2021) Inhibition of autophagy by CRMP2-derived peptide ST2-104 (R9-CBD3) via a CaMKKβ/AMPK/mTOR pathway contributes to ischemic postconditioning-induced neuroprotection against cerebral ischemia-reperfusion injury. *Mol Brain* 14: 123

Yorimitsu T & Klionsky DJ (2005) Autophagy: molecular machinery for self-eating. *Cell Death Differ* 12: 1542–1552

Young ARJ, Chan EYW, Hu XW, Köchl R, Crawshaw SG, High S, Hailey DW, Lippincott-Schwartz J & Tooze SA (2006) Starvation and ULK1-dependent cycling of mammalian Atg9 between the TGN and endosomes. *J Cell Sci* 119: 3888–3900

Young JE, Martinez RA & La Spada AR (2009) Nutrient Deprivation Induces Neuronal Autophagy and Implicates Reduced Insulin Signaling in Neuroprotective Autophagy Activation. *J Biol Chem* 284: 2363–2373

Yu J, Li X, Matei N, McBride D, Tang J, Yan M & Zhang JH (2018) Ezetimibe, a NPC1L1 inhibitor, attenuates neuronal apoptosis through AMPK dependent autophagy activation after MCAO in rats. *Exp Neurol* 307: 12–23

Zhang H, Bosch-Marce M, Shimoda LA, Tan YS, Baek JH, Wesley JB, Gonzalez FJ & Semenza GL (2008) Mitochondrial Autophagy Is an HIF-1-dependent Adaptive Metabolic Response to Hypoxia. *J Biol Chem* 283: 10892–10903

Zhang J-H, Chung TDY & Oldenburg KR (1999) A Simple Statistical Parameter for Use in Evaluation and Validation of High Throughput Screening Assays. *J Biomol Screen* 4: 67–73

Zhang X, Deguchi S, Deguchi K, Ohta Y, Yamashita T, Shang J, Tian F, Liu N, Liu W, Ikeda Y, *et al* (2011) Amlodipine and atorvastatin exert protective and additive effects via antiapoptotic and antiautophagic mechanisms after transient middle cerebral artery occlusion in Zucker metabolic syndrome rats. *J Neurosci Res* 89: 1228–1234

Zhang X, Fu C, Chen B, Xu Z, Zeng Z, He L, Lu Y, Chen Z & Liu X (2019) Autophagy Induced by Oxygen-Glucose Deprivation Mediates the Injury to the Neurovascular Unit. *Med Sci Monit Int Med J Exp Clin Res* 25: 1373–1382

Zhang X, Yan H, Yuan Y, Gao J, Shen Z, Cheng Y, Shen Y, Wang R-R, Wang X, Hu W-W, *et al* (2013) Cerebral ischemia-reperfusion-induced autophagy protects against neuronal injury by mitochondrial clearance. *Autophagy* 9: 1321–1333

Zheng YT, Shahnazari S, Brech A, Lamark T, Johansen T & Brumell JH (2009) The adaptor protein p62/SQSTM1 targets invading bacteria to the autophagy pathway. *J Immunol Baltim Md 1950* 183: 5909–5916

Zinnah KMA & Park S-Y (2019) Duloxetine Enhances TRAIL-mediated Apoptosis via AMPK-mediated Inhibition of Autophagy Flux in Lung Cancer Cells. *Anticancer Res* 39: 6621–6633